EFFECTS OF AMBIENT PRESSURE ON THE INSTABILITY OF A LIQUID BOILING EXPLOSIVELY AT THE SUPERHEAT LIMIT

Thesis by
David Lawrence Frost

In Partial Fulfillment
of the Requirements for the Degree of
Doctor of Philosophy

California Institute of Technology
Pasadena, California

1985
(Submitted 22 May 1985)

Dedicated to my parents

ACKNOWLEDGEMENTS

First of all I would like to thank my advisor, Professor Bradford Sturtevant, for his constant suggestions, advice, and motivation throughout the course of this work. I have especially benefitted from his keen physical insight and I feel that some of his enthusiasm for understanding new phenomena has rubbed off on me. His editorial assistance has also been invaluable.

I would also like to thank my fellow students, in particular Thomas Rösgen for his computer wizardry and brainstorming ideas, Jean-Francois Haas for help with my experiments and John Torczynski and Jean-Pierre Huot for many stimulating discussions.

Finally, I am grateful to all the members of the GALCIT community for their help and encouragement during my stay at Caltech.

This research was supported by the Department of Energy, Division of Chemical Sciences, under Project Agreement DE-AT03-80ER10634.

ABSTRACT

The effect of ambient pressure on the dynamical behaviour of a single droplet (1-2 mm diameter) of volatile liquid boiling explosively at the limit of superheat is studied experimentally and theoretically. In a series of experiments it is shown that the evaporative instability, observed earlier by Shepherd & Sturtevant (1982) during the rapid vapourization of butane droplets at atmospheric pressure, is suppressed at high pressure. Three other fluids (pentane, isopentane, and ether) are tested to establish the generality of the instability and other transient processes previously observed. Direct evidence is obtained showing that during violently unstable boiling small liquid particles are torn from the liquid-vapour interface. This ejection of fine droplets from the evaporating surface produces a mass flux orders of magnitude greater than that characteristic of ordinary boiling.

Raising the ambient pressure lowers the superheat attained at the superheat limit, which decreases the vapourization rate. At high pressure boiling consists of normal slow vapourization from a smooth interface. Observed bubble growth rates show reasonable agreement with theory. At intermediate pressures a transitional regime of stability occurs in which a drop initially vapourizes *stably* for several milliseconds while incipient instability waves develop on the evaporating interface. When only a small amount of liquid remains in the drop in the shape of a thin cap, heat transfer from the surrounding hot host fluid initiates violent boiling at the edge of the liquid cap. The subsequent rapid vapourization generates a radiated pressure field two orders of magnitude larger than during stable boiling, and sets the bubble into violent oscillation. The bubble is subject to the Rayleigh-Taylor instability and rapidly disintegrates into a cloud

of small bubbles.

Lowering the ambient pressure decreases the time delay between nucleation and onset of unstable boiling. For example, in ether at atmospheric pressure the instability is triggered less than 8 μsec after nucleation, shortly *after* the smooth vapour bubble contacts the droplet surface. Heterogeneous nucleation spreads out along the surface of the drop while disturbances (with a length scale of 100 μm) distort the *unstably* evaporating interface within the drop, substantially enhancing the vapourization rate. At early times, droplets torn from the evaporating surface evaporate before the instability-driven jet impinges upon the surrounding fluid, bulging the bubble surface. The last portion of liquid in a drop boils particularly violently and droplets ejected from the evaporating interface at this time remain intact to splatter the bubble surface. At subatmospheric pressures the most rapid vapourization occurs and temperature gradients within a drop produce spatial variations in vapourization rate.

The Landau mechanism for the instability of laminar flames is adapted to the case of evaporation to investigate the effects of variable ambient pressure. A spherical version of the theory, applicable before the vapour bubble contacts the droplet surface, predicts absolute stability at atmospheric pressure. At later times the spherical constraint is inappropriate and planar theory yields results in general agreement with observation. Differences in fluid properties make some fluids more prone to instability than others. The product of the maximum growth rate with the time interval the interface is predicted to be linearly unstable measures the susceptibility to instability. For practical estimates it is suggested that a value of 3 of this parameter be taken as the lower limit for instability. The sensitivity of the instability to temperature suggests that small temperature nonuniformities may be responsible for quantitative departures of the behaviour from predictions.

TABLE OF CONTENTS

LIST OF FIGURES

LIST OF TABLES

LIST OF SYMBOLS

Symbol	Description
b	Coefficient in dispersion relation (5.9), defined in equation (5.10)
c	Coefficient in dispersion relation (5.9), defined in equation (5.11)
c_p	Specific heat
D	Thermal diffusivity
F	Nondimensional "figure of merit" defined in equation (5.5)
g	Acceleration due to gravity
J	Mass flux
Ja	Jakob number defined in equation (5.12)
K	Nondimensional wavenumber = kR
k	Wavenumber
$k_{v,l}$	Thermal conductivity of vapour, liquid
L	Latent heat of evaporation
N_I	Inertia number defined in equation (5.3)
N_W	Weber number defined in equation (5.4)
n	Spherical harmonic index
p	Pressure
R	Vapour bubble radius
$\dot{R}$	Radial velocity
$\ddot{R}$	Radial acceleration
$R_{inertial}$	Bubble radius in the inertial growth regime given in equation (B.1)
$R_{thermal}$	Bubble radius in the thermally-dominated growth regime given in equation (B.2)
T	Temperature
T_b	Temperature of bubble surface

T_{bp}	Normal boiling temperature
t	Time
U	Radial bubble velocity
v	specific volume
W	Velocity relative to the evaporating interface
α	Density ratio, ρ_v/ρ_l
β	Fraction of liquid at the evaporating surface converted into vapour (see §5.2.2)
ε	Perturbation amplitude in the spherical instability theory discussed in §5.1.2
ζ	Vorticity
η	Perturbed interface shown in figure D.1
κ	Curvature
λ	Perturbation wavelength
ν_o	Natural frequency of ordinary surface waves defined in equation (D.4)
ρ	Density
σ	Surface tension
τ	Time interval during which a growing bubble is predicted to be linearly unstable
Ω	Nondimensional growth rate in the planar instability theory defined in equation (5.2)
ω'	Nondimensional growth rate in the spherical instability theory
ω	Dimensional growth rate
$(\,)_c$	Liquid
$(\,)_{max}$	Maximum

$( )_{sat}$	Saturation conditions
$( )_{sl}$	Superheat limit conditions
$( )_{v}$	Vapour
$( )_{2\varphi}$	Conditions in two-phase flow region discussed in §5.2.2

Chapter 1

INTRODUCTION

If heterogeneous nucleation is suppressed, a liquid may be heated to temperatures far above its normal boiling point. The maximum temperature attainable, the so-called limit of superheat, corresponds to the limit of mechanical stability of the liquid. When the superheat limit is reached, boiling begins spontaneously by homogeneous nucleation, and the subsequent evaporative fluxes, fluid accelerations and departures from thermodynamic equilibrium are orders of magnitude greater than in ordinary boiling. General reviews of the properties of superheated liquids can be found in Skripov (1974), Blander & Katz (1975), and Reid (1976, 1978). Several interesting phenomena which provide important insight into the behaviour of metastable liquids occur under the extreme conditions of superheat-limit vapourization. In particular, the rapid vapourization drives a dynamic instability at the evaporating surface which leads to violent unstable boiling.

The explosive effects observed at the superheat limit are consequences of a baroclinic interfacial instability similar to the Landau mechanism for the instability of laminar flames (Landau & Lifshitz, 1959), which was discovered in the context of evaporation of butane at the superheat limit by Shepherd & Sturtevant (1982). They observed that the instability distorts and roughens the liquid-vapour interface, and they *inferred* from their measurements that it tears the interface, producing a substantial increase in the surface area available for evaporation and a high-velocity two-phase flow away from the interface. They also observed several interesting dynamical effects that occur during the explosive vapourization of a drop of volatile liquid. For example, the instability-

driven mass flux generates a jet which impinges upon the surrounding fluid and produces a characteristic bulge in the bubble surface.

1.1. Motivation

The present work builds on the exploratory work of Shepherd & Sturtevant (1982) and was motivated by a desire to obtain a more detailed understanding of the physical processes that occur during unstable boiling at the superheat limit. The current experiments were undertaken to investigate (i) the occurrence of the instability in a variety of *different* liquids, (ii) the variation between different liquids of the dynamical effects that occur during explosive vapourization, and (iii) the effect of ambient pressure on the vapourization process. In the current investigation single small droplets (with typical diameters of 1-2 mm) of a volatile liquid are heated until they vapourize explosively at the superheat limit. Heterogeneous nucleation and ordinary boiling are suppressed by immersing the droplets in a hot nonvolatile liquid, thus isolating them from solid surfaces containing gas nuclei. When the superheat limit is reached, boiling begins spontaneously by homogeneous nucleation. High-speed microphotography and fast-response pressure measurements are used to document the explosion process.

The most important accomplishment of the present work is the elucidation of the transient physical processes that occur after the onset of the evaporative instability in highly superheated liquids. The detailed effects of ambient pressure on the occurrence of the instability in small droplets boiling explosively at the superheat limit has been systematically documented for the first time. In the following chapters, high-resolution photographs and pressure measurements are presented that illustrate the strong influence of ambient pressure on the vapourization rate and the onset of the instability. By increasing the external pressure it is shown that the instability may be inhibited altogether,

changing the nature of vapourization from an explosive event to that of stable growth of a smooth vapour bubble. A transitional regime of vapourization has been discovered, between unstable and stable boiling, that provides direct experimental confirmation of the earlier hypothesis (Shepherd & Sturtevant, 1982) that a two-phase jet forms during unstable boiling.

1.2. Large Scale Vapour Explosions

The explosive process caused by the rapid production of vapour in a liquid boiling at the superheat limit is known as a *vapour explosion*, and it can be very destructive when it occurs accidentally in industry or in nature. The hazards associated with industrial vapour explosions provide a strong impetus for investigating the underlying physical processes that occur during rapid evaporation. Over the last several decades a large number of investigators have attempted to identify the circumstances that lead to vapour explosions (also called *rapid phase transitions* or *fuel-coolant interactions*). The research effort has been hampered by the number of complicated processes that occur in practice during a vapour explosion (e.g., multiphase flow, fragmentation, boiling heat transfer, and non-equilibrium evaporation).

Reid (1983) reviews the occurrence of vapour explosions in a variety of industries as well as related laboratory-scale studies. Other authors that have reviewed the widespread incidence of vapour explosions include Witte, Cox, & Bouvier (1970), Anderson & Armstrong (1974), and Strehlow (1980). Large-scale experiments that have been conducted to study vapour explosions typically involve either dropping or injecting a hot fluid into a cooler volatile liquid and observing if an explosion takes place. Experiments of this type usually provide little insight into the details of the events that lead to the explosion, and consequently there is still considerable controversy regarding the underlying mechanisms that govern vapour explosions. The diversity of situations in which vapour

explosions occur has contributed to the variety of physical mechanisms that have been hypothesized. A qualitative and comprehensive theory of vapour explosions currently does not exist and none of the existing models that deal with fuel-coolant interactions treat the important role of the evaporative instability discovered by Shepherd & Sturtevant (1982). The necessity of incorporating the significant effects of the instability into future theories provides incentive for conducting small-scale exploratory experiments in simple systems to investigate the basic phenomena.

After comparing explosive boiling incidents from different industries, Reid (1983) suggested two criteria that are necessary for the initiation of a rapid phase transition. First, intimate contact between a hot fluid and a cooler volatile fluid is needed, and secondly the temperature of the hot fluid must exceed a threshold value that is related to the superheat limit of the cooler liquid (see Henry et al., 1975). For large-scale explosions a rapid increase in interfacial area is necessary to provide efficient heat transfer for the rapid formation of vapour. Many investigators have assumed that prefragmentation of the hot fluid is a necessary condition for the onset of a vapour explosion. This assumption (often left unstated) is based on comparisons that show that heat transfer rates estimated to occur during vapour explosions in industry are much larger than characteristic heat transfer rates that occur in conventional boiling processes (for example see Witte et al., 1970). Classical diffusive heat transfer during stable boiling is not sufficient to supply the energy for rapid evaporation unless the surface area for heat transfer is greatly enlarged. The distortion and tearing of the liquid-vapour interface observed in the present experiments that occur during the violent phase of the instability sufficiently enhance the transport of energy to explain the large observed rates of vapourization. Therefore, fragmentation is effectively built into the instability mechanism.

Various fragmentation mechanisms have been presented to explain large-scale explosions. For example, Board et al. (1974) carried out a series of experiments that generated explosions by contacting molten metal with water. They proposed that when the vapour film surrounding the molten metal collapses, a jet of cold liquid is formed. The jet then penetrates the hot molten metal and rapidly vapourizes, fragmenting the molten metal. The collapse of the vapour film triggers an interaction that produces more vapour and the bubble growth/collapse cycle in some cases may escalate into a large explosion. This feedback process is elaborated in more depth by Buchanan & Dullforce (1973) and Buchanan (1974). Unfortunately none of the researchers who have proposed the vapour blanket collapse mechanism have ever observed the process to actually occur. This mechanism may play a role in some explosions, particularly ones involving liquid metals, but in other systems it fails to explain the observations. The time scale required for the formation and collapse of a vapour film (on the order of milliseconds) invalidates the appropriateness of this model in many cases in which an explosion is observed to occur microseconds after a volatile cold liquid contacts a hot fluid (for example, in spills of some cryogens onto water, Reid, 1983). The instability in the present experiments occurs during the ***growth*** phase of vapour bubbles, while, for example, the Rayleigh-Taylor instability, which is another mechanism for jetting but which occurs only upon bubble ***collapse*** plays no role.

The physical processes involved in the escalation of a small-scale vapour explosion into a large, coherent explosion are not well understood at present. Hall & Board (1979) (see also Baines et al., 1980) have proposed that vapour explosions may propagate in a manner analogous to a detonating chemical explosion. Initially, a quasi-stable coarse mixture of fuel and coolant is assumed to be present. The propagation of a shock wave, generated by an external disturbance, through the mixture would initiate fragmentation and energy

transfer. The rapid production of vapour may then be sufficient to sustain the propagation of the shock front. However, this model gives no insight into the causes of the initial fragmentation of the hot liquid fuel in contact with the coolant. Some authors (Drumheller, 1979; Witte et al., 1973; Reid, 1983 among others) believe that in large-scale interactions under certain conditions there must be a triggering phase, by which, after some incubation time, the explosion is initiated. The present experiments suggest that under conditions in which the boiling is neutrally stable (e.g., at elevated pressure) an external disturbance can trigger the instability producing violently unstable boiling. It is likely that the occurrence of a marginally stable situation is relatively common in applications. Under these circumstances a variety of mechanisms may trigger unstable vapourization.

1.3. Previous Related Work

Many experimental and theoretical studies have been carried out to study the growth of a vapour bubble in a superheated liquid. Plesset & Zwick (1954) obtained a solution for an asymptotic stage of bubble growth, dominated by heat transfer in a thin thermal boundary layer surrounding the bubble, in which the square of the bubble radius grows linearly in time (see Appendix A). Dalle Donne & Ferranti (1975) integrated the differential equations governing bubble growth numerically, without prior assumption of a thin thermal boundary layer, and obtained radial bubble growth rates for the vapourization of sodium at very high superheats. Results from a more recent version of the classical theory of the growth of a smooth bubble in a uniformly superheated liquid, that are in reasonable agreement with the results of Dalle Donne & Ferranti (1975), can be found in Prosperetti & Plesset (1978). Theofanous et al. (1969) and Jones & Zuber (1978) theoretically investigated the effects of a variable pressure field on bubble growth and the role of a nonuniform temperature field has been

considered by Zuber (1961).

Experimental studies utilizing high-speed movies (for example Dergarabedian, 1953, 1960; Hooper & Abdelmisseh, 1966; Kosky, 1968) show that at relatively low superheats a growing vapour bubble has a smooth surface. Previous experiments at the superheat limit (Apfel & Harbison, 1975; Avedisian & Glassman, 1981a) reported the explosive vapourization of droplets but had inadequate temporal and spatial resolution to resolve the details of the instability observed by Shepherd & Sturtevant (1982). The production of a two-phase flow during unstable boiling observed in the present experiments seems to be most similar to that seen during the flashing of free liquid surfaces by Grolmes & Fauske (1974). They studied the behaviour of a saturated or slightly subcooled column of liquid that was suddenly depressurized. After the expansion wave reached the interface they observed a violent flashing action in which vapour plus entrained liquid left the free surface. The superheats attained were less than 37°C, much smaller than that attained at the superheat limit, and the measured mass flux was an order of magnitude smaller than that estimated in the present expermiments.

1.4. Role of Ambient Pressure

The results of the present investigation show that the occurrence of the instability may be suppressed by increasing the ambient pressure. The role of ambient pressure may be understood by examining the p-T diagram shown in figure 1.1. The saturation curve is calculated from the Reidel equation of state (Reid et al., 1977) and the spinodal (defined by $(\partial p/\partial v)_T = 0$) is obtained by differentiating the Peng-Robinson equation of state (Peng & Robinson, 1976). The limit of superheat is observed to occur close to the liquid spinodal (Skripov, 1974), the locus of points of neutral mechanical stability of the liquid. It is well known (Reid, 1976; Avedisian & Glassman, 1981a,b) that the limit of superheat is

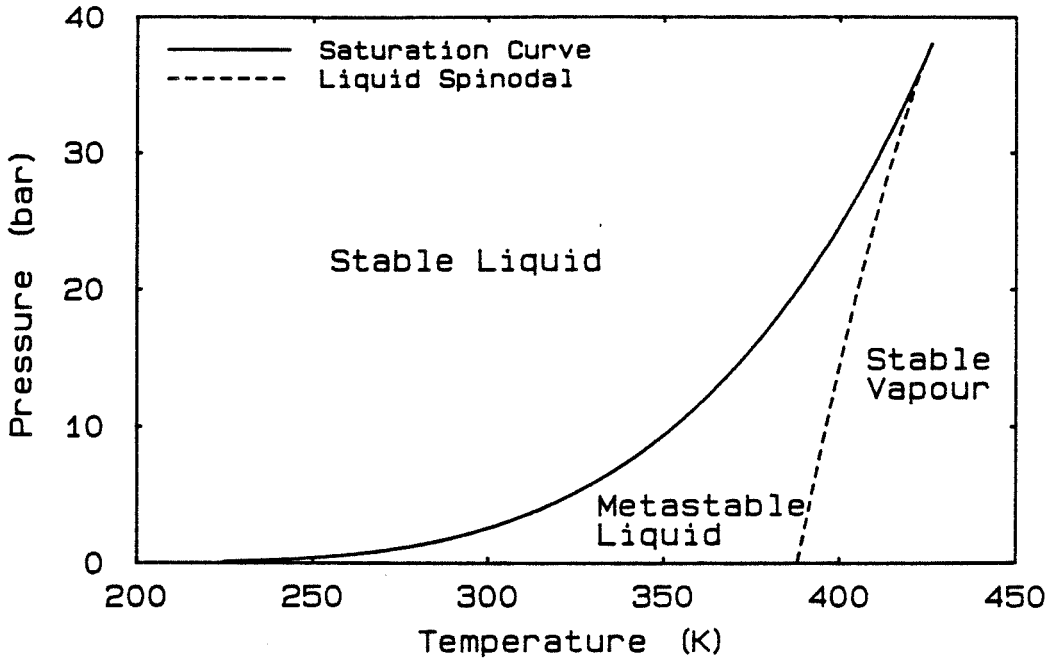

Figure 1.1 Pressure-temperature diagram for butane

relatively insensitive to ambient pressure. However, experiments reported by Avedisian (1982) have shown that the substantial reduction of superheat at the liquid spinodal (i.e., $T_{sl} - T_{sat}$) as the critical point is approached has a strong effect on the rate of vapourization of droplets after nucleation occurs. He used high-speed photography to study the boiling of liquid droplets of n-octane at the superheat limit at ambient pressures of 1, 6.8, and 12.1 bar. At atmospheric pressure the droplets boiled in a violent manner although the vapourization process is not resolved in the published photographs. At elevated pressures the boiling was much less intense and the growing vapour bubble appears smooth. The moderating effect of superheat reduction due to an increase in the external pressure has been noted by a number of authors in the context of models for large-scale vapour explosions (Buchanan, 1974; Drumheller, 1979; Henry & Fausky, 1979). It has been observed that only a modest increase in ambient pressure is needed to suppress the onset of vapour explosions in some fuel-coolant interaction systems (Nelson & Buxton, 1978). Until now it was not known that

the moderating effect may be directly attributable to the suppression of the intrinsic instability of rapid vapourization.

1.5. Outline of Present Work

The present work is an experimental investigation of the physical processes that occur during the explosive boiling of small liquid droplets at the superheat limit. The experimental facility and instrumentation used to study the rapid evaporation of droplets is described in chapter 2. Chapter 3 reports experiments that were performed to determine whether the evaporative instability discovered earlier in butane is found in other fluids. The various bubble growth phases are documented with small-scale photographs and pressure measurements.

Chapter 4 presents the outcome of experiments at elevated pressures and contains the most important results of the present investigation. The moderating effect of an increase in ambient pressure on bubble growth is demonstrated. Increasing the external pressure delays the onset of the instability and provides a situation in which a great deal about the physics of unstable boiling may be learned. In a transitional boiling regime, the instability is triggered in a late stage of bubble growth, and the two-phase jet generated at the evaporating interface is clearly visible. After the suppression of the instability at high pressures, the bubble growth rate is predicted reasonably well by existing classical bubble growth theories.

Chapter 5 contains a discussion of the Landau instability theory, first applied to rapid evaporation by Sturtevant & Shepherd (1982), in which the effects of variable ambient pressure are included. The relevance of planar and spherical versions of the theory is discussed in light of the experimental results. Finally, the behaviour of unstable boiling is investigated, and in particular the implications of the relatively simple quasi-steady nature of unstable boiling noted by

Shepherd & Sturtevant (1982) is discussed.

Chapter 2

EXPERIMENTAL FACILITY AND INSTRUMENTATION

2.1. Bubble Column Apparatus

The apparatus in the present experiments is a modified version of the bubble column apparatus of Shepherd & Sturtevant (1982), redesigned for operation at elevated pressures and temperatures. The basic apparatus consists of a vertical column of host fluid in which a droplet of buoyant, immiscible test fluid is immersed. A heater at the top of the column, and cooling coil at the bottom produce a stable temperature gradient in the host fluid. The temperature in the test section at the top of the column is monitored and maintained at the superheat limit of the test fluid. A small drop of test fluid is injected into the bottom of the vertical tube containing the host fluid. The test drop slowly rises up the column and is heated by the transfer of heat from the surrounding host. When the drop reaches the test section, homogeneous nucleation occurs and the drop evaporates with an explosive pop. The explosive process is examined with high-speed high-resolution microphotography and fast-response pressure instrumentation.

The bubble column apparatus, shown in figure 2.1, is constructed of anodized aluminum and consists of a test section (12.8 cm high, 10.2 cm square) mounted on top of a pipe (5.1 cm o.d., 30.4 cm long) which together contain the host fluid. The pipe is supported by a baseplate that contains the injection needle, viewing port and drainage valve. The baseplate is cooled by means of a spiral cooling coil attached to the bottom of the baseplate. Good thermal contact between the coil and baseplate is achieved by using high thermal conductivity epoxy to mount the coil to the plate. Circulating tap water through the

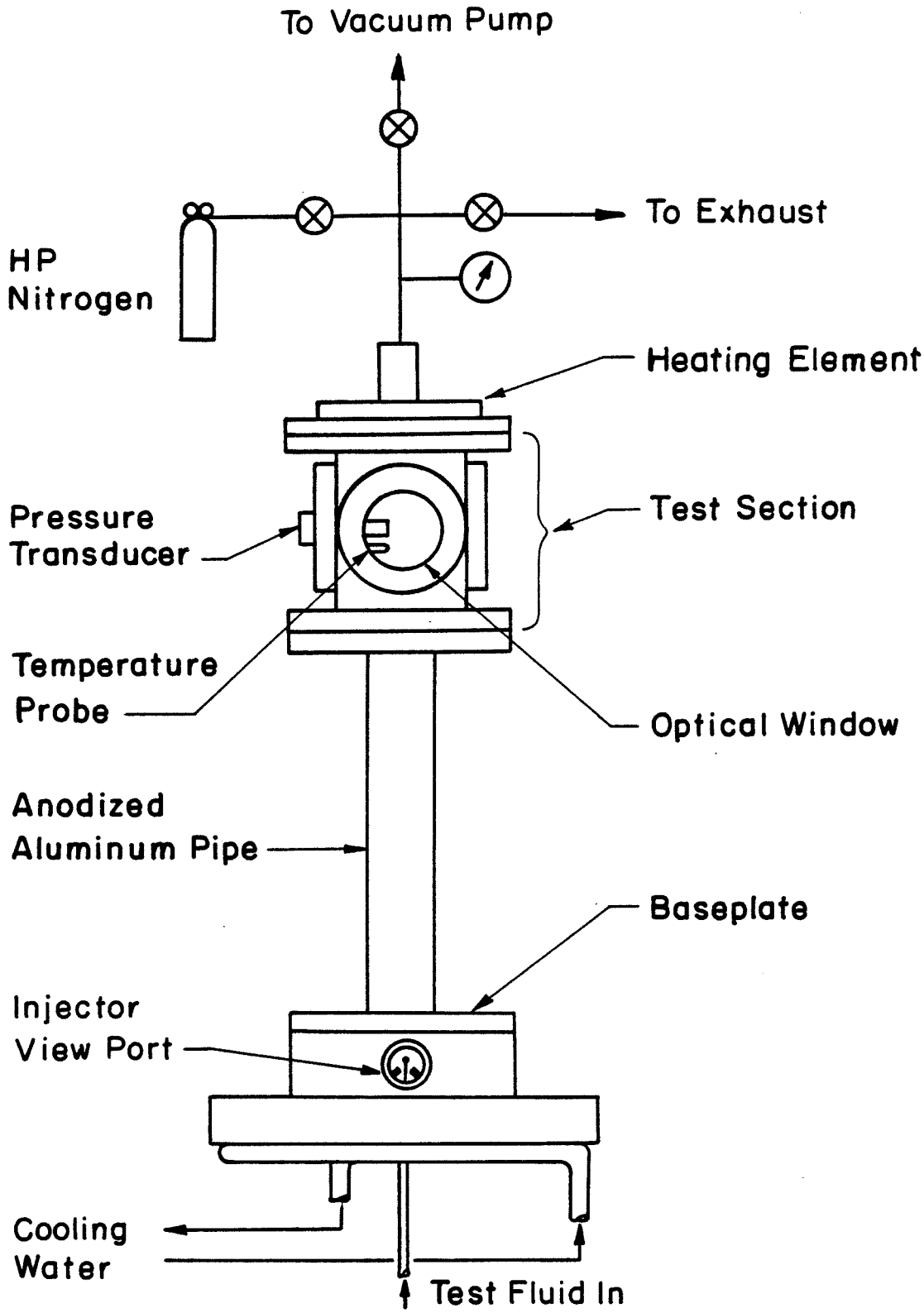

Figure 2.1 Bubble column apparatus

coil maintains the temperature of the baseplate near room temperature.

The host fluid is heated by a heating element (500 W) that is clamped to a plate above the test section. With the test section and column insulated, the heater is capable of heating the fluid in the test section up to a maximum temperature of about 175°C. The temperature in the test section is regulated by an OMEGA model 4201 temperature controller. The controller utilizes a resistive thermometer probe that protrudes into the test section to monitor and digitally display the temperature to within 0.1°C. The controller directs current to the electric heater with a magnitude that is proportional to the difference between a preset temperature value and the temperature measured in the test section. With a judicious choice of the set-point temperature value, determined by trial and error, it is possible to maintain the temperature in the middle of the test section at the superheat limit temperature of the test fluid to within 0.5°C.

Experiments were carried out with the ambient pressure inside the test section varying between 0.25 and 4.5 bar absolute. To maintain the fluid within the test section at high temperatures (typically 150°C) and under pressure it is necessary to use high temperature viton o-rings rather than conventional o-rings to seal the test section windows. To operate the experiment at elevated pressures, high pressure nitrogen gas is applied above the fluid in the test section through a hollow aluminum cylinder that extends upwards from the top of the test section. To obtain pressures below atmospheric pressure, a vacuum pump is used to partially evacuate the air above the host fluid within the test section. To control the flow rate of air out of the test section, a fine metering valve (.79 mm orifice diameter) is utilized between the vacuum pump and the test section.

A schematic of the droplet injection system is shown in figure 2.2. The plug containing the injection needle is mounted in the bottom of the baseplate and

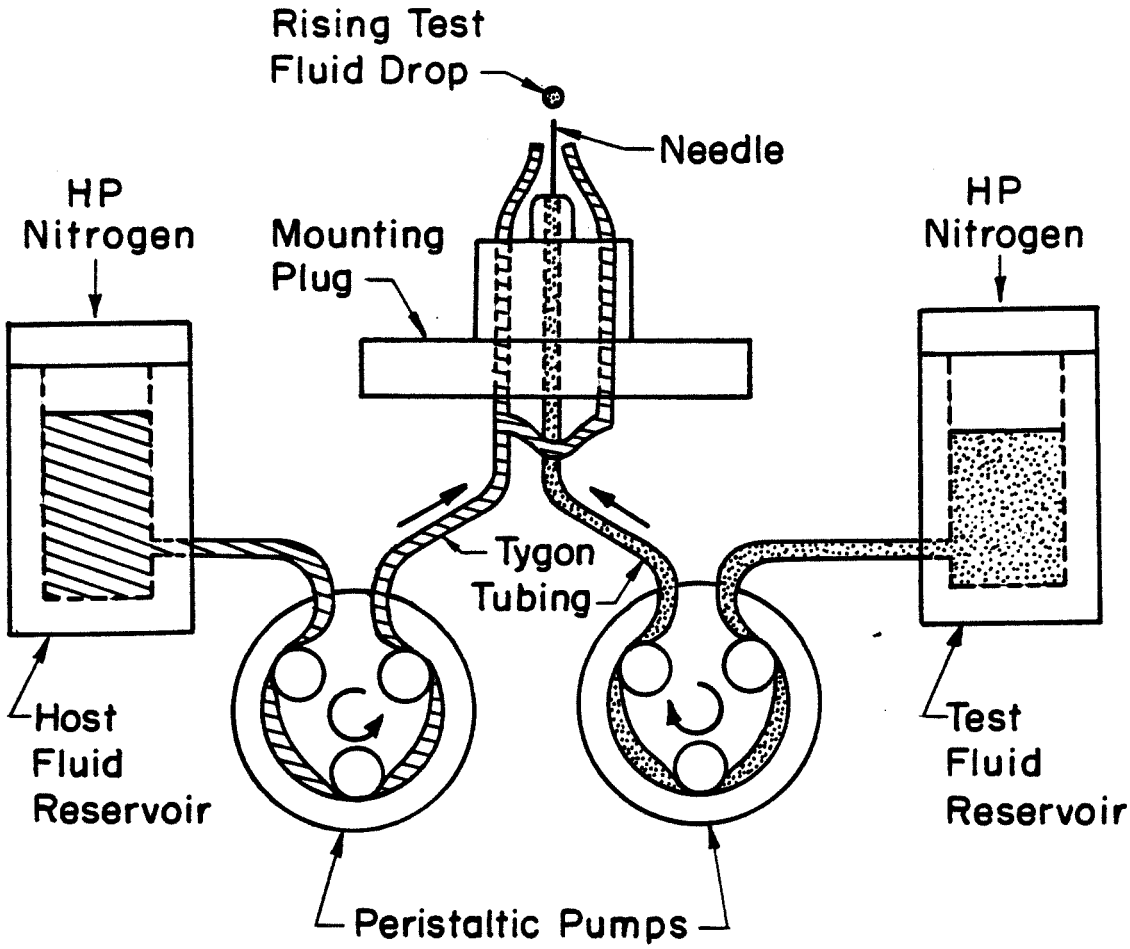

Figure 2.2 Injection system

the needle extends upwards into the host fluid in the lower part of the column. Test fluid is injected into the bottom of the column through a #27 gage hypodermic needle that is connected to the test fluid reservoir via standard LUER-LOK fittings and tygon tubing (.76 mm i.d.). A droplet of test fluid is formed on the end of the needle by manually operating an OMEGA MASTERFLEX peristaltic pump. Small drops (typically 1 mm diameter) remain attached to the needle due to surface tension. A small jet of host fluid is used to dislodge a drop from the needle. The jet is generated with another peristaltic pump and is directed towards the drop on the needle by two tubes that are located adjacent to and below the needle tip. The injection needle is viewed through a telescope

attached to a viewing port. The test fluid and host fluid reservoirs are pressurized to the same pressure level as the test section to facilitate droplet injection when the experiment is operated at elevated pressures.

The injection system has no refrigeration capability and the test fluid droplets are injected at room temperature. This limits the injection system to operating at ambient pressures above the vapour pressure of the test fluid at room temperature. Butane has a normal boiling point of -0.5°C and a vapour pressure of about 2.2 bar at room temperature (22°C) and as a result butane can only be injected and studied while the bubble column is pressurized. Ether, with a vapour pressure of about 0.63 bar at 22°C can be studied at subatmospheric pressures. Experiments have been carried out at pressures as low as 0.25 bar by first injecting a droplet at an ambient pressure above its vapour pressure, then lowering the pressure as the droplet rises up the column.

To operate the experiment the heater is first turned on and tap water is circulated through the cooling coil. It takes about two hours for the temperature of the fluid within the test section to reach 150°C. The temperature probe readout is monitored to determine when a steady state temperature gradient is obtained within the test section. A number of test drops with the same diameter are injected to determine the vertical location within the test section where homogeneous nucleation occurs. A time interval of several minutes between the injection of each drop allows the mixing generated by the explosion to subside and the temperature measured in the test section to return to its steady state value. Small changes to the temperature of the host fluid in the test section are made until the drops explode near the centre of the test section. After aligning the optics and readying the electronics in anticipation of an explosion, an experimental run can begin.

2.2. Description of the Host and Test Fluids

The choice of host and test fluids is dictated largely by convenience and the experience of previous investigators. The selection of a host fluid is limited by the requirements that it must (i) be immiscible with the test fluid, (ii) be more dense than the test fluid, (iii) have a surface tension sufficiently high to insure homogeneous nucleation, and (iv) have a boiling point higher than the superheat limit of the test fluid. Glycerol satisfies the above criteria and is used as the host fluid. After prolonged use at elevated temperatures, glycerol develops a slight yellowish discolouration. When this becomes noticeable the column is drained and refilled with fresh glycerol.

Three volatile hydrocarbons are primarily used as test fluids: pentane, isopentane, and ethyl ether. All three are liquid at room temperature and have superheat limits (148°C, 139°C, 147°C, respectively, at atmospheric pressure) low enough to allow the use of conventional piezoelectric pressure transducers immersed in the test section. At the superheat limit superheats of typically 112°C are attained, slightly higher than the 105°C achieved using butane at atmospheric pressure in the previous experiments by Shepherd & Sturtevant (1982), and much higher than most early experiments (Dergarabedian, 1953; Florshuetz et al., 1969; Hewitt & Parker, 1968; Kosky, 1968). Butane and acetone are also used as test fluids in the present experiments although no photographs were obtained for acetone. Representative properties of the host and test fluids can be found in tables 2.1, 2.2, and 2.3.

The fluids used are all of "reagent" grade except acetone which was labelled as "spectrophotometric" grade with a stated minimum purity of 99.5%. The glycerol, pentane and isopentane are obtained from the J.T. Baker Chemical Co., and the ether and acetone are from Mallinckrodt Inc., and American Scientific Products, respectively. No extra measures were taken to purify the test fluids.

In earlier experiments, Shepherd (1981) used technical grade butane and found that every drop containing only pure test fluid reached the superheat limit before exploding. In the present experiments the drops consistently explode within the temperature range reported by other experimenters (Blander & Katz, 1975).

2.3. Pressure Measurements

The pressure field generated by an exploding droplet is recorded using a fast-response piezoelectric pressure transducer. The pressure signal provides information about the explosive vapourization process as well as providing a trigger for photographing the drop. The transducer used is a PCB model 112A02 high-sensitivity quartz transducer manufactured by Piezotronics. Relevant features of the transducer include short response time (rise time = 2 μsec), high temperature operation (maximum temperature = 200 °C) and low sensitivity of the output to temperature changes (temperature coefficient = 0.02 %/°C). The transducer is able to detect very small pressure fluctuations. The resolution of the transducer is limited by the background noise level which has a peak-to-peak value of about 3 mbar when the transducer amplifier is set for maximum sensitivity.

The transducer is flush-mounted in an aluminum or brass plug that is located inside the test section in one of the two configurations shown in figure 2.3. In configuration A the transducer is located near the exploding drop (the drop/transducer distance is typically 5-6 mm) to obtain a signal that is used to trigger the light source used for photography. From table 2.1, the sound speed in glycerol at 150°C is 1.6 mm/μsec, so it takes about 4 μsec for the primary blast wave generated by an exploding droplet to reach the transducer. The pressure measured by the transducer is the sum of the primary waves that travel directly from the drop and the secondary waves that reach the transducer after

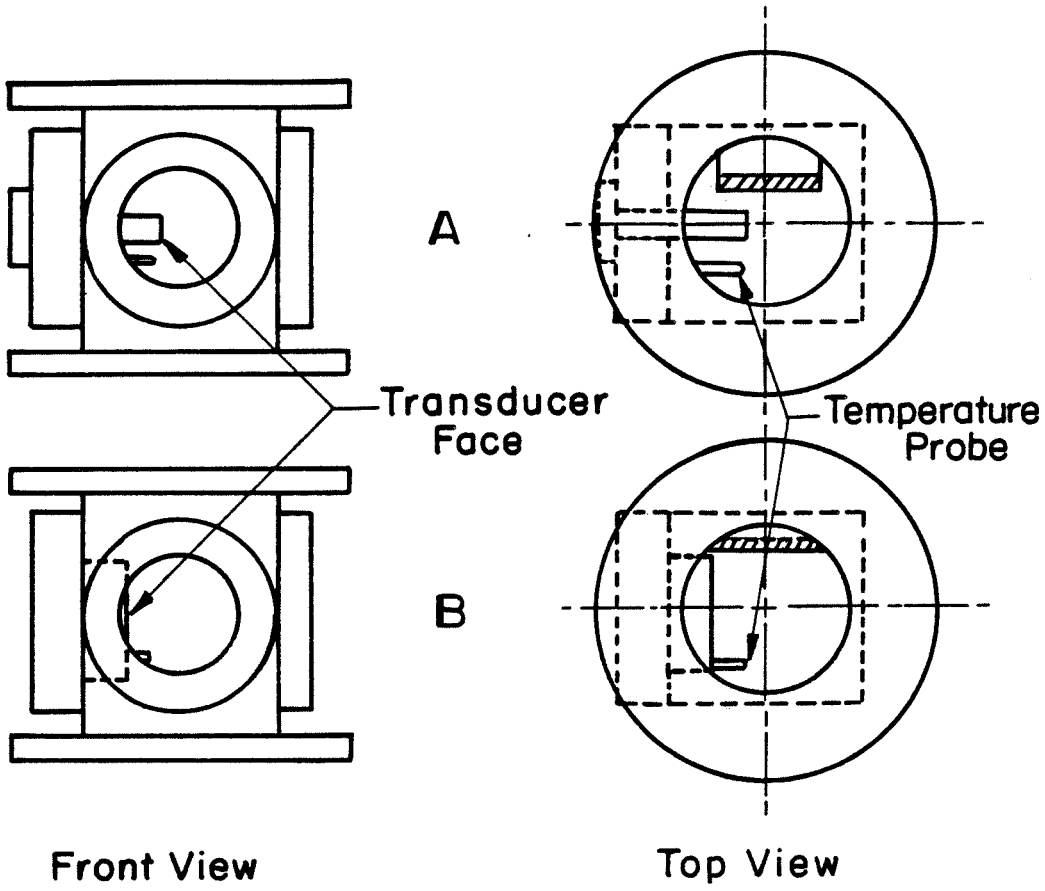

Figure 2.3 Transducer locations within test section

reflections within the test section. The contribution to the total recorded pressure from the secondary waves will be much less than that of the primary waves as a result of the intrinsic rapid decay in amplitude of a spherical acoustic wave with distance from the source. Configuration B is used to obtain information about the early stage of the explosion (the first 20 μsec) before any secondary waves reach the transducer.

The proximity of the transducer baffle to the exploding droplet has no discernible effect on the dynamics of the vapour bubble growth within the droplet. However, after the vapourization is complete and the vapour bubble has grown to a large size, in some cases it comes into contact with the transducer baffle. If

this occurs, the shape of the bubble as it collapses and oscillates is strongly affected by the presence of the baffle. The bubble behaviour under these circumstances is remniscent of the collapse of a cavitation bubble near a wall (see Appendix A). Thus, for the majority of photographs, the transducer baffle is located sufficiently far from the exploding drop to have no effect on the vapourization process.

The pressure signal detected by the transducer is recorded by a Nicolet 4094 digital oscilloscope, and stored on a 5¼" format floppy disk. The digital pressure data are then transferred via a GP-IB interface to a PDP 11/23 computer for data analysis and plotting.

The Nicolet oscilloscope has several convenient features that facilitate the triggering of the light source for photography. In particular, the threshold level for triggering can be displayed and adjusted while simultaneously viewing the live input signal. Secondly, when a triggering event occurs, a TTL-compatible pulse is generated at an external output. This pulse is used to trigger a Wavetek 50 MHz pulse generator which subsequently triggers the light source after a variable time delay. Finally, the "pretrigger" option on the oscilloscope allows a portion of the pressure signal to be saved that is detected prior to the occurrence of the triggering signal.

2.4. Photography

The large differences in the indices of refraction of the host liquid ($n_{20°C}$ = 1.47), the test fluids ($n_{20°C}$ = 1.33 - 1.36) and the test fluid vapour (n = 1.000) produce difficulties in photographing the vapour bubble within the liquid drop. If parallel back-illumination is used, the drop refracts the incoming light, causing the image of the drop to appear opaque and obscuring the details of the interior of the drop. The key to obtaining good pictures lies in the use of very diffuse back-illumination (Shepherd, 1981). An efficient opal glass diffuser is

used and is located as close as possible (about 15 mm) to the exploding droplet (see figure 2.4).

Figure 2.4 shows the photographic setup that is usually employed, although the camera to record the side-scattered light is not always used.

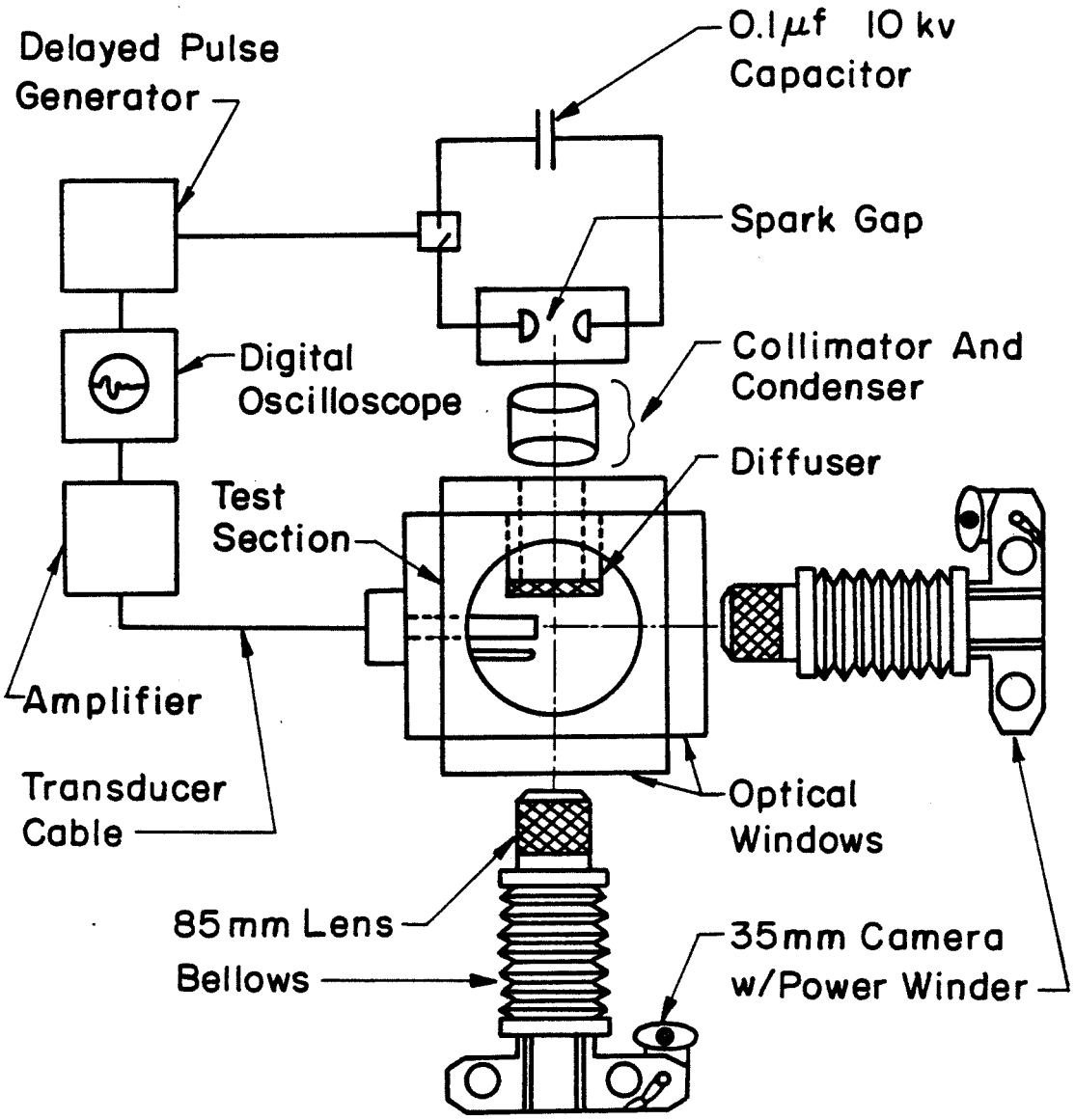

Figure 2.4 Photographic setup

Two Nikon FE2 35 mm cameras with 85 mm lenses and bellows attachments are used to obtain simultaneous, perpendicular views of a vapourizing drop. For the camera recording the back-lit view of the drop, an aperture setting of f/16 and a magnification of about 1.5 on the negative give the optimum trade-off between depth of field and resolution for the given amount of light available. The camera with the side-lit view receives much less light and it is necessary to open the aperture a further three stops to a setting of f/5.6, at the expense of depth of field, to obtain a satisfactory image with the same magnification. The light source used is a spark gap that produces a linear spark with a length of 7 mm and a typical duration of 1 μsec. The upper electrode is charged to 10 kV and the spark gap is triggered by applying a high voltage pulse to a small wire mounted concentric with the lower electrode. The electrodes are contained in a plexiglas enclosure that is filled with an Ar/Air (70%/30%) gas mixture. Kodak 400 ASA TRI-X film is used in both cameras. For the camera in line with the spark gap, the film is developed using HC-110 developer, while for the camera receiving only side-scattered light, the film is push-processed to 1600 ASA using an ultra-fine grain developer (DIAFINE).

The pressure signal that is detected by the transducer during the explosion of a droplet is used to trigger the electronic circuitry that sends a triggering pulse to the spark gap after a preset time delay. When the pulse arrives at the spark gap, after a short delay (usually less than 5 μsec), the spark gap fires. At this time the room lights are off, the camera shutters open, and the image of the evaporating droplet is recorded. The electromagnetic noise generated when the spark gap fires produces a sharp spike on the transducer pressure trace recorded by the oscilloscope. By measuring the time interval from the beginning of the pressure signal to the appearance of the spike, and adding the drop/transducer acoustic transit time, a time corresponding to each photograph can be determined. This is the time that is used to label the photographs

Table 2.1. Physical Properties of Glycerol

Property	Symbol	Value	Units
Melting temperature	T_{mp}	18	°C
Boiling temperature	T_{bp}	290	°C
Critical temperature	T_c	453	°C
Critical pressure	P_c	66	atm
Density (20°C)	ρ	1.26	g/cm^3
Specific Heat (20°C)	c_p	1.2	J/g°C
Thermal Conductivity (20°C)	k	2.6×10^{-3}	W/cm°C
Viscosity (20°C)	μ	1490	cP
(100°C)[1]		37	cP
(150°C)[1]		2.7	cP
Index of refraction (20°C)	n	1.475	
Sound speed (25°C)[2]	a	1904	m/s
(150°C)[2]		1629	m/s
Acoustic impedance (150°C)[3]	ρa	1.59×10^5	g/cm^{2}s

1. Estimated using the Andrade correlation (Reid et al., 1977)
2. From CRC Handbook of Chemistry and Physics
3. Density estimated from Rackett (1970)

discussed in the following chapters.

Table 2.2. Properties of Butane, Pentane and Isopentane

Property	Butane	Pentane	Isop.
Critical pressure P_c (atm)	38.0	33.7	33.8
Critical temperature T_c (°C)	156	196.5	187.3
Boiling temperature T_{bp} (°C)	-0.5	36.1	27.9
Superheat limit[1] T_{sl} (°C)	105.0	147.8	139
Liquid density (@ bp)[2] ρ_l (g/cm^3)	0.613	0.633	0.629
Vapour density (@ bp)[3] ρ_v (g/cm^3)	2.66×10^{-3}	2.91×10^{-3}	2.98×10^{-3}
Specific heat (@ bp)[4] c_p (J/g°C)	2.35	2.40	2.32
Latent heat (@ bp)[5] L (J/g)	385	357	339
Thermal diffusivity (@ bp) D (cm^2/s)	8.4×10^{-4}	7.3×10^{-4}	8.0×10^{-4}
Surface tension (@ bp)[6] σ (dyn/cm)	14.81	14.27	14.09
Jacob number (@ bp)[7] Ja	0.643	0.751	0.760

1. Measured values from Blander & Katz (1975)
2. Estimated using the Tyn and Calus Method (Reid et al., 1977)
3. Estimated using the Thompson correlation (Thompson & Sullivan, 1979)
4. Estimated using a corresponding-states method (Reid et al., 1977)
5. Estimated using the Chen Method (Reid et al., 1977)
6. Estimated using a corresponding-states method (Reid et al., 1977)
7. $Ja = c_p(T_{sl} - T_{bp})/L$

Table 2.3. Properties of Ethyl Ether and Acetone

Property	Ether	Acetone
Critical pressure P_c (atm)	36.4	46.4
Critical temperature T_c (°C)	193.6	235
Boiling temperature T_{bp} (°C)	34.6	56.3
Superheat limit[1] T_{sl} (°C)	147	174
Liquid density (@ bp)[2] ρ_l (g/cm^3)	0.709	0.822
Vapour density (@ bp)[3] ρ_v (g/cm^3)	3.12×10^{-3}	2.54×10^{-3}
Specific heat (@ bp)[4] c_p (J/g°C)	2.24	2.28
Latent heat (@ bp)[5] L (J/g)	358	513
Thermal diffusivity (@ bp) D (cm^2/s)	7.7×10^{-4}	8.4×10^{-4}
Surface tension (@ bp)[6] σ (dyn/cm)	15.30	19.93
Jacob number (@ bp)[7] Ja	0.703	0.522
Sound speed (@ T_{sl})[8] a (m/s)	391	504
Acoustic impedance (@ T_{sl})[9] ρa (g/cm^{2}s)	2.07×10^4	3.11×10^4

1. Measured values from Blander & Katz (1975)
2. Estimated using the Tyn and Calus Method (Reid et al., 1977)
3. Estimated using the Thompson correlation (Thompson & Sullivan, 1979)
4. Estimated using a corresponding-states method (Reid et al., 1977)
5. Estimated using the Chen Method (Reid et al., 1977)
6. Estimated using a corresponding-states method (Reid et al., 1977)
7. $Ja = c_p(T_{sl} - T_{bp})/L$
8. From CRC Handbook of Chemistry & Physics
9. Density estimated from Rackett (1970)

Chapter 3

EXPERIMENTAL RESULTS AT ATMOSPHERIC PRESSURE

3.1. Introduction

In this chapter experiments are reported whose purpose was to determine (i) whether the evaporative instability discovered by Shepherd & Sturtevant (1982) in butane is found in other liquids, and (ii) the generality of the wide range of phenomena they observed earlier during the explosive boiling of a droplet. This chapter presents a selection of photographs and pressure traces that provides a survey of the various physical processes that are observed to occur during the vapourization of a highly superheated droplet at atmospheric pressure. The effects of ambient pressure on the dynamics of rapid vapourization are considered in the next chapter. It will be shown that by varying the ambient pressure the onset of the instability on the evaporating interface can be delayed substantially, a feature that can effectively be used to elucidate a great deal more about the physics of vapour explosions.

To investigate the occurrence of the instability in other fluids, three different fluids are studied at atmospheric pressure in the current investigation: pentane, isopentane, and ethyl ether. The interfacial instability, which develops on the surface of the vapour bubble growing within a drop, occurs in each fluid and substantially enhances the vapourization rate. Similar repeatable, dynamical effects are observed in each case. In this chapter a series of detailed photographs is used to document the behaviour of unstable boiling at atmospheric pressure. The results are organized to illustrate (i) the onset of the instability, (ii) the unstable growth of the vapour bubble within a drop, (iii) the structure of the nonevaporating bubble surface and evaporating interface, and (iv) the

subsequent behaviour of the vapour bubble after the completion of vapourization.

3.2. Onset of the Instability at Atmospheric Pressure

Figure 3.1 shows a series of photographs taken at early times during the explosive vapourization of ether droplets (with typical diameters of 1-2 mm) at atmospheric pressure. The time listed below each drop is the elapsed time since the pressure wave first left the drop. The drops are shown immersed in glycerol, which appears light grey or white in the photographs. Each picture depicts the vapourization of a different drop; the nucleation of the vapour bubble occurs at random asymmetric locations within the drops, always rather close to the drop boundary.

From the photographs alone, it is impossible to show definitely that the vapour bubble nucleates inside the drop (homogeneous nucleation) rather than on the surface of the drop (heterogeneous nucleation). The location where nucleation occurs for a drop immersed in a host fluid is a function of the surface tensions of the test and host fluids and the interfacial tension between the two fluids. The vapour nucleus will form in a configuration that requires the least energy to generate the new surface. Jarvis et al. (1975) investigated the various mechanisms of bubble nucleation, theoretically and experimentally, and concluded that homogeneous nucleation occurs for droplets of n-pentane immersed in ethylene glycol. The surface tensions of pentane, isopentane and ether are comparable (see tables 2.2 and 2.3) and the surface tension of ethylene glycol is close enough to that of glycerol to suggest that the same conclusion holds in the present experiments. The observation that the droplets always explode at, or very close to the superheat limit is also a good indication that homogeneous nucleation occurs. So in summary, the evidence is strong that the vapour nucleus forms inside the drop near the surface, grows, and

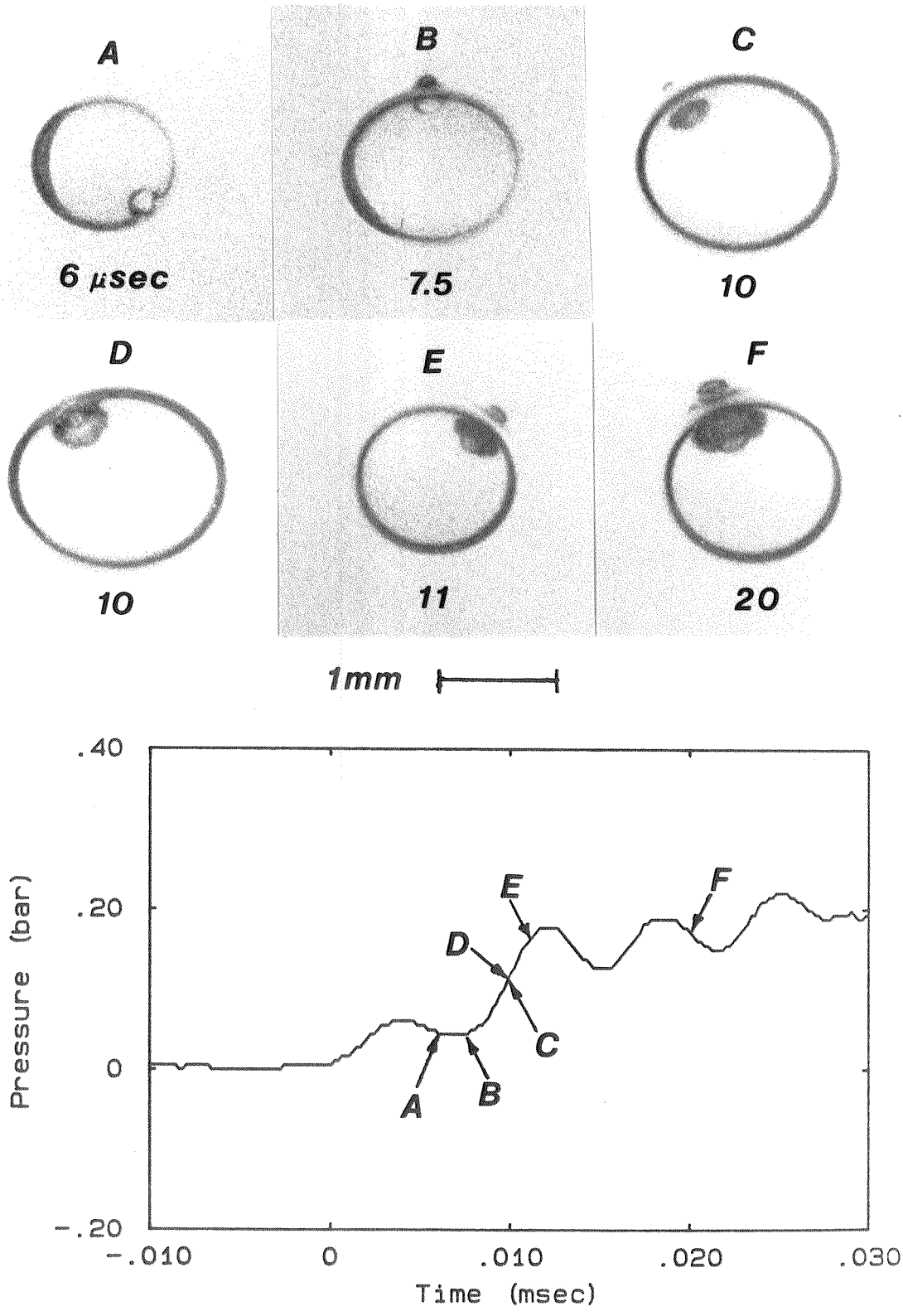

Figure 3.1 Onset of the instability in ether at atmospheric pressure

comes into contact with the drop surface after a short period of time (typically less than 6 μsec).

In each photograph in figure 3.1, the vapour bubble has grown large enough to contact the surface of the drop. The impact of the growing bubble with the drop surface produces a protrusion of the nonevaporating part of the bubble into the host fluid. Drops *A* and *B* contain vapour bubbles that appear transparent and have smooth surfaces. At some time between photographs *B* and *C* a small-scale roughness develops on the bubble surface. This surface instability appears to be initiated near the line of contact between the evaporating bubble surface and the hot host fluid. The contact between the vapour bubble and the host fluid plays a role in the onset of the instability but in some cases (e.g., at high pressure) it is not sufficient to initiate unstable boiling. A large *pre-instability* mass flux across the evaporating surface must also be present. In the next chapter it will be shown that by increasing the ambient pressure, and thereby decreasing the bubble growth rate and evaporative mass flux, it is possible to suppress the onset of the instability altogether.

After the vapour bubble contacts the bubble surface, unstable heterogeneous nucleation spreads out on the surface of the droplet while the vapour bubble continues to grow towards the centre of the droplet. This dual character of the vapourization near the edge of the droplet at early times is clearly exhibited in figure 3.2. The photograph of the pentane drop was taken 10 μsec after the initial nucleation. The vapour bubble nucleated on the side of the drop away from the viewer so that the evaporating interface is viewed through the drop. The bubble appears to be embedded in a patch of vapour that spreads out away from the bubble near the drop surface. The rough surface of this region surrounding the bubble indicates rapid unstable boiling. At this stage of bubble growth, the cooling effect of vapourization causes the temperature of the liquid

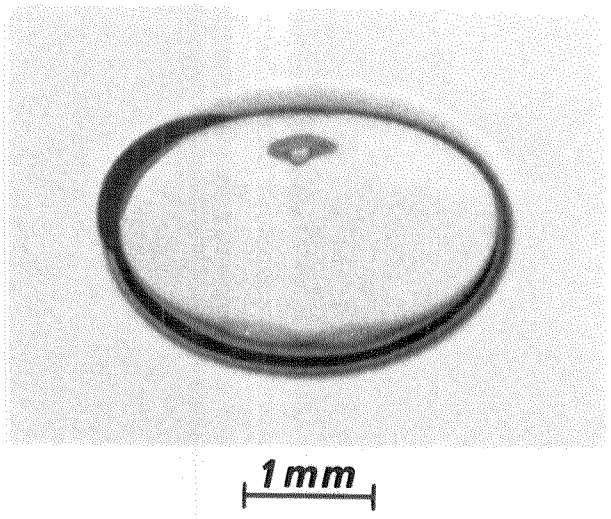

Figure 3.2 Early stage of vapourization in pentane at atmospheric pressure

at the smooth bubble surface to be near the saturation temperature, substantially lower than that of the nearby host fluid (see Appendix B). The large temperature gradients near the bubble imply large gradients in surface tension. The surface tension of the pentane near the drop edge (at the superheat limit temperature) is lower (by more than a factor of 4, 14.3 dyn/cm to 3.3 dyn/cm) than that of the liquid at the bubble surface (approximately at the saturation temperature) within the drop. It is plausible that the relatively lower surface tension at the drop edge promotes the spreading of unstable boiling along the surface of the drop.

After the onset of the instability, disturbances develop on the initially smooth evaporating surface within the drop, substantially enhancing the vapourization rate. The small-scale surface distortions refract incoming light and cause the vapour region to appear opaque in the photographs. In photographs E and F of figure 3.1 the central portion of the evaporating interface appears to have a smoother surface than the outer part of the interface that is closer to the edge of the drop. This small nonuniformity is presumably a remnant of the initial

smooth growth of the vapour bubble. This feature is not evident at later times, when the small-scale perturbations appear uniformly distributed across the evaporating surface.

Each exploding droplet produces a pressure field that is characteristic of the growth of the vapour bubble within the drop. The pressure trace shown below the photographs in figure 3.1 is the overpressure measured by the pressure transducer a short distance (9 mm) away from an exploding droplet of ether with a diameter of 1.3 mm. The first two pressure peaks are remarkably repeatable from one explosion to the next. The first pressure pulse, which peaks after about 4 μsec, is a result of the blast wave produced by the initial nucleation and growth of the smooth vapour bubble. The sudden pressure rise after about 8 μsec coincides with the onset of the instability and an increase in the vapourization rate. The subsequent small-scale pressure oscillations are probably due to the reverberations within the drop of the compression wave generated by the initiation of unstable bubble growth. The large difference in the acoustic impedances of glycerol and ether (see tables 2.1 and 2.3) causes a portion of the acoustic wave incident on the ether/glycerol interface to be reflected back into the drop. The fact that the round-trip acoustic transit time (about 6.5 μsec) matches the period of the pressure perturbations supports the above hypothesis.

3.3. Unstable Vapour Bubble Growth

After the onset of the instability, the vapour bubble grows rapidly, consuming the liquid within the drop. An overview of the unstable vapourization process and a discussion of the pressure field generated by the explosion will now be given.

3.3.1. *Overview of Bubble Growth.* Figure 3.3 shows a series of photographs of droplets of ether illustrating the growth of the vapour region after the onset of the instability. A number of repeatable features are evident from these photographs, the most important of which is the small-scale roughness on the evaporative liquid-vapour interface. The opaqueness of the bubble prevents a direct observation of the unstable boiling process at the evaporating interface. The rough surface of the vapour bubble is quite different from that observed in boiling liquids at lower superheats, where the bubble surface usually has a smooth, glassy appearance. The instability that distorts the evaporating surface appears in the earliest pictures shown here and persists at a nearly constant amplitude during the vapourization of the drop. After the vapour bubble comes into contact with the host fluid, a portion of the bubble surface becomes nonevaporating. This evaporatively dormant surface exhibits a considerable amount of small-scale structure.

Another feature of the bubble growth is a characteristic bulging into the host fluid that is observed in each case when the initial bubble has grown large enough to contact the boundary of the drop. In figure 3.3, the photographs taken at 31, 44 and 65 μsec show views of the evaporating surface and the smooth cap structure in profile. In the drop photographed after 58 μsec, the orientation of the protrusion is towards the viewer. The final photograph in the figure was taken after the liquid in the drop has completely evaporated. The smooth portion of the bubble surface is the remnant of the cap structure that was formed during the unstable boiling.

3.3.2. *Pressure Signals.* Figure 3.4 shows a typical pressure trace recorded for each exploding droplet shown in figure 3.3. The overall shape of the pressure trace is repeatable, although the small-scale structure varies from one explosion to the next. After nucleation and the onset of the instability, the pressure

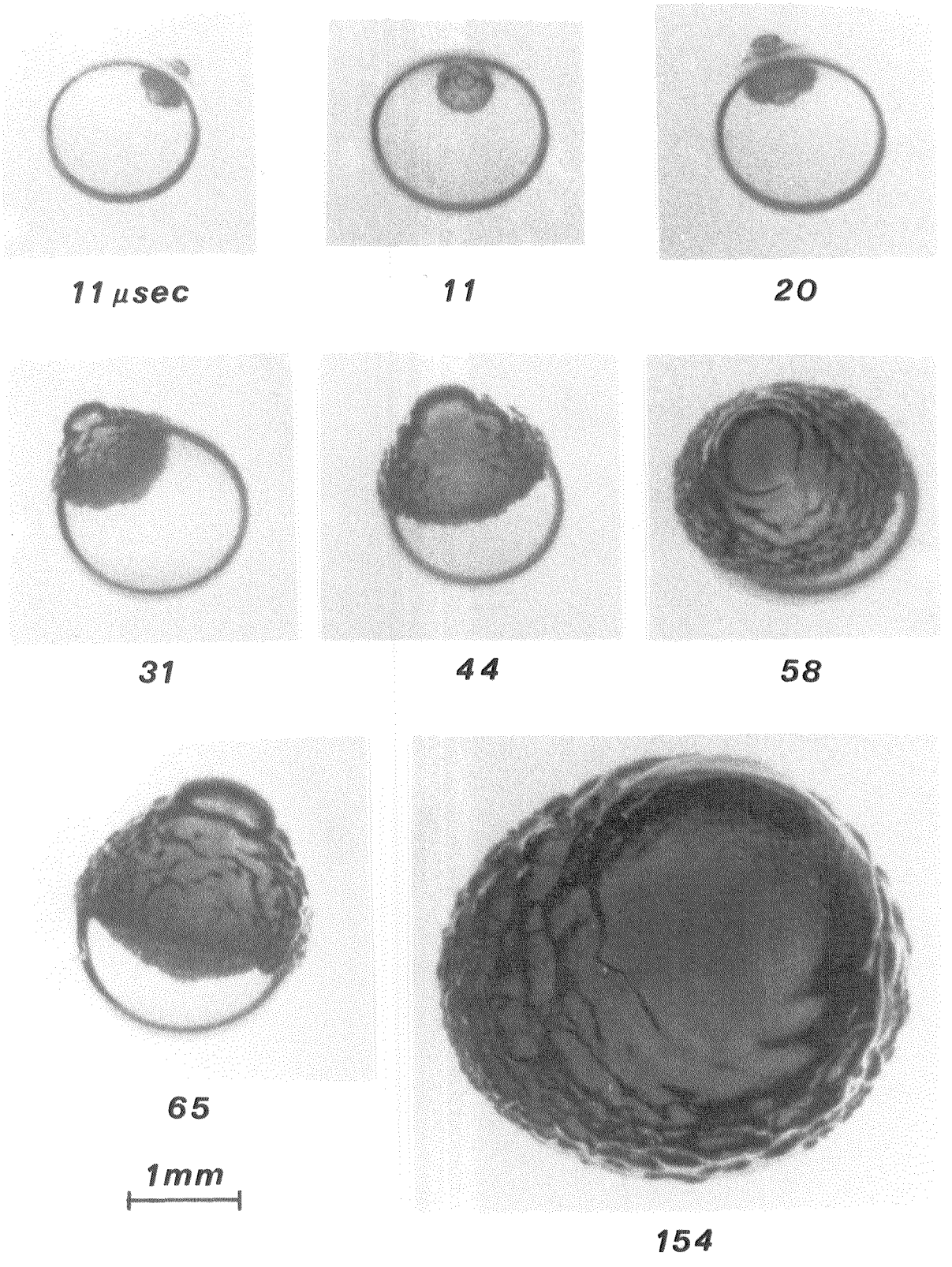

Figure 3.3 Bubble growth in ether droplets at atmospheric pressure

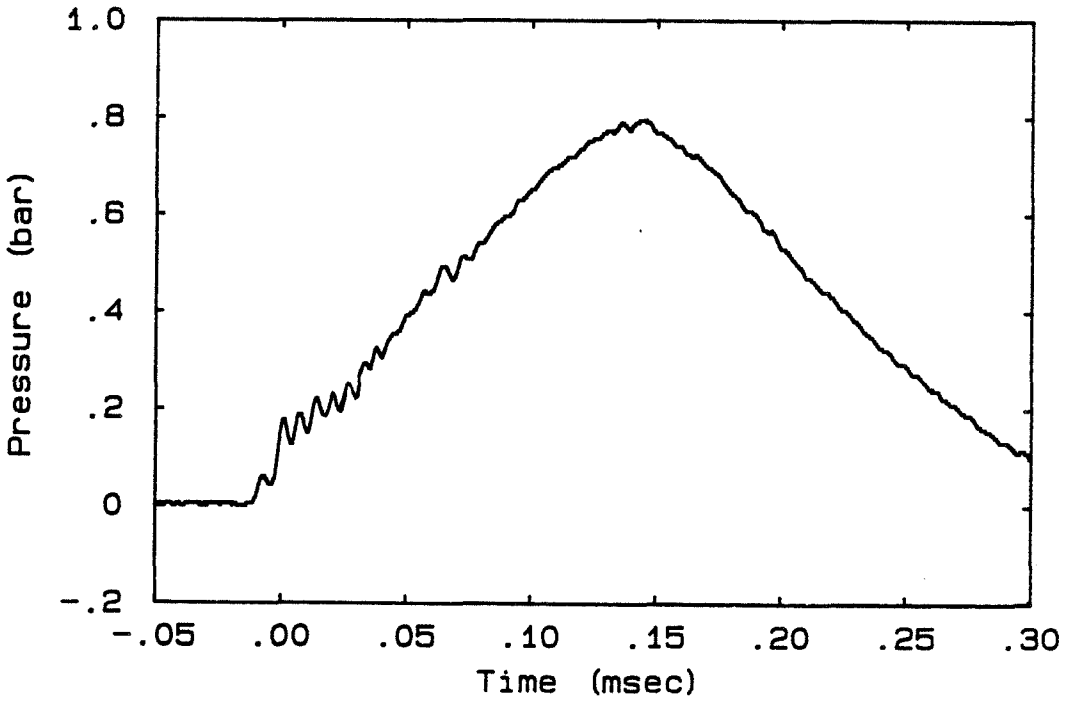

Figure 3.4 Pressure trace for an exploding ether droplet

increases roughly linearly. The effective radius of the vapour region also grows linearly (Shepherd & Sturtevant, 1982). During this quasi-steady unstable boiling period, the growing vapour bubble acts like an expanding volume source and radiates compression waves. The pressure reaches a maximum (after about 150 μsec for a 1.3 mm diameter drop) when the liquid in the drop is completely vapourized. The overpressure within the bubble and the radial motion of the liquid surrounding it cause the bubble to continue to grow and overshoot its equilibrium radius. Further expansion relieves the overpressure and the radial bubble growth is retarded. The decelerating bubble radiates expansion waves and the pressure recorded by the transducer falls, as shown in figure 3.4.

Well-defined small-scale pressure oscillations are observed on the initial portion of each of the pressure traces recorded at atmospheric pressure. The oscillations persist typically for several cycles before they decay and are replaced by random small-scale pressure fluctuations. Changes in the drop-transducer

orientation and the random location of the bubble within the drop lead to variations in the detailed structure of the pressure trace from one explosion to the next. Factors that produce systematic differences between the pressure traces include variations in the drop diameter and drop-transducer distance.

Figure 3.5 shows a pressure trace in which the early pressure oscillations have a particularly large amplitude and persist for at least 80 μsec. This pressure trace was generated by the explosion of a 1.7 mm diameter drop of isopentane located 4 mm away from the transducer baffle. The photograph of the drop was taken 40 μsec after the initial pressure wave left the drop. The proximity of the drop to the transducer baffle shown in the photograph, and the specific orientation of the vapour region in the drop with respect to the transducer both contribute to the large pressure amplitude recorded. The time interval between successive pressure minima from the pressure trace is plotted as a function of time in figure 3.6. The frequency of the small-scale pressure oscillations increases with time as the drop evaporates. This behaviour supports the earlier hypothesis that the oscillations are caused by the reverberations within the drop of the blast wave generated by the onset of the instability. As the liquid within the drop evaporates, the round-trip transit time for an acoustic wave within the drop will subsequently decrease. The transit time should go to zero when the liquid in the drop is completely evaporated. In fact, if the data in figure 3.6 are extrapolated, the oscillation period goes to zero at roughly the same time as the pressure trace in figure 3.5 reaches a maximum which corresponds to the completion of the evaporation.

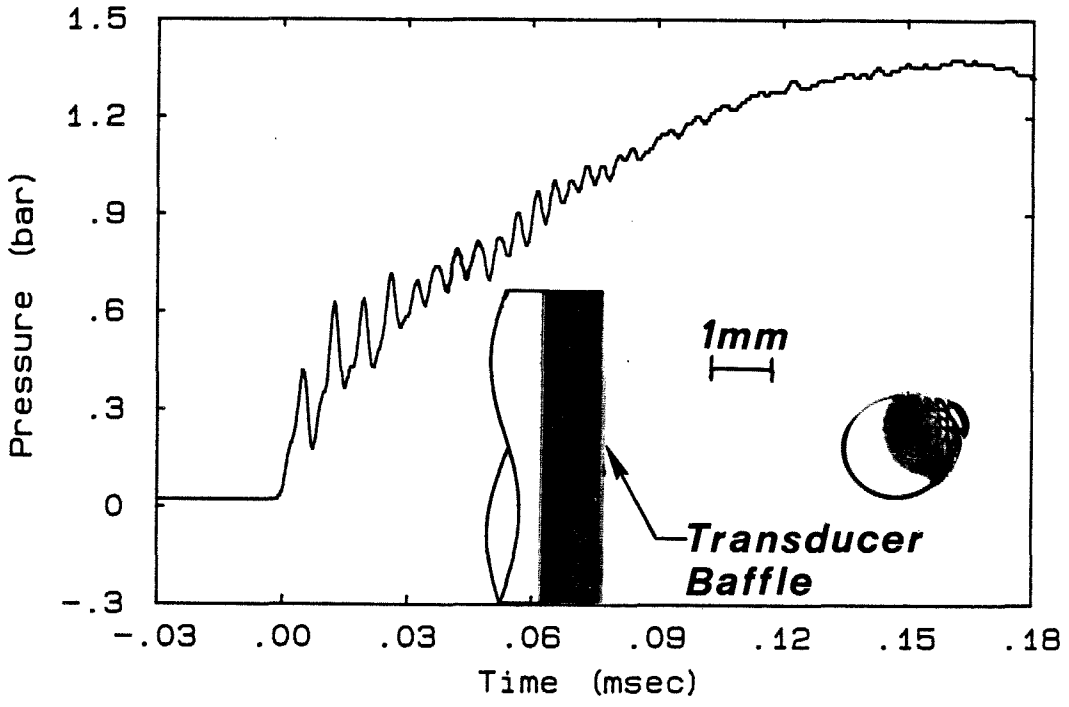

Figure 3.5 Radiated pressure field from an isopentane drop

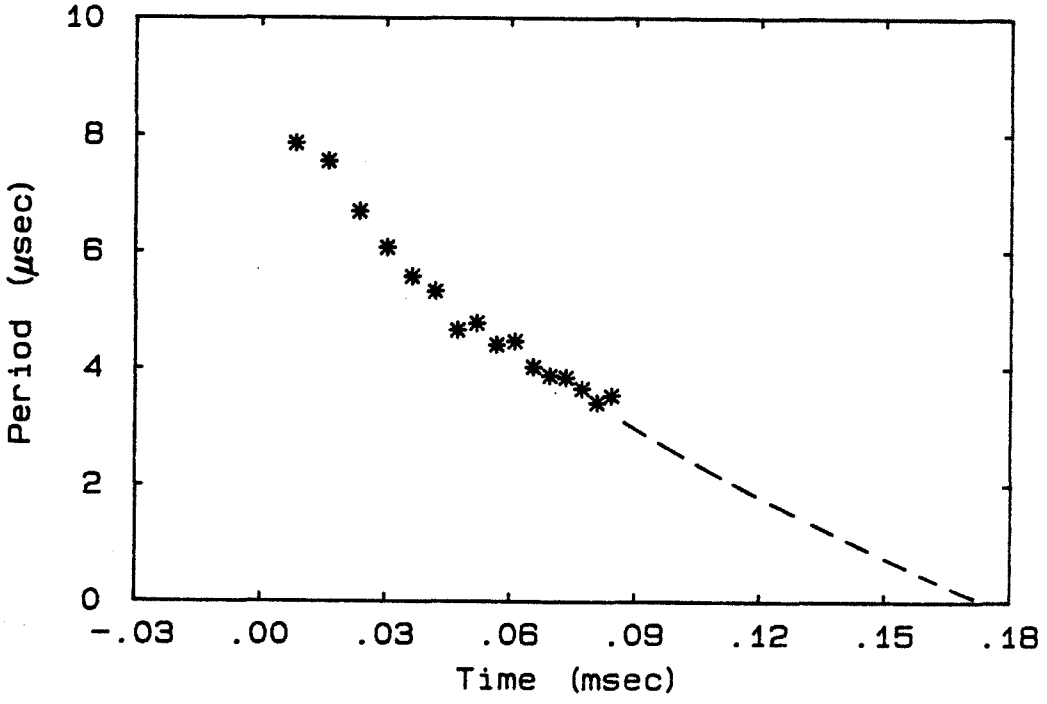

Figure 3.6 Variation of the period of small-scale pressure oscillations in figure 3.5 (- - -, extrapolation)

3.4. Structure of the Unstable Evaporating Interface

The structure of the evaporating interface plays an important role in the dynamics of bubble growth. By distorting the interface and increasing the surface area available for evaporation, the presence of the instability causes a substantial increase in the vapourization rate. After the initial development of the instability, the growth of the disturbances becomes nonlinear, saturates, and the amplitude remains roughly constant during the evaporation of the drop. The evaporating surface is only visible in certain photographs, depending on the orientation of the initial nucleation. Figure 3.7 shows a drop of isopentane that is nearly completely vapourized.

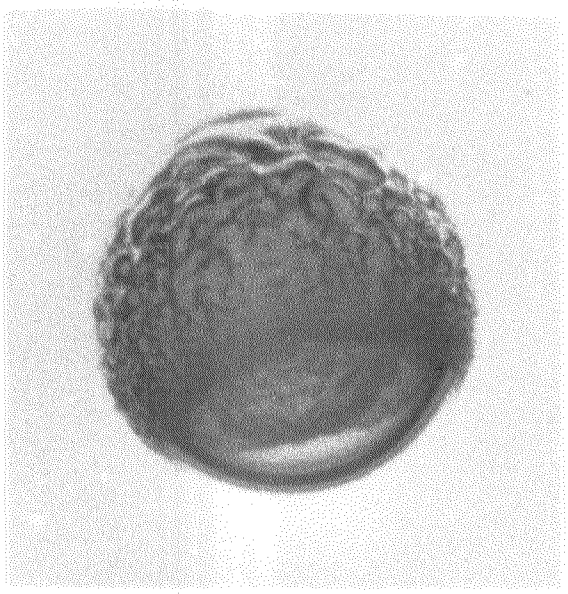

Figure 3.7 View of the evaporating interface in a 2.4 mm diameter drop of isopentane

The drop has been evaporating for 94 μsec, and only the lower portion of the drop remains liquid. Subject to the "fish-eye" lensing effect of the remaining liquid, it is possible to see up inside the drop and view the perturbations on the evaporating surface. The portion of the liquid-vapour interface in view has a regularly wrinkled appearance.

Figure 3.8 shows a series of photographs of isopentane drops in which the initial vapour bubble and subsequent cap structure have formed on the side of the drop *away* from the viewer.

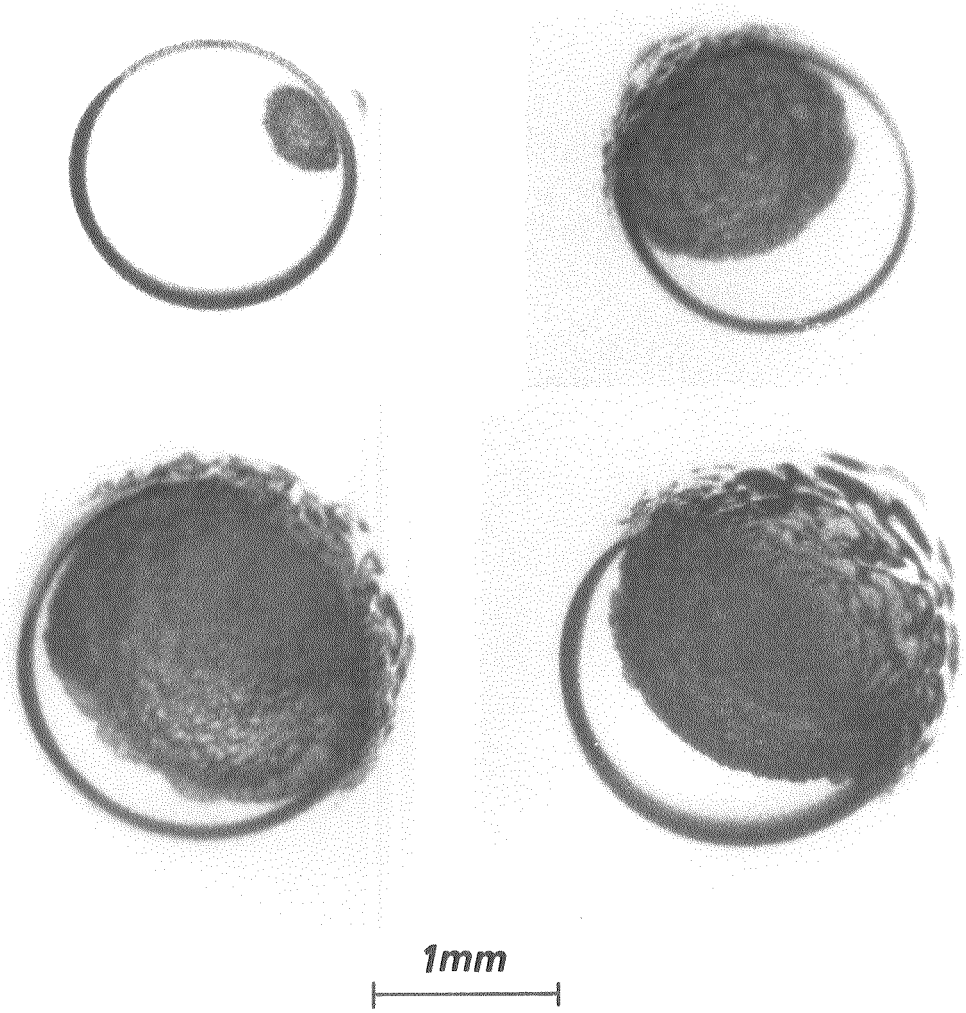

Figure 3.8 The active evaporating surface of isopentane vapourizing at atmospheric pressure viewed from below at 11, 43, 67, and 67 μsec, respectively

As a result, the scale of the perturbations on the evaporating surface may be observed. Although the roughening appears random in orientation and many length scales are present, the length scale of the smallest perturbations appears to remain roughly constant throughout the evaporation process. This

observation will be relevant later in the discussion of the theoretical models for the instability. Figure 3.9 contains an enlargement of the third photograph in figure 3.8 and shows that the length scale of the disturbances visible on the lower portion of the evaporating surface is on the order of 100 μm.

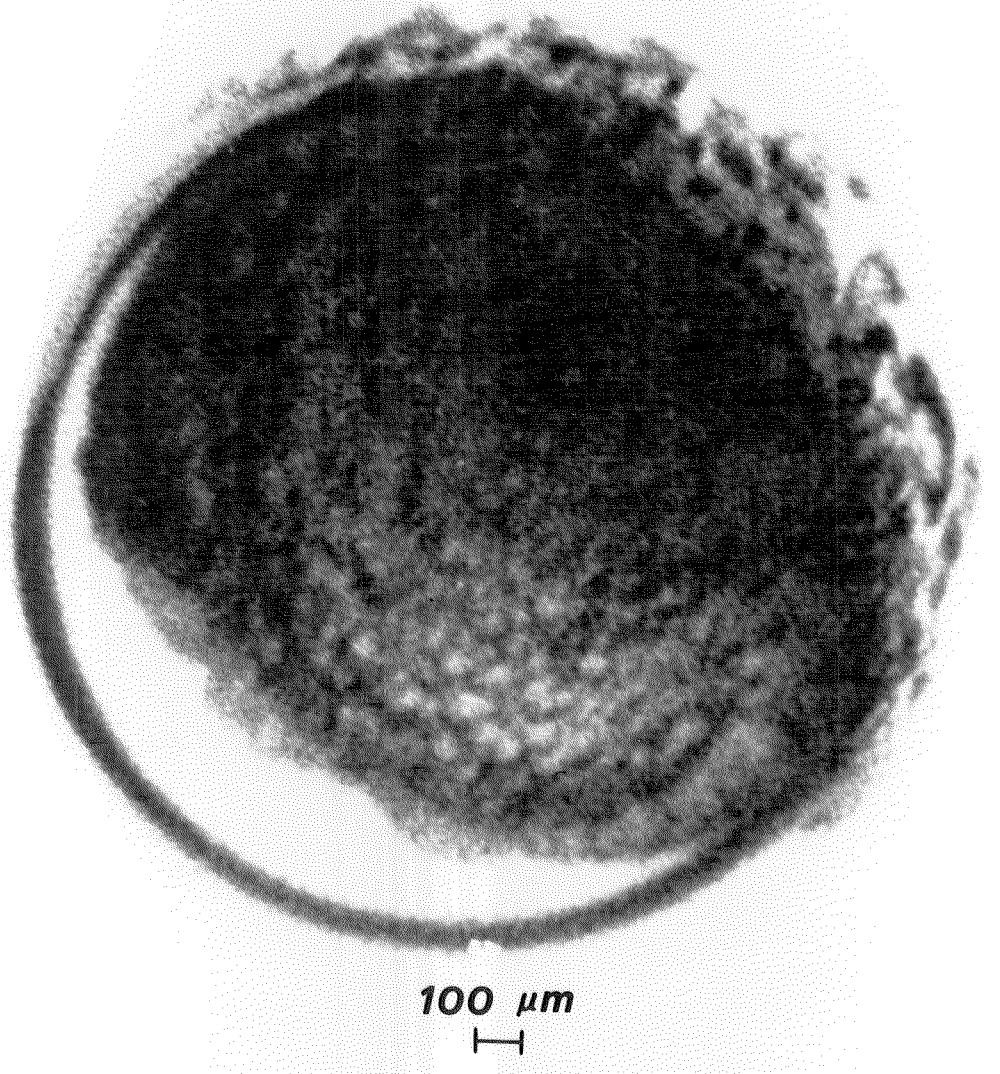

Figure 3.9 Small-scale disturbances on the evaporating surface within an isopentane droplet

The evaporating surface has a similar appearance in the other liquids tested. For example, figure 3.10 shows an oblique view of the evaporating surface in a

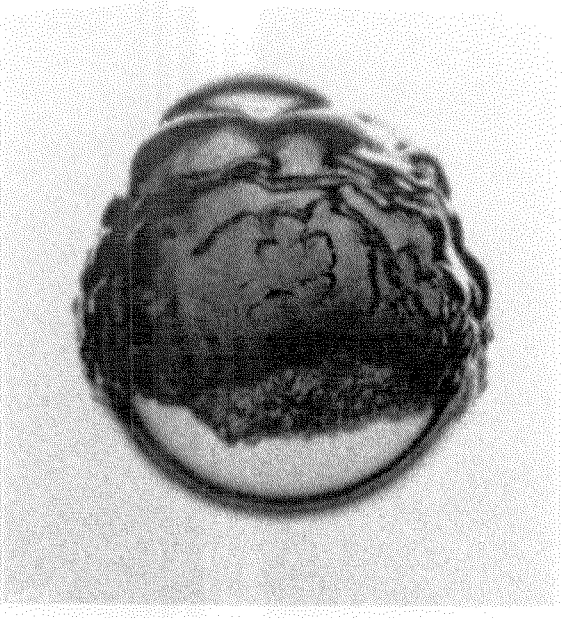

Figure 3.10 Oblique view of the evaporating interface in a 2.5 mm diameter drop of butane

partially vapourized drop of butane. Once again the length scale of the smallest perturbations is on the order of 50-100 μm.

3.5. Structure of the Bubble Surface

The nonevaporating portion of the vapour bubble that is in contact with the host fluid displays a considerable amount of small-scale structure. This surface structure is a remnant of the contact between the highly distorted evaporating interface and the host fluid, but it is, in addition, subject to the smoothing effects of surface-wave propagation. The surface perturbations persist even after the drop is completely vapourized. Figure 3.11 shows two completely vapourized drops of ether photographed after 154 μsec and 182 μsec, respectively. Both photographs exhibit a gradation in length scale of the structure on the surface of the bubbles. The most recently formed surface, for example near the bottom of bubble *A*, has the smallest scale, whereas the *older* surface structure at the top of the bubble has a larger scale, presumably due to surface-wave

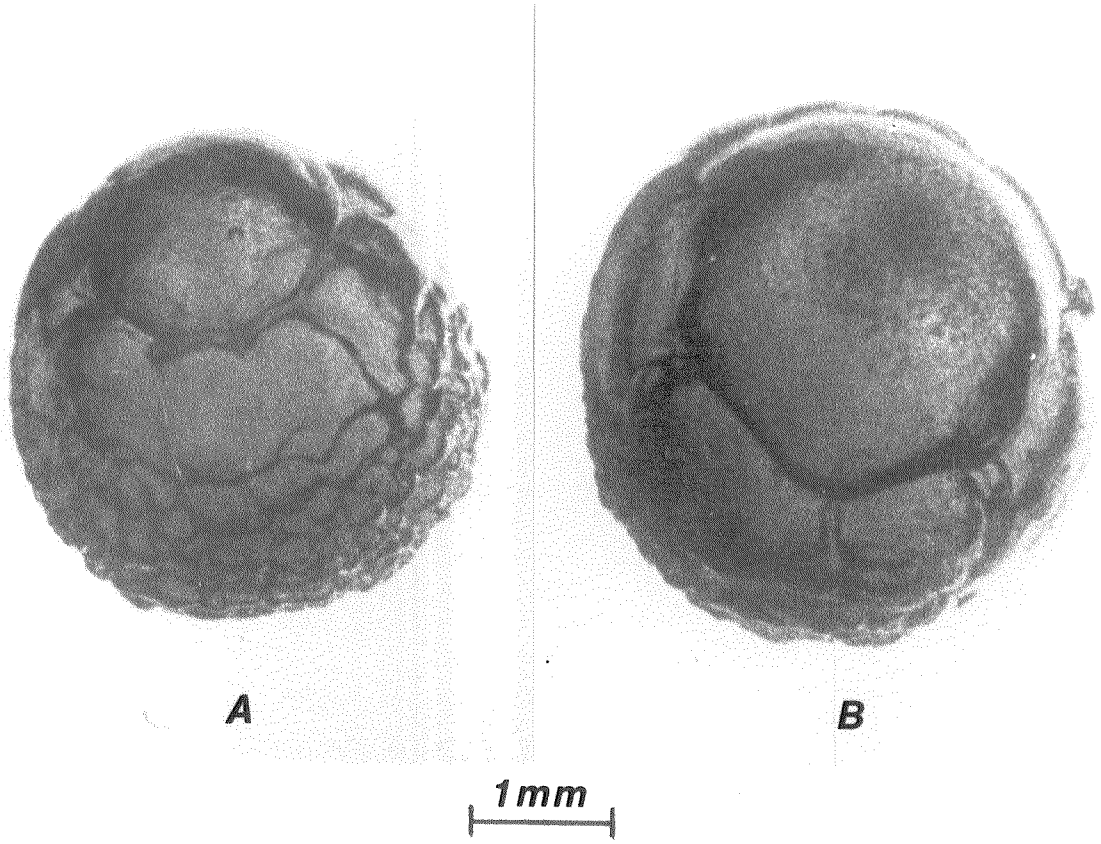

Figure 3.11 Bubble surface structure on fully vapourized drops of ether spreading.

The hemispherical cap structure visible on the upper portion of each bubble in figure 3.11 is a remnant of the smooth protrusion that was observed at earlier times in the photographs in figure 3.3. This characteristic bulging of the vapour bubble into the host fluid was observed in butane by Shepherd & Sturtevant (1982) and occurs in all three liquids photographed at atmospheric pressure in the present experiments (see figure 3.12). Shepherd & Sturtevant (1982) conjectured that the protrusion and associated circumferential waves are both driven by a vapour jet that is generated at the evaporating surface and impinges on the opposing bubble surface. They also speculated that a substantial amount of liquid may be torn from the liquid-vapour interface during the time when the

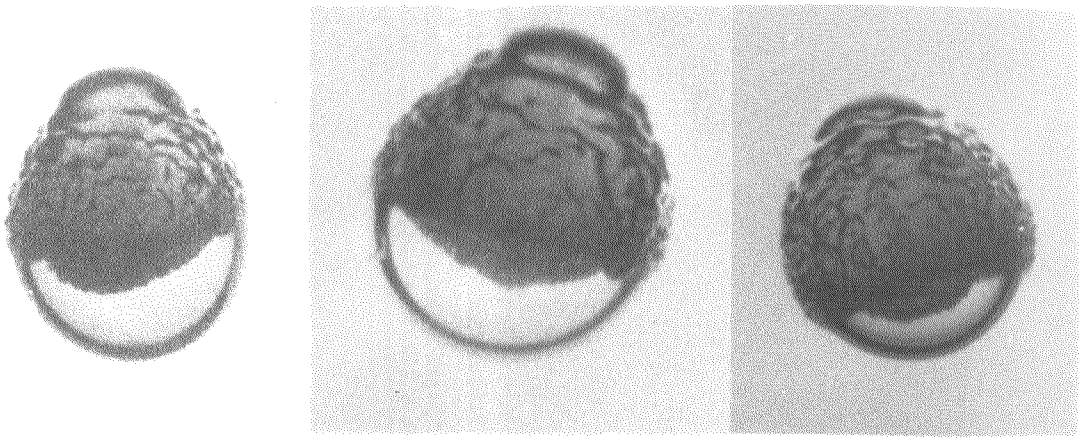

Figure 3.12 Smooth cap structure on drops exploding at atmospheric pressure. Drop diameters; pentane, 2.0 mm; ether, 2.0 mm; isopentane, 2.5 mm.

mass flux across the interface is at a maximum. In the present work, direct evidence of the existence of a two-phase evaporative jet during unstable boiling has been obtained and will be presented in the next chapter. It will also be shown that the last portion of liquid to vapourize in a drop boils in a particularly violent fashion as a result of additional heating by the host fluid. At this late stage, the drops torn from the evaporating surface may be large enough to remain intact and splatter on the opposite side of the bubble. Judging by the smooth appearance of the caps in figure 3.12, at early times the liquid particles in the jet are small enough that they evaporate before reaching the host fluid.

Figure 3.13 shows a sequence of photographs of isopentane drops evaporating at atmospheric pressure together with a characteristic pressure trace. A small amount of liquid remains in the lower portion of the drop in photograph *A*. The remaining photographs document the subsequent expansion of the vapour bubble and corresponding changes in the bubble surface structure. The smooth cap visible near the top of each bubble grows in size with time as the surface waves

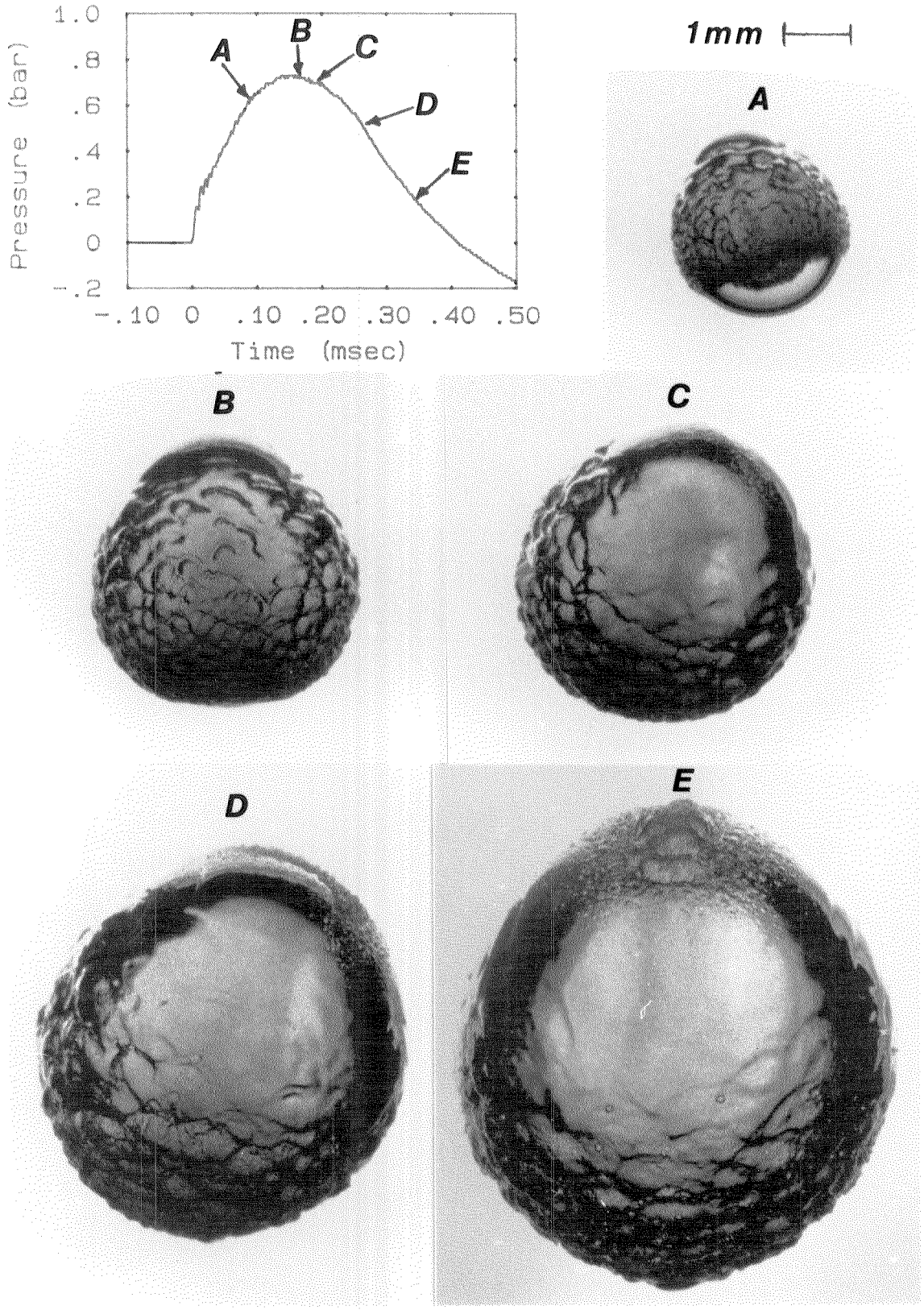

Figure 3.13 Structure of the bubble surface for isopentane drops exploding at atmospheric pressure

spread and decay in amplitude. Of particular interest is the small-scale roughness that first appears in photograph *C* on the otherwise smooth remnant cap. This splattered appearance becomes more prominent at later times and by photograph *E* a significant cratering of the surface has occurred. This surface disturbance is caused by small liquid droplets torn from the evaporating surface that survive the flight across the inside of the bubble to impact the hot host fluid and vapourize in a spray of micro-explosions. The velocity of the particles ejected from the evaporating surface (estimated to be approximately 50 m/s in the next chapter) is larger than the growth rate of the bubble so the spray contacts the bubble surface before the bubble stops expanding.

3.6. Bubble Collapse and Oscillation

After a drop is completely vapourized the bubble continues to expand (see figure 3.11 for example) as a result of the overpressure within the bubble and kinetic energy stored in the outward radial motion of the liquid surrounding the bubble. The pressure within the bubble falls below the ambient pressure causing the bubble to slow its expansion and ultimately collapse and oscillate violently on a millisecond time scale. Figure 3.14 shows the characteristic behaviour of the far-field radiated pressure during bubble oscillation. The pressure rises sharply and reaches a maximum when the vapourization of the liquid in the drop is completed. The pressure decreases to a broad minimum as the bubble reaches its maximum radius. The bubble then collapses causing the radiated pressure to rise and reach a maximum when the bubble reaches its minimum radius. The bubble rebounds and the process repeats itself.

The points on the pressure trace in figure 3.14 labelled *A* and *B* correspond to the times for the two photographs shown in figure 3.15. Photograph *A* shows an ether bubble shortly after it has started to collapse. Disturbances have begun to distort the bubble surface from its initial spherical shape. When the bubble

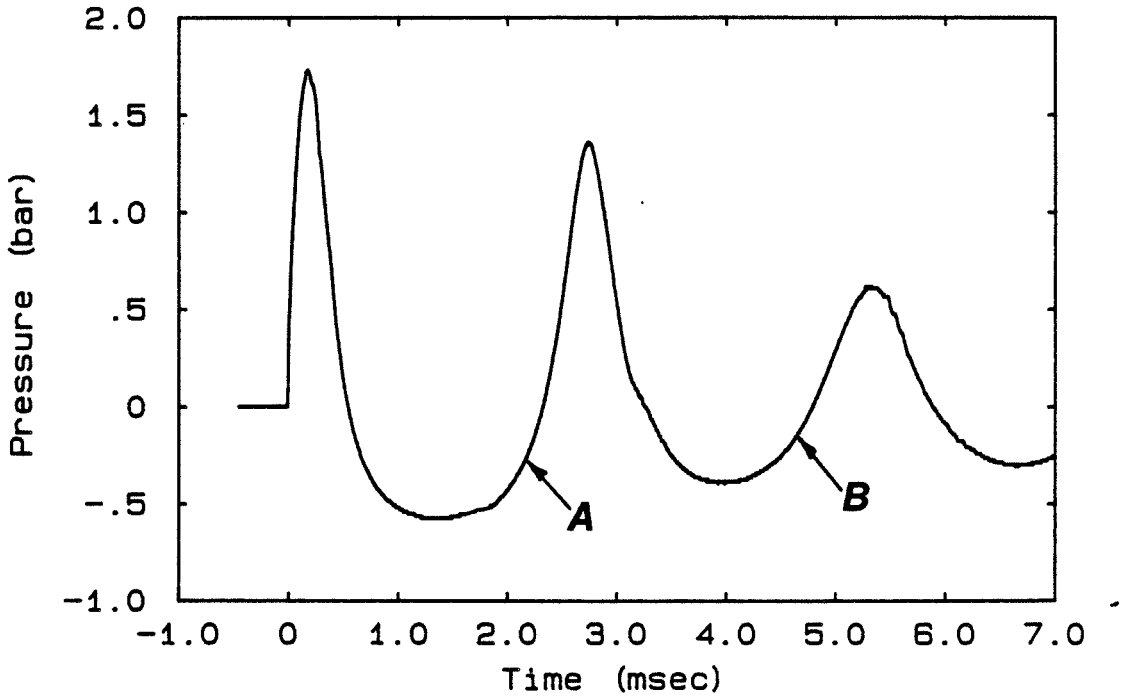

Figure 3.14 Long time behaviour of pressure radiated from exploding and oscillating drop of ether. (*A* and *B* refer to the photographs in figure 3.15)

reaches its minimum radius and rebounds the bubble surface is subject to tremendous radial accelerations (estimated to be on the order of $10^4 g$ by Shepherd & Sturtevant, 1982), and the surface breaks up subject to the Rayleigh-Taylor instability (Taylor, 1950). The isopentane bubble in photograph *B* was photographed during the second collapse of the bubble and illustrates the extent of the surface deformation after only one bubble oscillation cycle. The distortions grow as the bubble continues to oscillate and eventually the surface breaks up into a cloud of small bubbles. The amplitude of the radiated pressure signal decays as the energy contained in the radial bubble motion is dissipated. However, the frequency of the pressure oscillation remains remarkably constant even after the break-up of the bubble, indicating that the cloud of small bubbles that is formed oscillates effectively like one bubble. The collapse and oscillation of butane bubbles has been well documented by Shepherd (1981) and nothing

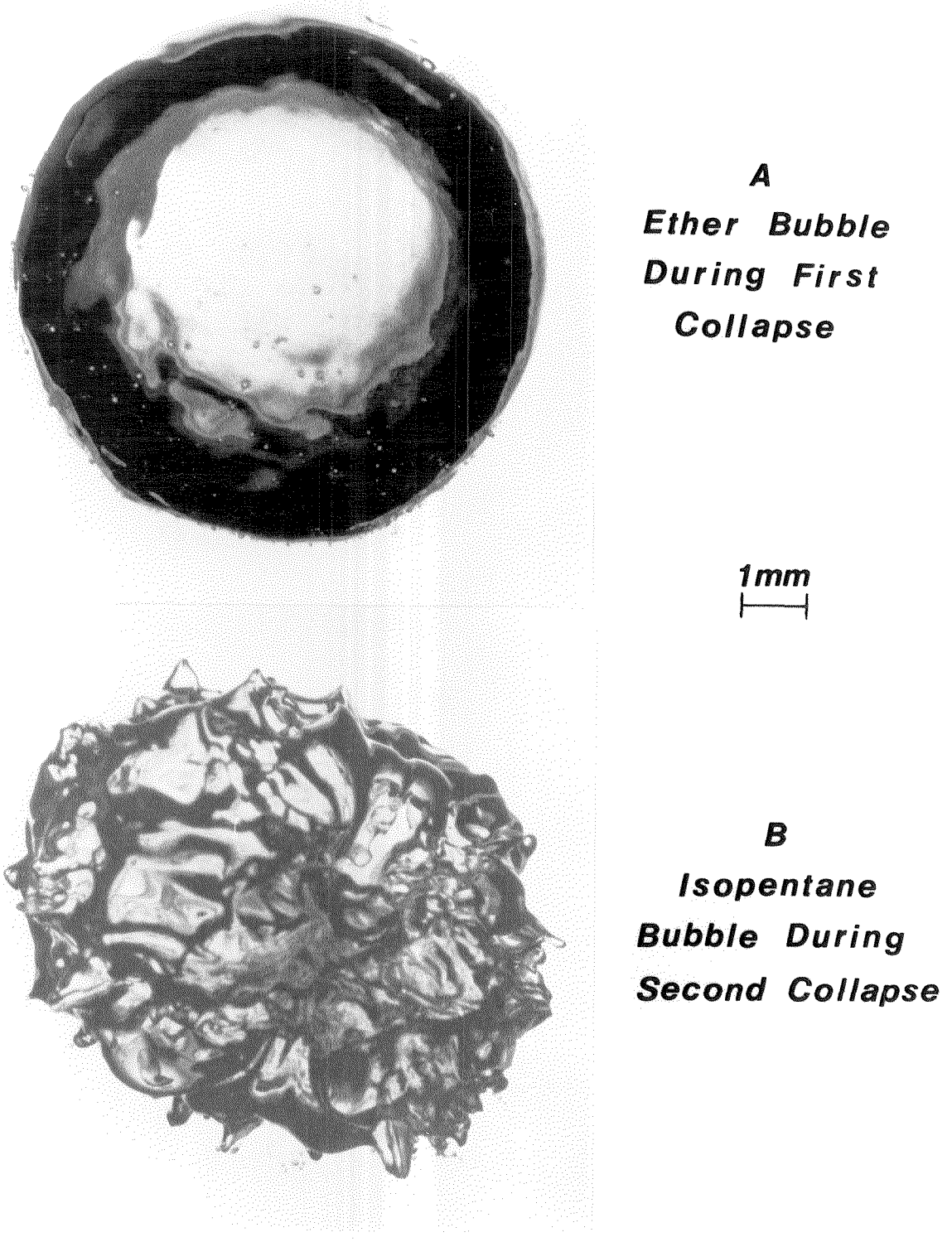

Figure 3.15 Bubble collapse and oscillation

fundamentally new has been observed during this stage with different fluids in the present experiments.

Chapter 4

EFFECTS OF AMBIENT PRESSURE ON THE EVAPORATIVE INSTABILITY

4.1. Introduction

The explosive behaviour of a liquid vapourizing at the superheat limit is particularly sensitive to the magnitude of the ambient pressure. The value of the ambient pressure determines the superheat at the liquid spinodal (i.e., $T_{sl} - T_{sat}$). Increasing the ambient pressure decreases the superheat and has a moderating effect on vapour bubble growth. Conversely, lowering the ambient pressure below atmospheric pressure enhances the vapourization rate and makes the drops boil even more explosively.

The importance of being able to control the violence of rapid vapourization by varying the ambient pressure becomes particularly apparent at elevated pressures. Increasing the ambient pressure slows the vapourization rate and provides a convenient opportunity to view the onset of the instability and the development of unstable boiling. In fact, if the pressure is raised high enough, it is possible to inhibit the instability altogether and change the nature of the vapourization from an explosive event to that of stable growth of a smooth vapour bubble. In this chapter results are presented that show the effect of ambient pressure on the vapourization process and illustrate the physical processes that occur during unstable boiling.

4.2. Enhanced Explosive Boiling

The intensity of the explosion generated by a drop boiling at the superheat limit can be enhanced by running the experiment under a partial vacuum. Lowering the ambient pressure leads to an increase in the superheat achieved at the spinodal. For example, for ether at 0.25 bar the superheat attained is about 145°C, a 30% increase over the corresponding value at atmospheric pressure. An increase in the vapourization rate is reflected in the magnitude of the far-field pressure field generated by bubble growth. The pressure level recorded by the transducer is a function of the size of the drop and the distance from the drop to the transducer, so it is difficult to quantitatively compare the pressure traces from different explosions.

Figure 4.1 shows three drops of ether vapourizing at ambient pressures of 0.25, 0.50, and 0.65 bar that were photographed after 20, 18, and 11 μsec, respectively. The pressure traces recorded by the transducer are shown below the photographs. These particular drops and the corresponding pressure traces were selected for the purpose of comparison because they are all roughly the same size (with an average diameter of 1.7 mm) and because they each exploded at the same location with respect to the transducer (7 mm from the transducer face). Note that as the ambient pressure decreases, the slope of the pressure rise recorded by the transducer increases, indicating an enhanced vapourization rate. The increase in the vapourization rate is modest and the time for a drop to completely evaporate (corresponding to the time the radiated pressure reaches a maximum) only decreases slightly at lower pressures. The drop shown boiling at 0.65 bar was photographed shortly after the onset of the instability, and a portion of the original smooth vapour bubble is still visible. The bubble growth rate before the onset of unstable boiling is also more rapid at lower pressures. As a result, the bubble comes into contact with the host fluid and the instability is triggered at a slightly earlier time than at atmospheric pressure.

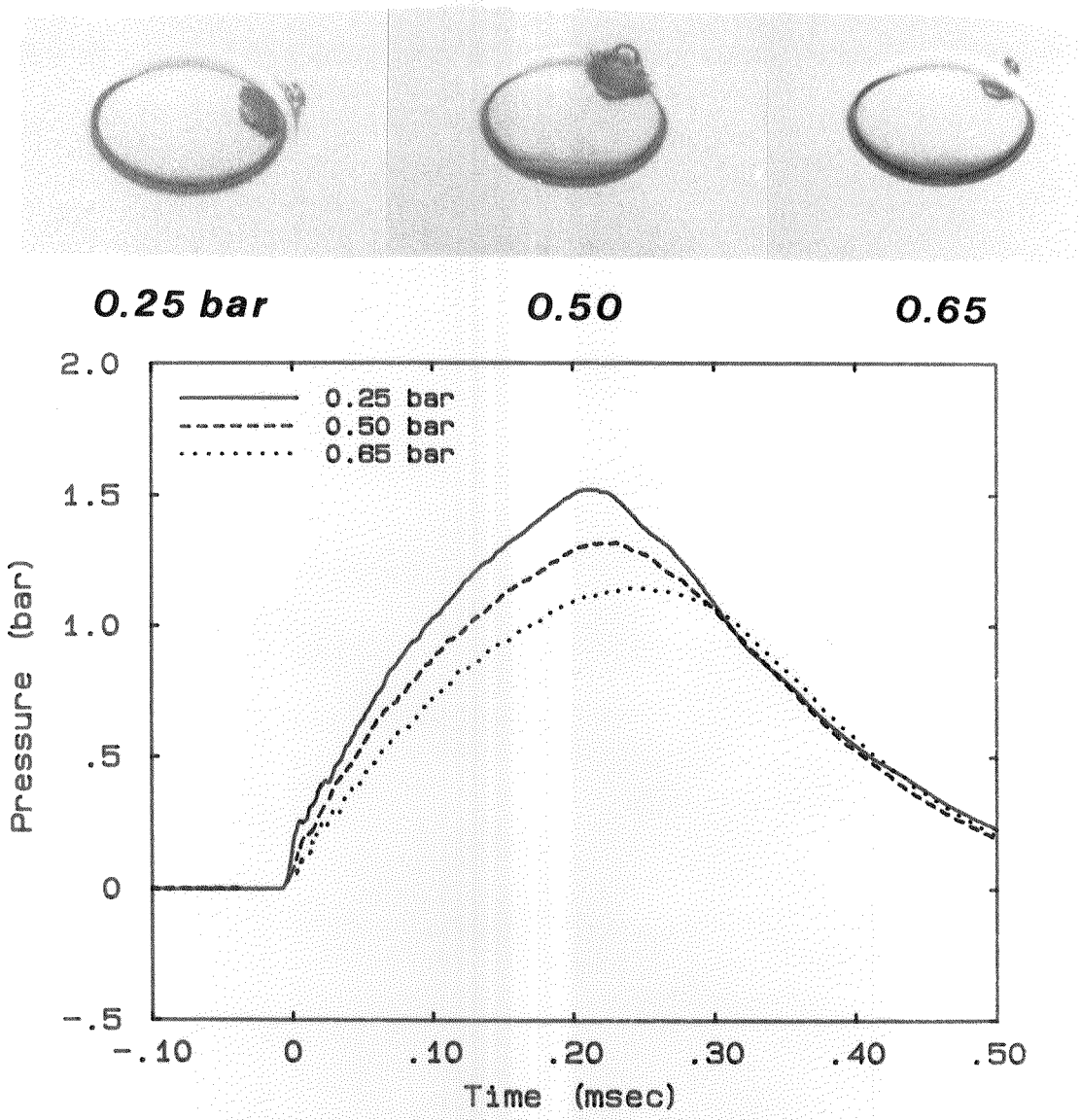

Figure 4.1 Ether drops vapourizing under a partial vacuum

Figure 4.2 shows a sequence of drops of ether evaporating at an ambient pressure of 0.6 bar. The unstable vapour bubble growth is remniscent of the behaviour at atmospheric pressure (see figure 3.3) although systematic differences in the appearance of the evaporating interface and the structure of the nonevaporating surface are apparent. The first three photographs in figure 4.2 show various views of the evaporating surface at early times. The dual appearance of the evaporating surface that was noted earlier at atmospheric

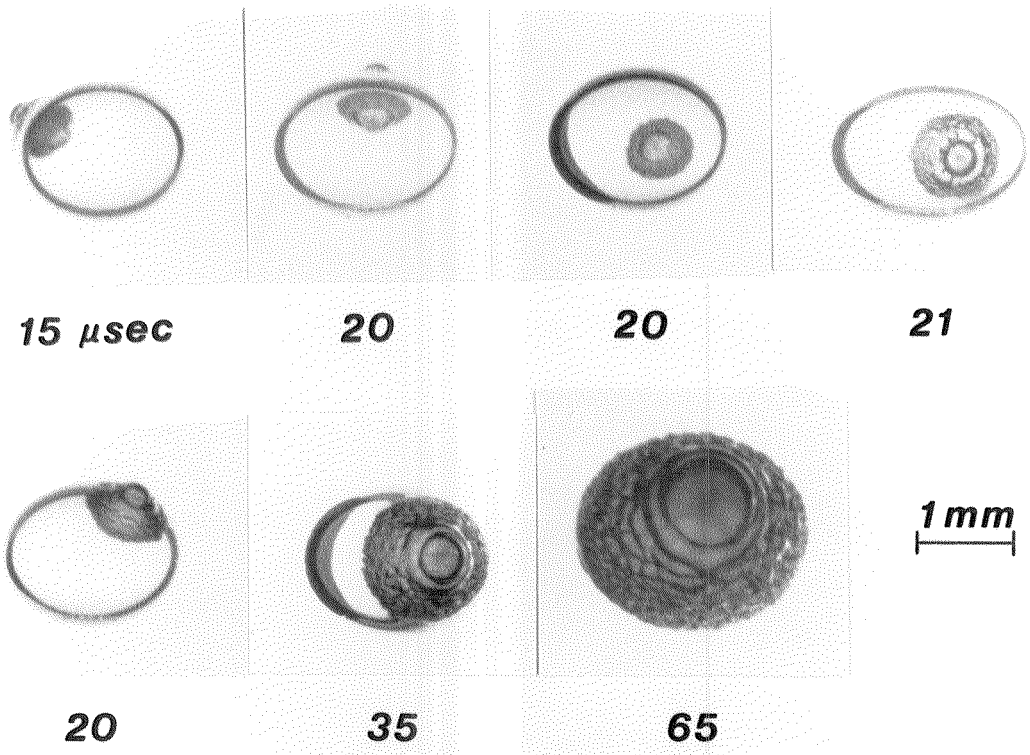

Figure 4.2 Drops of ether vapourizing at an ambient pressure of 0.6 bar

pressure (see photographs *E* and *F* in figure 3.1, and figure 3.2) is more prominent at lower pressures, presumably due to the more rapid growth of the initially smooth vapour bubble. At later times (see in particular the last two photographs in figure 4.2) the smooth cap appears reentrant, and the nonevaporating surface exhibits a fine scale roughness. The larger unstable vapourization rate at low pressure implies that there is less time for the action of surface waves to smooth out the disturbances on the bubble surface.

If the ambient pressure is lowered to 0.3 bar the vapour production rate is increased still further. The superheat attained at this pressure is 141.3°C. Figure 4.3 shows three photographs of ether drops vapourizing at 0.3 bar. The first photograph provides an oblique view of the evaporating surface and shows that the smooth hemispherical bulge in the evaporating interface exists for a considerable time during the bubble growth. The persistence of the dual character of

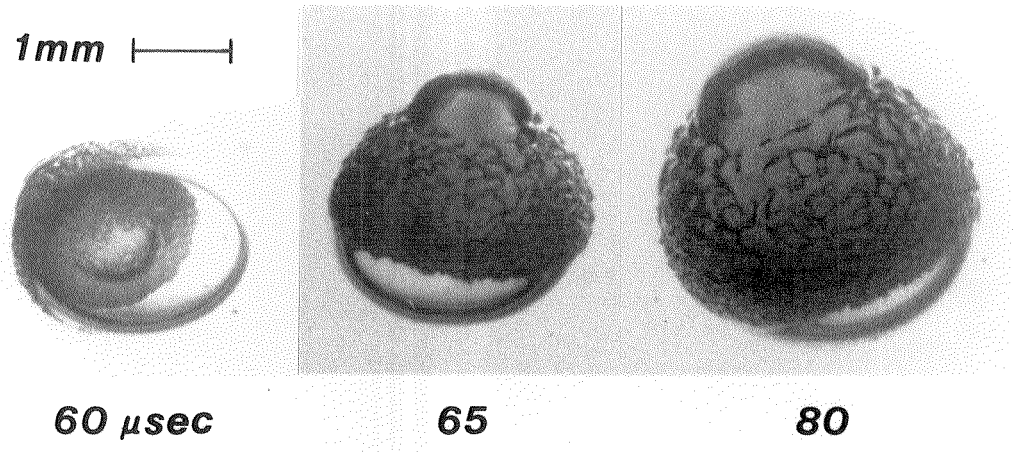

Figure 4.3 Drops of ether vapourizing at an ambient pressure of 0.3 bar

the evaporating surface may be related to the proximity of the host fluid. Heat transfer from the adjacent host fluid to the periphery of the evaporating interface serves to augment the vapourization rate in this region. The outer section of the unstably evaporating surface near the host fluid always exhibits a fine scale roughness indicative of intense unstable boiling. The more stable smooth portion of the interface is always located in the centre of the evaporating interface, farthest from the hot host fluid. So it is likely that the spatial variations in vapourization rate are caused by temperature gradients within the drop. The thermal nonuniformity that develops even in this nominally isothermal host fluid-droplet configuration is very similar to that which is inherent in rapid vapourization in spills. Therefore, the fringe of unstable vapourization observed in these photographs may occur rather generally. The last two photographs in figure 4.3 illustrate the increased prominence of the protrusion in the nonevaporating bubble surface at low pressure. Lowering the ambient pressure has the effect of enhancing the evaporative mass flux and thereby strengthening the vapour jet that creates the characteristic bulge by impinging on the bubble surface.

4.3. Moderated Unstable Boiling

Raising the ambient pressure lowers the attainable superheat and moderates the explosive nature of unstable bubble growth. For example, if the ambient pressure is increased to 3 bar, a drop of ether achieves a superheat of 80°C before exploding, a 29% reduction from the value at atmospheric pressure. Reducing the superheat causes the initially smooth vapour bubble to grow more slowly within the drop. By lowering the mass flux at early times across the stably evaporating interface, the susceptibility of the liquid to the instability decreases. As a result the onset of the instability may be delayed for a short time following the formation of the original vapour nucleus. When the instability occurs at elevated ambient pressures the vapourization rate rises sharply but does not reach the level attained at atmospheric pressure. Also with slower growth rates, the bubble oscillations that follow the completion of the evaporation tend to be much less violent than at lower pressures.

4.3.1. *Delayed Onset of the Instability.* Increasing the ambient pressure by the moderate amount of one bar produces a noticeable delay in the onset of the instability. Figure 4.4 shows a sequence of photographs of drops of ether all of approximately 1 mm diameter at various stages of vapourization. The typical pressure trace shown below the drops illustrates the behaviour of the pressure field 5 mm from the drops. Note that at early times (especially picture 1) the surface of the vapour bubble appears smooth. During this time the radiated pressure is at a low level. Picture 4 shows a drop that was photographed shortly after the onset of the instability and about 19 μsec after the initial nucleation. Then after about 25 μsec (picture 5) considerable roughness has developed and the vapour region appears opaque. The distortion of the interface corresponds to a dramatic increase of the far-field pressure by as much as a factor of 5, indicating a jump in the vapourization rate.

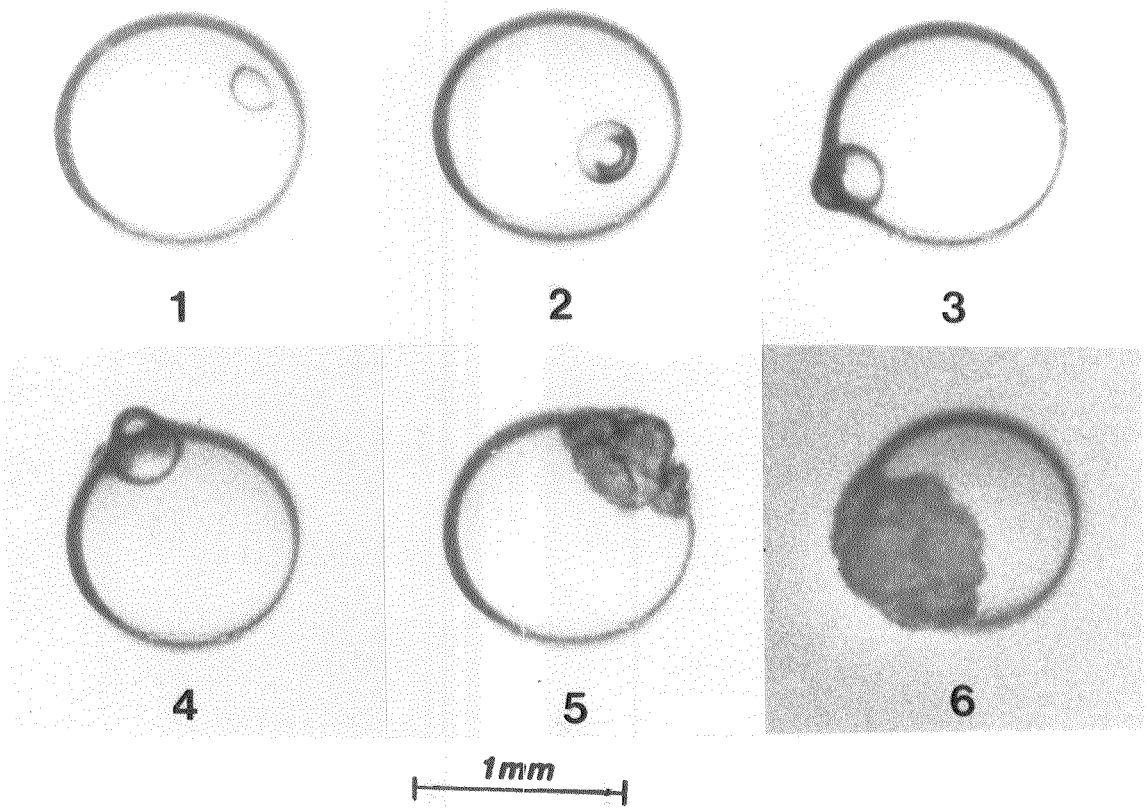

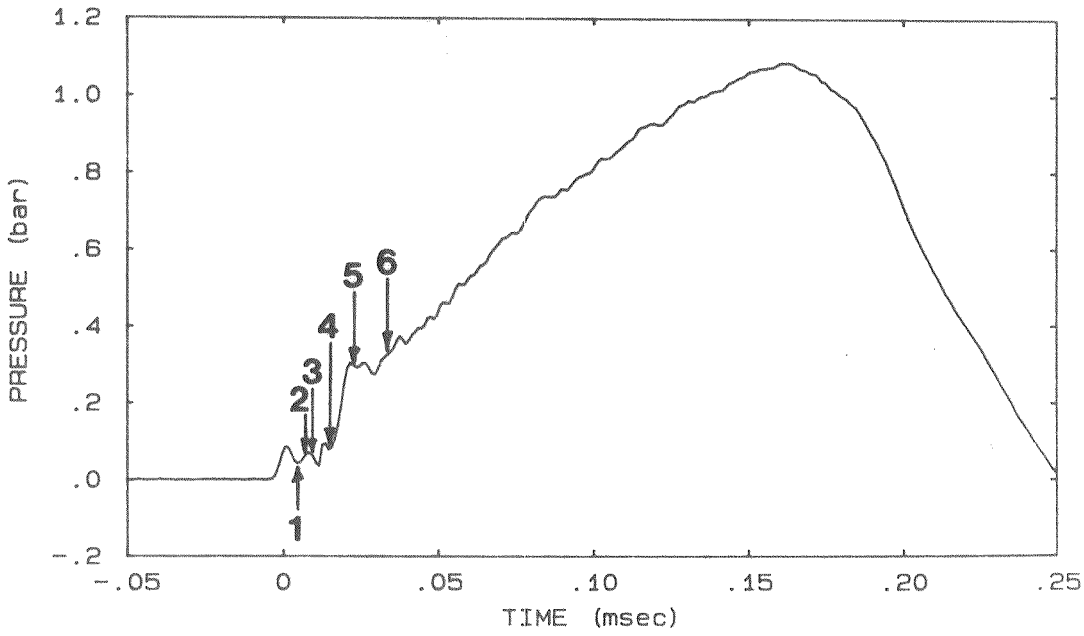

Figure 4.4 Photographs and pressure trace of ether drops exploding at an ambient pressure of 2 bar

Increasing the ambient pressure increases the time delay between the formation of the vapour nucleus and the onset of the instability. The maximum pressure that is radiated following the onset of the instability also decreases with increasing ambient pressure. These stabilizing effects are observed in all the liquids tested although at a given ambient pressure some liquids appear to be more susceptible to the instability than others. Variations in fluid properties lead to quantitative differences in the sensitivity of the liquids to the instability, and in subsequent bubble growth rates. The influence of fluid properties on the behaviour of unstable boiling will be discussed in the next chapter.

Increasing the ambient pressure to 4 bar provides a convenient situation for exhibiting the details of the onset of the instability in ***butane***. Figure 4.5 shows photographs of drops of butane evaporating at 4 bar together with a typical pressure trace. The radiated pressure field displays an interesting behaviour: following the sharp spike produced by the nucleation, the overpressure measured 5 mm away is less than 0.003 bar for several hundred microseconds. During this time the smooth vapour bubble grows stably within the drop (see picture *A*). The exact length of the stable growth phase varies somewhat randomly from drop to drop but the onset of the instability typically occurs between 150 μsec and 300 μsec after nucleation. Pictures *B* and *C* show the early development of a disturbance on the bubble surface 25-30 μsec after the onset of the instability. The instability appears to be initiated in the volatile fluid near the circle that forms the intersection between the growing vapour bubble, the test fluid in the drop and the host fluid. The onset of the instability in other liquids occurs in a similar fashion (e.g., see picture 4 of figure 4.4 for ether). Picture *D* was taken 120 μsec after the onset of unstable boiling and illustrates the small-scale roughness that forms on the evaporating surface. The length scale of the smallest perturbations is on the order of 100 μm, the same scale observed at atmospheric pressure (see figure 3.9).

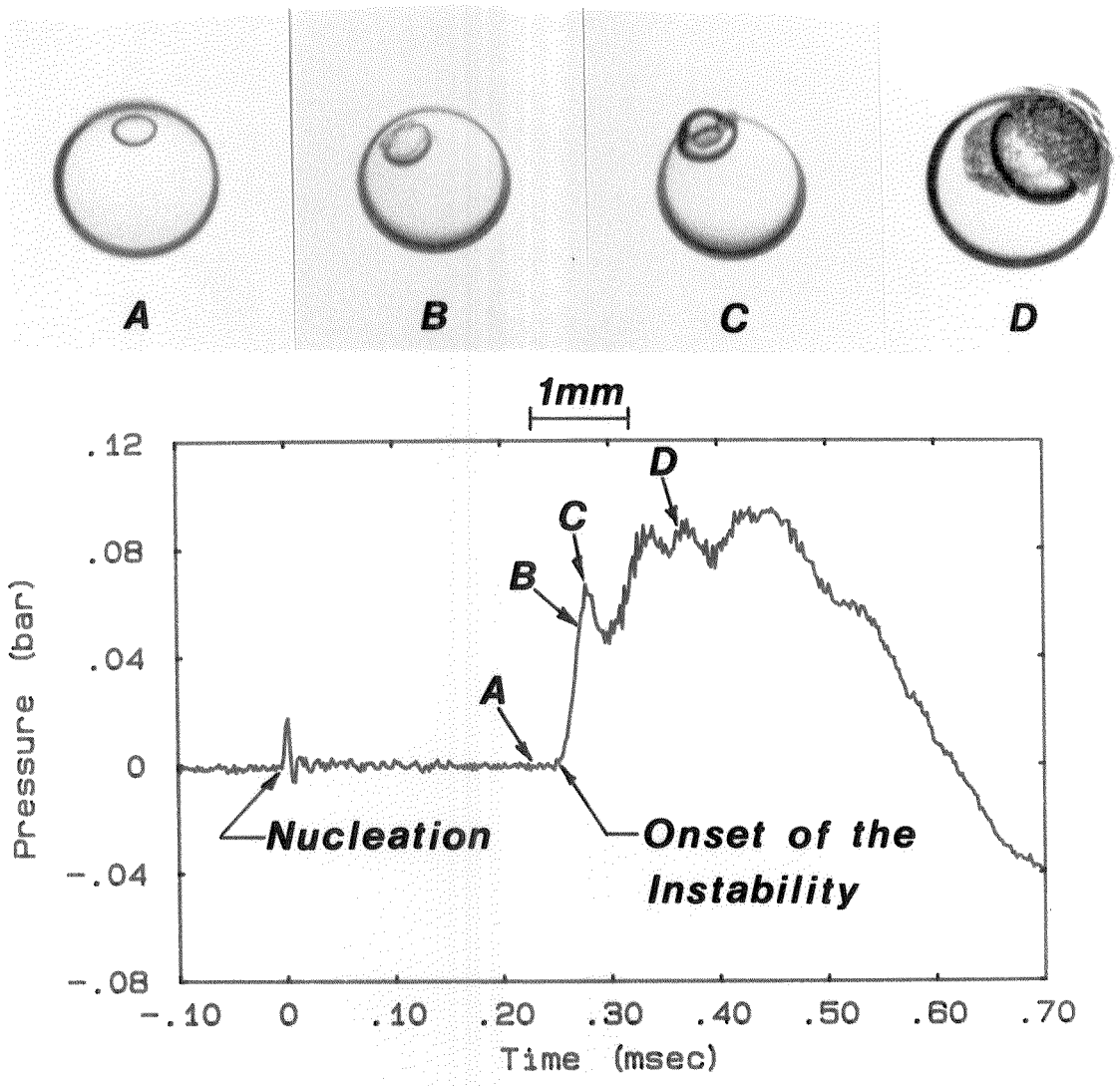

Figure 4.5 The onset of the instability in butane at an ambient pressure of 4 bar

4.3.2. *Reduced Unstable Vapourization Rates.* During the transition from stable boiling to unstable boiling, the radiated overpressure rises sharply. However, from figure 4.5, the maximum overpressure attained 5 mm from the drop is only about 0.1 bar, an order of magnitude lower than the corresponding value at atmospheric pressure. This moderation of the intensity of explosive boiling at elevated pressures is a reflection of the reduced superheat. In fact the

superheat attained for drops of butane exploding at the superheat limit at 4 bar is only 66.5°C (c.f. 105.3°C at atmospheric pressure), which is the *lowest* level of superheat attained for an exploding drop in the present experiments.

Figure 4.6 shows a series of photographs illustrating the behaviour at later times of drops of butane vapourizing at an ambient pressure of 4 bar. Picture *A* shows a drop that is nearly completely vapourized. The edge of the evaporating surface in view appears quite rough although the action of wave-spreading has considerably smoothed the nonevaporating bubble surface. The portion of the bubble surface near the evaporating interface appears to be darker than the surface nearer the central portion of the bubble. This dark horizontal band just above the evaporating interface may be caused by refraction due to the mist of fine particles that is ejected from the evaporating surface. In this case the vertical extent of the dark region would indicate the distance the fine liquid droplets travel before evaporating. The last portion of liquid in the drop appears to evaporate in a particularly violent fashion presumably due to small temperature nonuniformities on the evaporating surface (this will be discussed further in the next chapter). The liquid droplets that are torn from the evaporating surface at this late time are large enough to survive the flight across the inside of the bubble and impinge on the host fluid. Pictures *C* and *D* in particular show the cratering of the bubble surface that occurs when the spray of volatile liquid particles contacts the hot host fluid.

The pressure trace shown in figure 4.6 shows the behaviour of the radiated pressure on a millisecond time scale. The appearance of the pressure trace is notably different from the behaviour at atmospheric pressure (see figure 3.14). In particular, the violent bubble collapse and oscillation illustrated in figure 3.15 are absent at 4 bar. Apparently at high pressure the unstable growth rate is slow enough that when the evaporation is completed the resulting vapour bubble

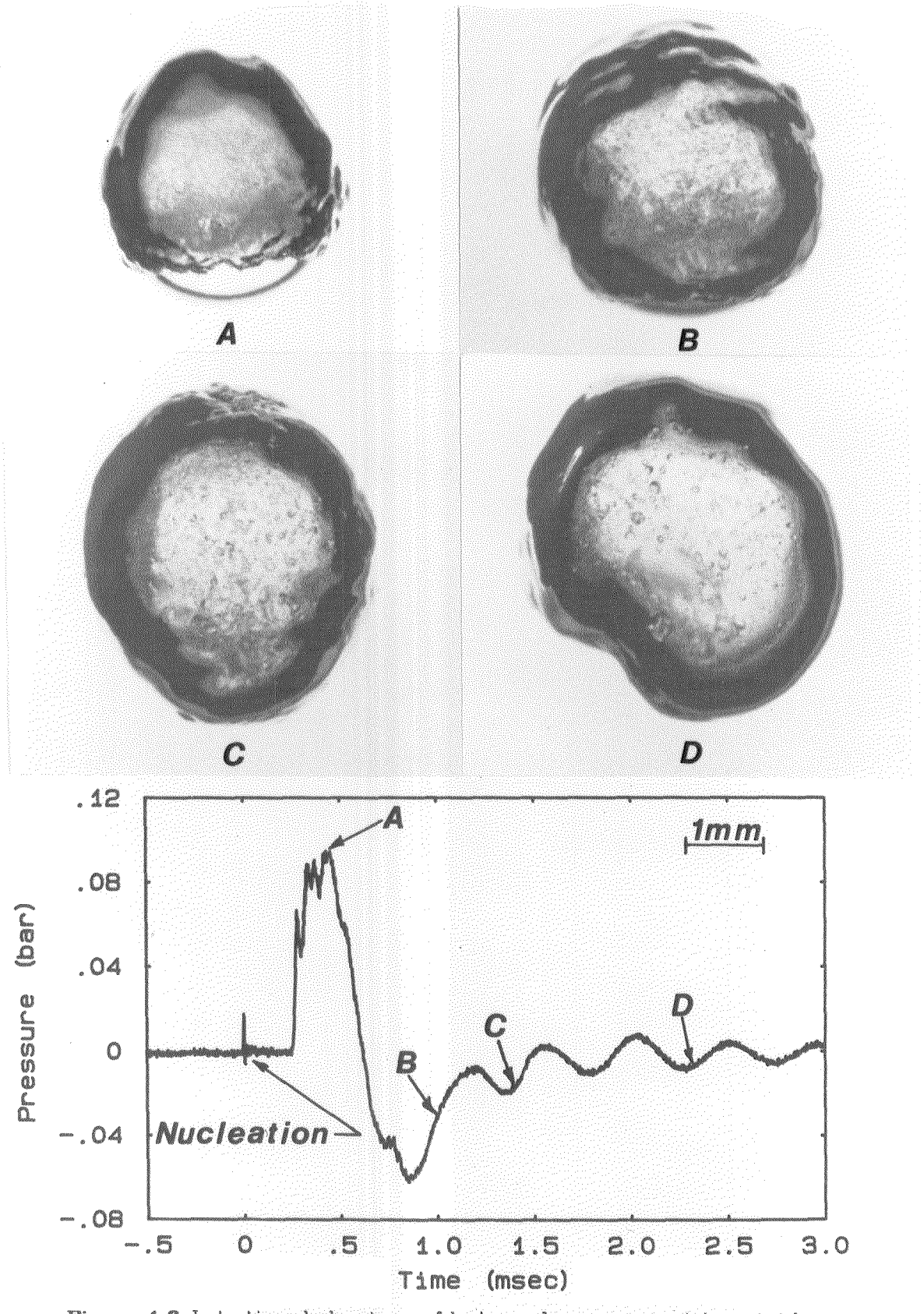

Figure 4.6 Late time behaviour of butane drops vapourizing at 4 bar

deforms and oscillates at a very small amplitude. The butane bubble in picture *D* of figure 4.6 was photographed after 3 weak volume oscillations and the bubble surface appears largely intact.

4.4. Stable Bubble Growth

If the ambient pressure is increased above 3 bar it is possible to suppress the instability in ether altogether. Figure 4.7 shows the vapourization of drops of ether at 4.2 bar (69°C superheat). In each case the instability is no longer present and the growing vapour bubble has a smooth surface. With the absence of the instability, the vapour bubbles grow much more slowly than at atmospheric pressure. Times for the first five photographs are 20 μsec, 80 μsec, 240 μsec, 1.22 msec, and 1.42 msec, respectively. The violent bubble oscillations that occur at atmospheric pressure following the completion of the vapourization are completely eliminated at high pressure and the vapour bubble retains its spherical shape. As has been noted by other authors (e.g., Avedisian & Glassman, 1981b; Avedisian, 1982), the characteristic popping sound accompanying the explosion at atmospheric pressure is no longer evident at high pressure.

At an ambient pressure of 3 bar the onset of the instability in ether is delayed until late times (on the order of milliseconds) or occasionally suppressed entirely. Figure 4.8 shows a series of drops of ether vapourizing stably at 3 bar (80°C superheat). The smooth vapour bubble within each drop appears in a variety of orientations. The times for the drops range from 12 μsec for picture 1 to 1.6 msec for picture 18. The impact of the growing vapour bubble with the surface of the drop is sufficient to produce a smooth protrusion of the bubble surface into the host fluid (e.g., see pictures 3 and 11). However, at later times (e.g., picture 18) this characteristic bulge is less prominent than the cap structure that was observed during *unstable* boiling at lower pressure (e.g., see figure 4.3) when, in addition, the impact of the strong evaporative jet with

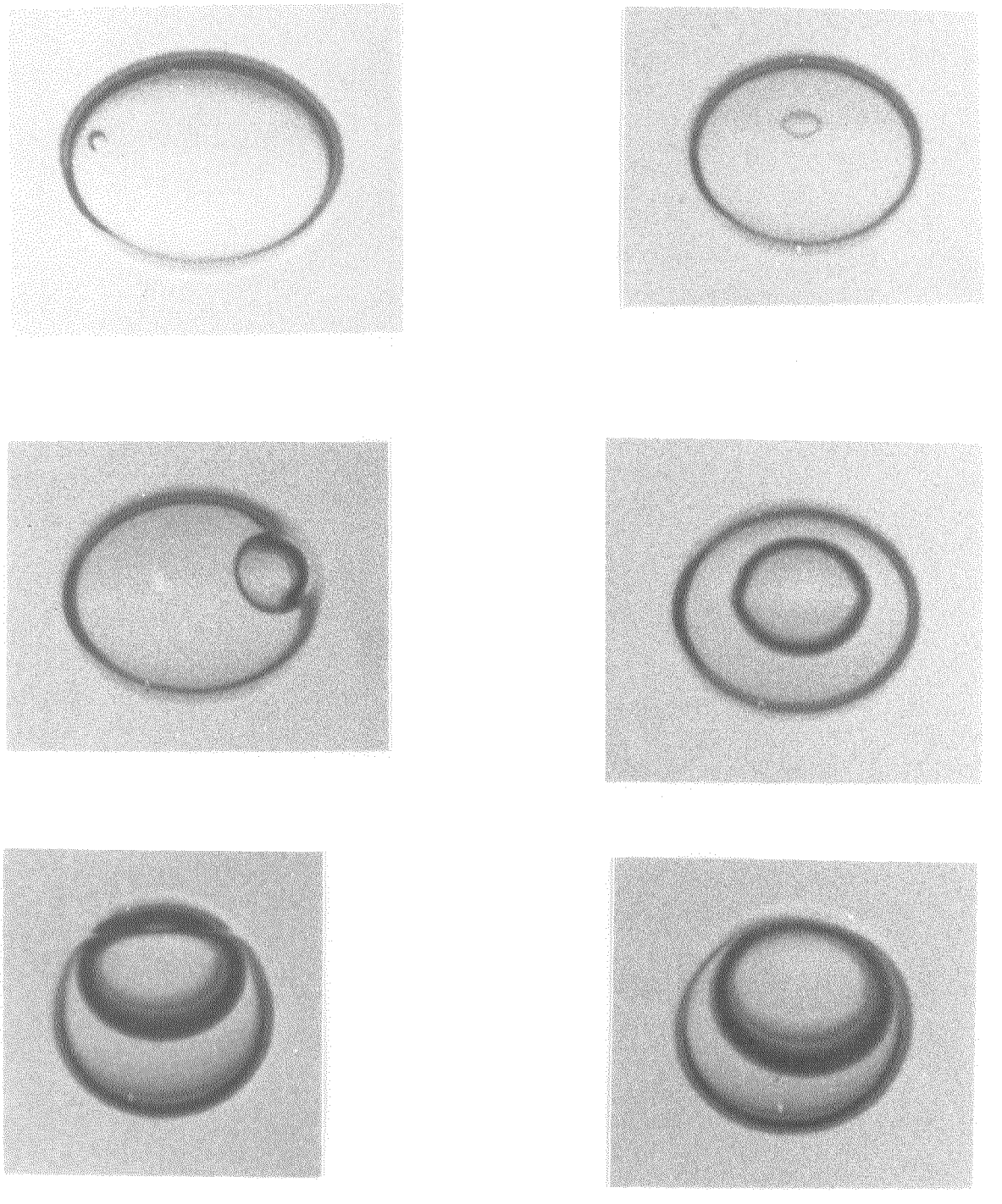

Figure 4.7 Ether droplets vapourizing at an ambient pressure of 4.2 bar

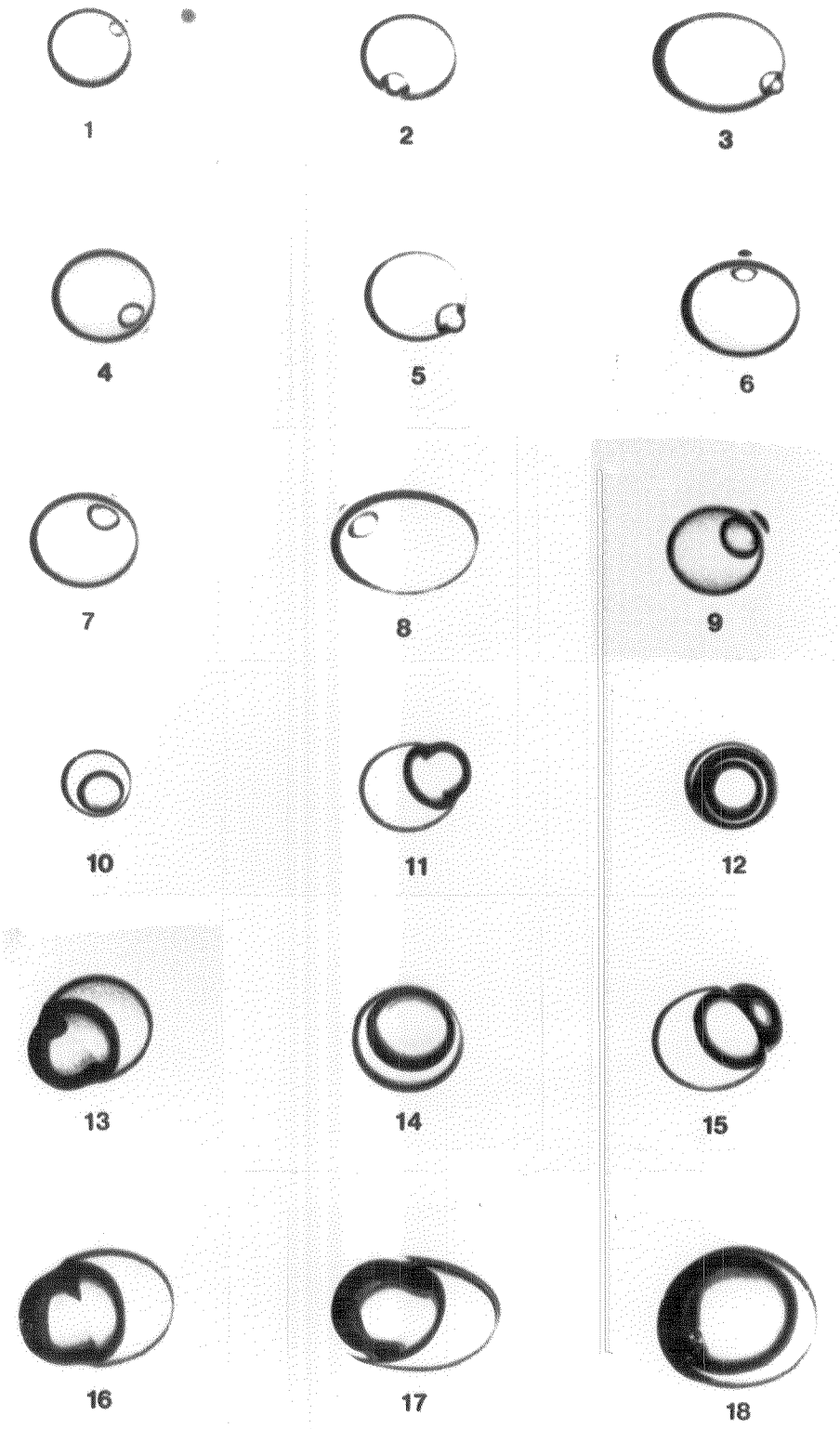

Figure 4.8 Stable bubble growth in ether at 3 bar

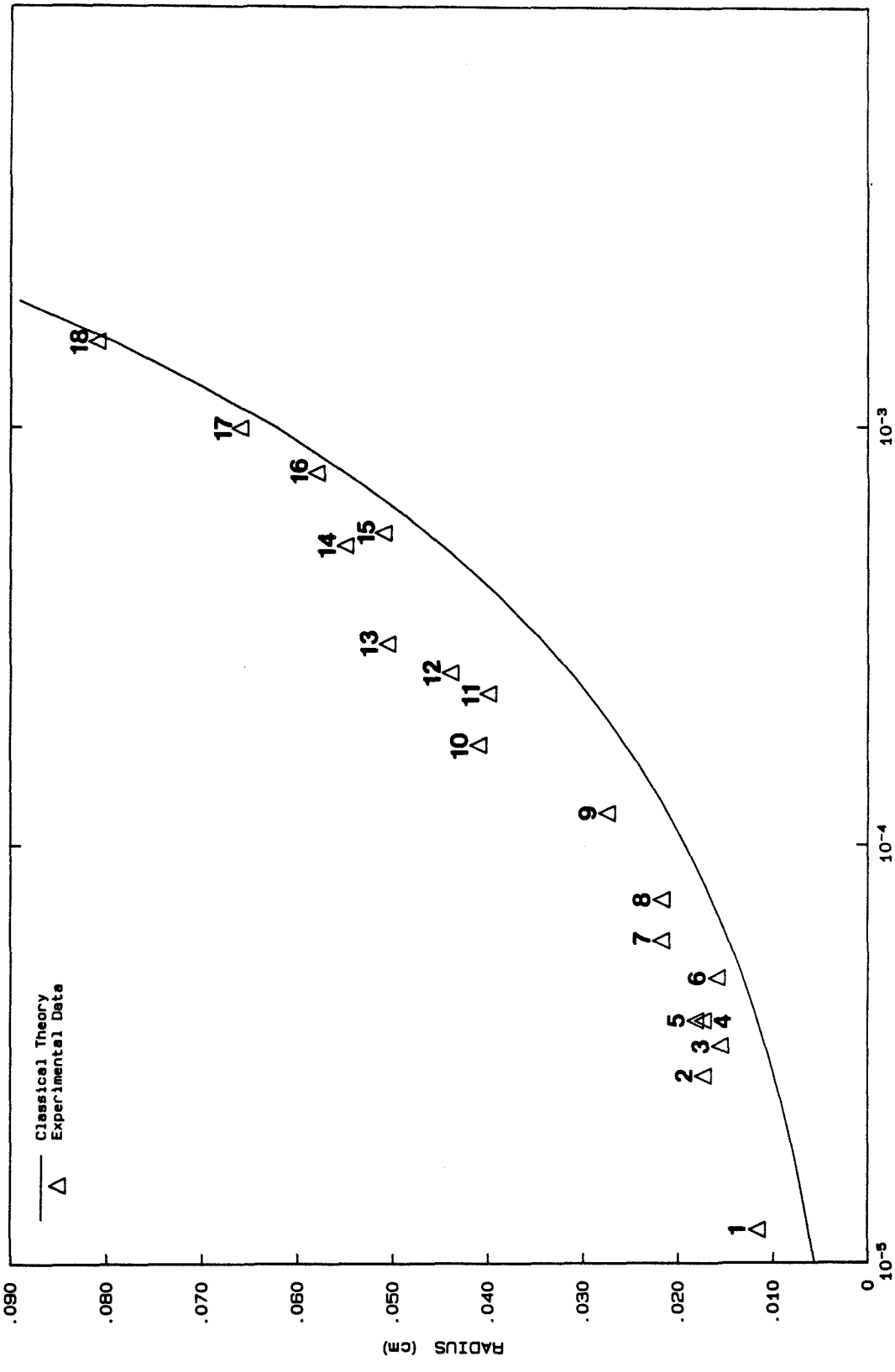

Figure 4.9 Comparison between theory and experiment for stable bubble growth at 3 bar

the bubble surface serves to increase the extent of the bulge. The average bubble radius was estimated from each photograph in figure 4.8 and plotted versus time in figure 4.9. The curve denoted *classical theory* was generated using the theory of Prosperetti & Plesset (1978) for the growth of a vapour bubble in a uniformly superheated liquid. The agreement is rather remarkable considering the many approximations we have used in applying the theory. The assumptions used in deriving the theoretical curve are discussed in Appendix B. The theory considers the growth of a vapour bubble in an infinite liquid, in contrast with the finite drop size in experiments. As a result, in applying the theoretical predictions to experimental results, no provision in the theory is made for (i) heat transfer from the host fluid to the test fluid, (ii) heat transfer from the host fluid to the vapour, and (iii) the fact that evaporation takes place across only a fraction of the bubble surface after the bubble contacts the droplet surface. The theoretical curve lies below the experimental data (this discrepancy is discussed in Appendix B), but the agreement is much better than when the instability is present (Shepherd & Sturtevant, 1982).

During the stable bubble growth, the radiated overpressure generated is extremely small. Figure 4.10 shows a superposition of three pressure traces for drops of ether, all of approximately the same size (typically 1.4 mm), at ambient pressures of 1, 2, and 3 bar. The pressure recorded when the instability is suppressed at 3 bar is several orders of magnitude less than at atmospheric pressure. Also, the time for the drop to completely evaporate is substantially increased. For example, a 1.5 mm diameter drop takes about 170 μsec to vapourize at atmospheric pressure. This time is increased by roughly a factor of 30 to about 5 msec at 3 bar.

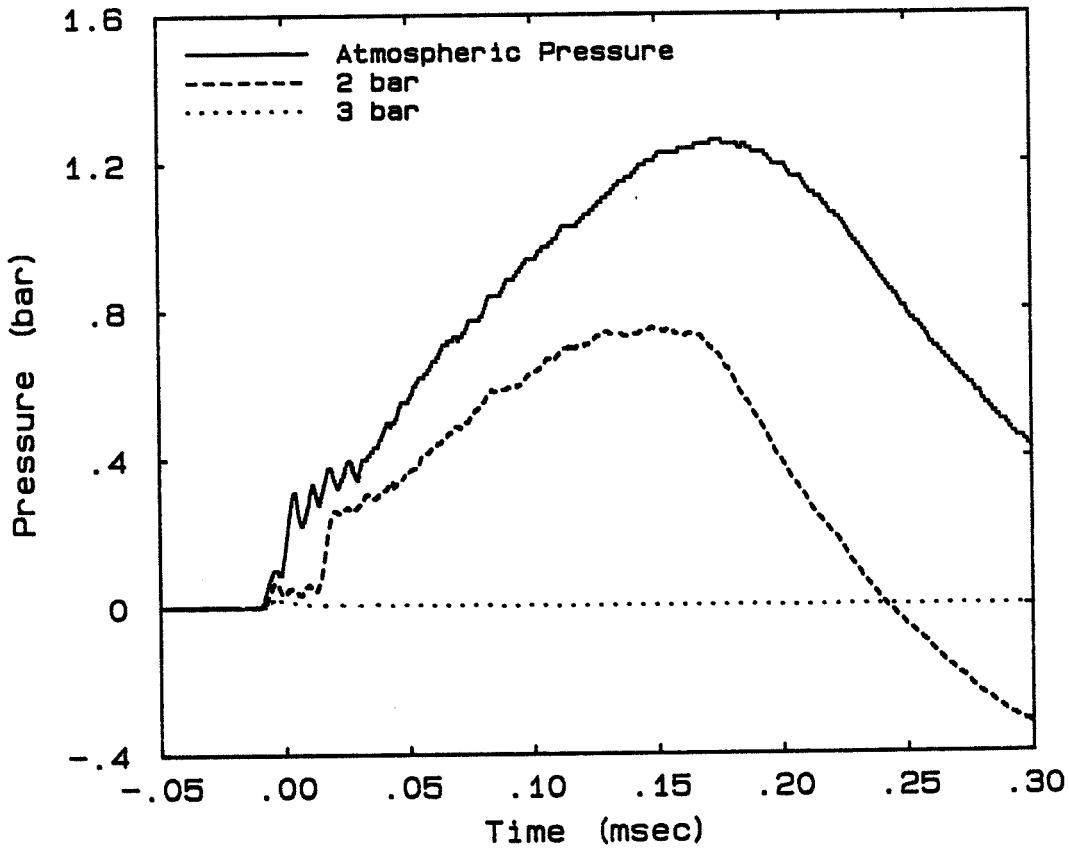

Figure 4.10 Superposition of pressure signals radiated from ether drops. Pressure, drop diameter, and distance from baffled pressure transducer: top, atmospheric pressure, 1.2mm, 6mm; middle, 2 bar 1.3mm, 6mm; bottom, 3 bar, 1.6mm, 4.4mm

4.5. Transitional Boiling

4.5.1. *Overview.* The range of ambient pressures between violently unstable boiling and stabilized boiling in which a kind of metastable or transitional stability is found, provides an important opportunity for documenting the detailed behaviour of explosive boiling. In this regime (which occurs at an ambient pressure of about 3 bar for ether) the instability is delayed until a late time when the majority of the liquid in the drop has vapourized, so, when the explosive boiling finally does occur, the interior of the vapour bubble is clearly visible.

Figure 4.11 provides an overview of the behaviour of ether boiling at 3 bar.

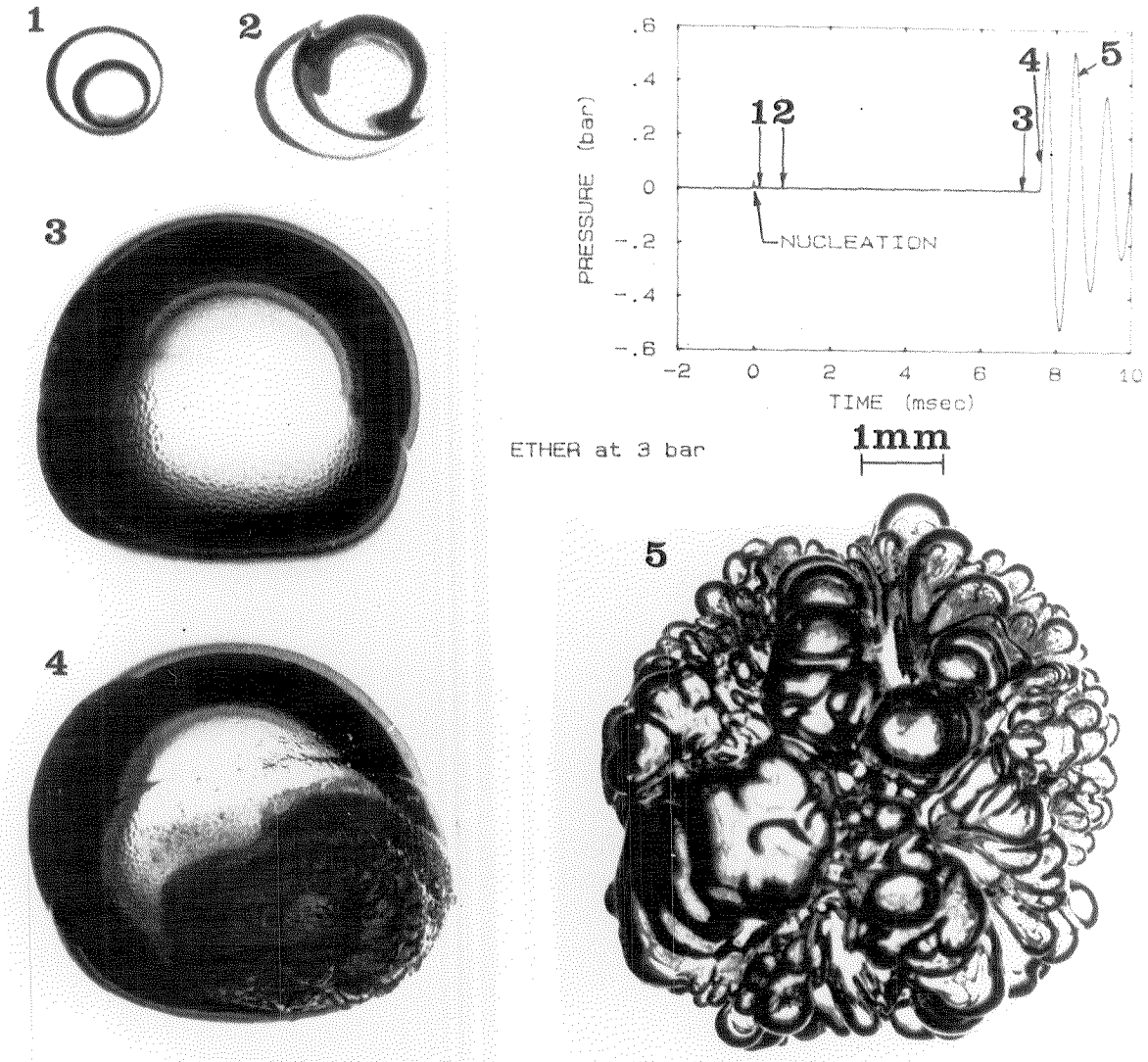

Figure 4.11 Overview of ether boiling at 3 bar

The pressure trace in the figure shows a remarkable behaviour, in which for about 7 ms, while the droplet is evaporating stably (pictures 1 to 3), the over-pressure measured 6 mm away is less than 0.005 bar. Then a sudden impulse causes the bubble to grow rapidly and oscillate violently. The photographs in figure 4.11 show that during the early stages of vapourization at these conditions the bubble surface is completely smooth, but later, when the remaining

liquid forms only a thin cap at the end of the bubble (picture 3), the liquid-vapour interface of the *stably* vapourizing liquid develops small-amplitude short-wavelength disturbances (giving the appearance of "orange-peel"). Finally (picture 4), the instability is initiated at some point near the edge of the liquid cap, rapidly spreads out radially, and the remaining liquid boils explosively. Picture 5 shows the consequences of the action of the Rayleigh-Taylor instability on the bubble surface after only one rebound. A more detailed discussion of the evaporative behaviour in this transitional boiling regime will now be given.

4.5.2. *Initial Stable Growth.* During the early stages of vapourization of ether at an ambient pressure of 3 bar, the surface of the growing vapour bubble is completely smooth. However, after several milliseconds of stable growth, small-amplitude disturbances begin to appear on the liquid-vapour interface. Figure 4.12 shows a droplet of ether that has been evaporating stably for 2.82 ms.

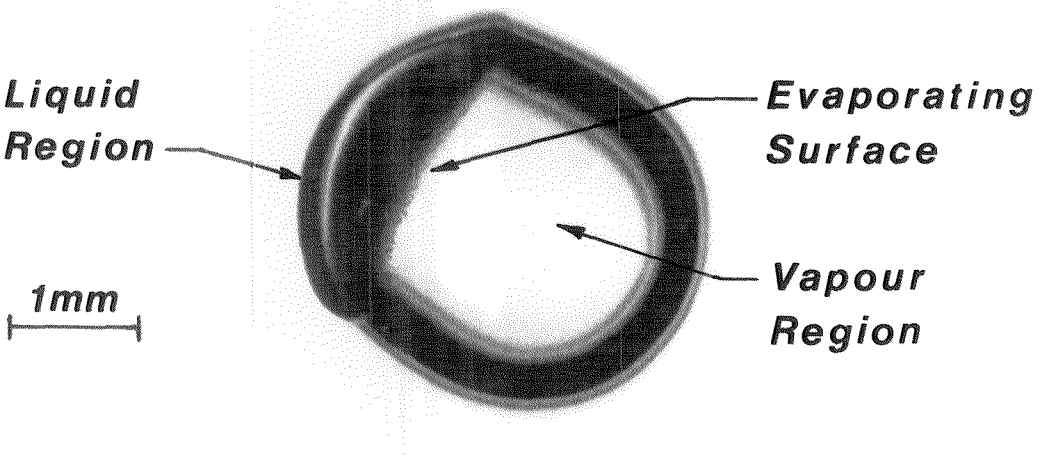

Figure 4.12 Stable bubble growth for ether at 3 bar. Note disturbances on evaporating surface.

The ether vapour is contained in the U-shaped region in the lower right portion of the photograph. The black band around the vapour region is a consequence

of the large difference between the index of refraction of the vapour and the surrounding host fluid. The remaining liquid forms a thin lens-shaped cap at the end of the bubble. Note that the evaporating liquid-vapour interface, here viewed in profile, has a roughened appearance.

The high wavenumber disturbances that develop on the evaporating surface slowly increase in amplitude with time. Figure 4.13 shows oblique views of the liquid caps on two different ether bubbles, each photographed after evaporating stably for 7.47 ms.

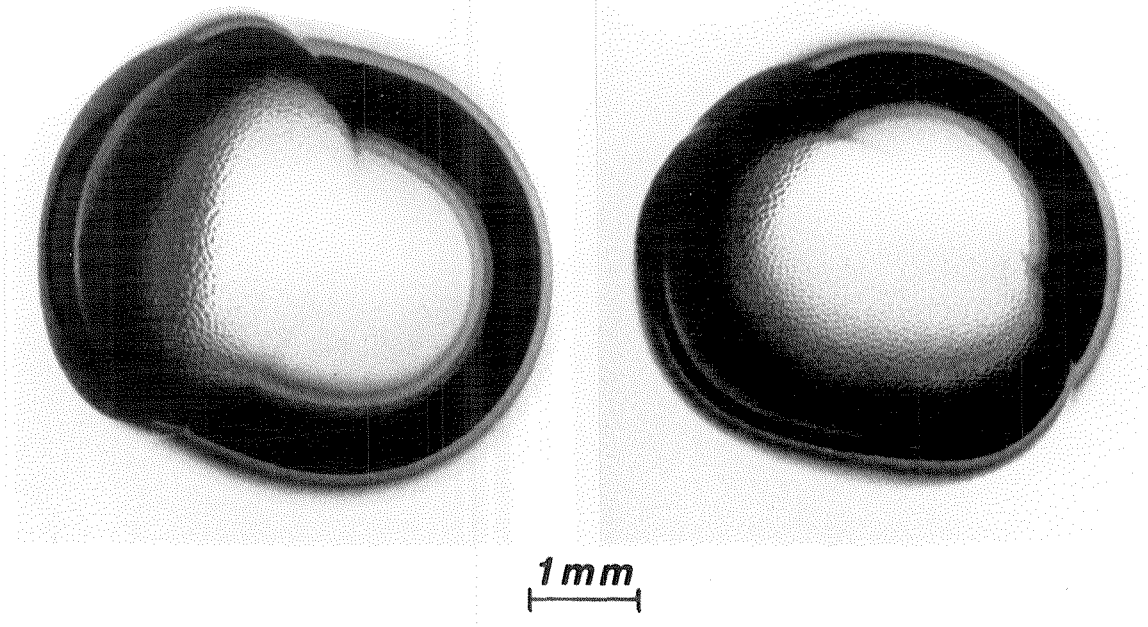

Figure 4.13 Disturbances on stably evaporating surface in ether at 3 bar

The regular small-amplitude waves visible on the liquid-vapour interface give the surface a corrugated appearance. Figure 4.14 shows a drop of ether photographed after 7.04 ms together with an enlargement from the same photograph of the liquid region illustrating the small-scale structure on the evaporating surface. As a result of diffraction by the curved surface of the liquid region, it is difficult to determine the exact length scale of the perturbations. However,

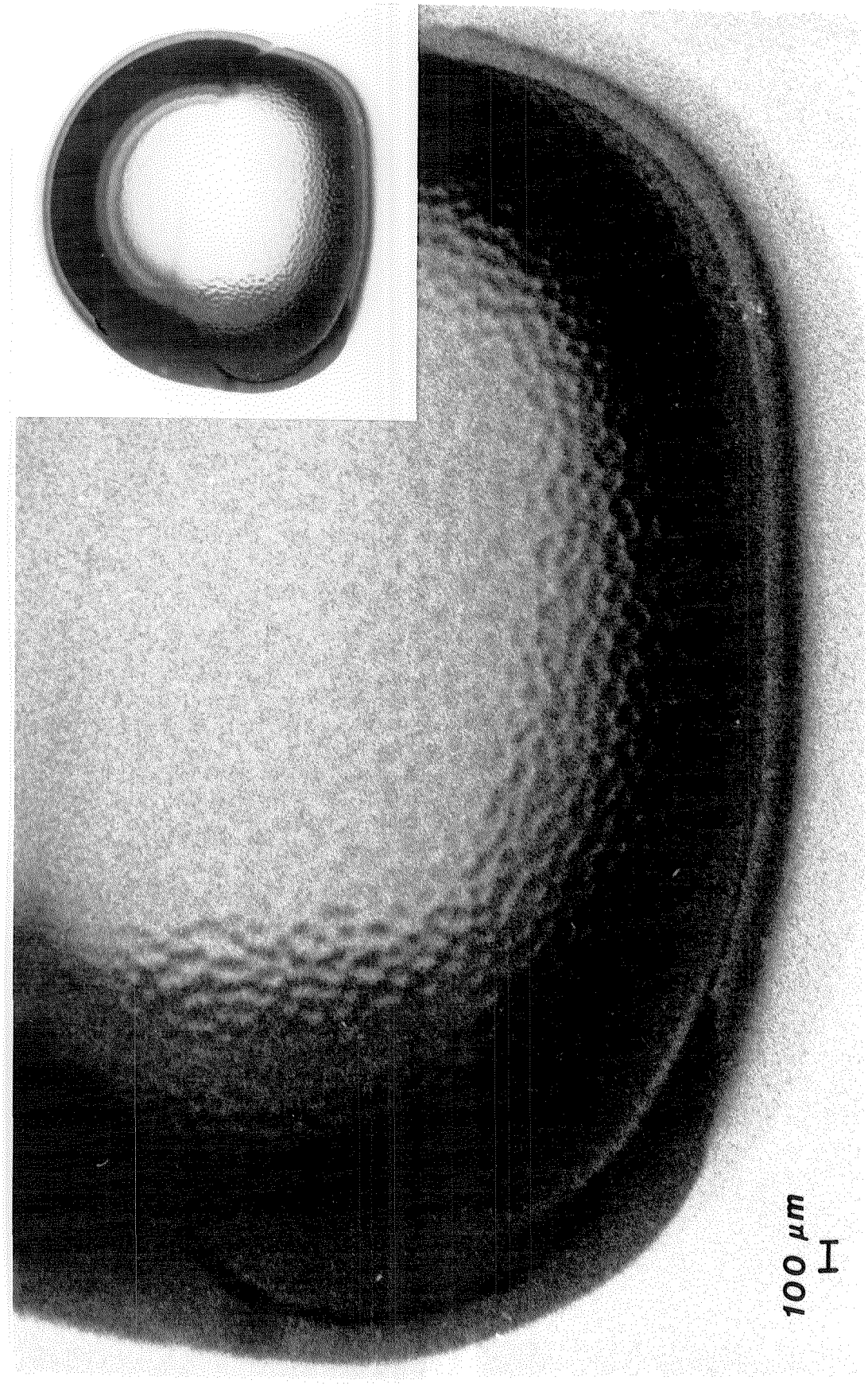

Figure 4.14 Enlargement of perturbations on the evaporating surface in ether at 3 bar

from the photograph, the disturbances appear to have a scale of the order of 50-100 μm. This is the same order of magnitude as found earlier for the smallest length scale of the disturbances on a fully-developed unstably evaporating surface.

4.5.3. *Initiation of the Instability*. In this late stage of bubble growth the occurrence of some disturbance may serve to trigger a breakdown to violent instability. Figure 4.15 shows two drops of ether shortly after the transition to unstable boiling has occurred.

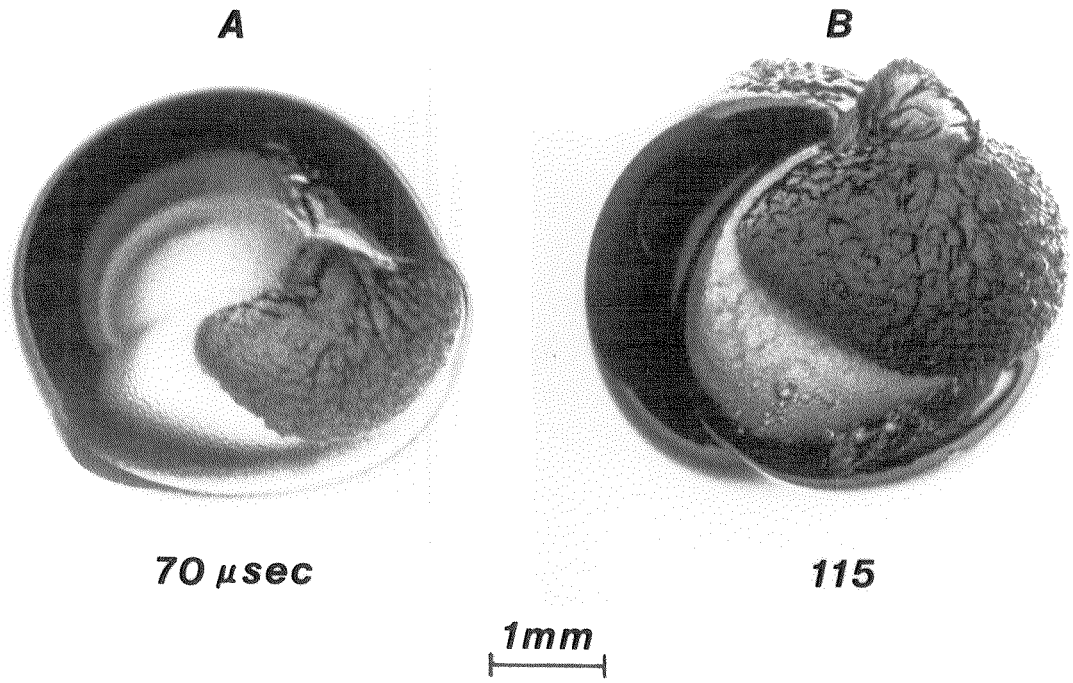

Figure 4.15 Ether drops shortly after the initiation of unstable boiling at 3 bar

The photographs show exterior views of the liquid cap with a "clam-shell" shaped unstable region visible on the surface. The time shown below each photograph (and in all subsequent photographs in this chapter) is the time elapsed since the onset of the instability. The violent boiling in each case starts at the edge of the

liquid region and rapidly spreads out radially, consuming the remaining liquid, typically in 150-200 μsec.

The presence of the hot host fluid plays a role in the transition to unstable boiling. Shortly before the onset of the instability, the remaining liquid is contained in a cap-shaped region that becomes very thin at the edges. Local heating at the edge of this thin liquid lens by the host fluid may generate a band of higher-temperature fluid at the edge of the evaporating interface that is hot enough to undergo a breakdown to violent boiling. The effect of temperature perturbations on the stability of a stably boiling interface will be discussed in the next chapter in the context of linear stability theory.

The transitional boiling regime occurs in pentane at an ambient pressure between 3.5 and 4.0 bar. The dynamical features observed in pentane in this regime are similar to those that occur in ether at 3 bar. Figure 4.16 shows two pentane drops photographed 36 μsec and 66 μsec after the onset of unstable boiling, respectively. The photographs were taken at different values of the ambient pressure, as noted in the figure. Both drops exhibit the incipient instability waves on the evaporating surface and the unstable boiling region.

The appearance of the unstable region in the photographs in figures 4.15 and 4.16 suggests an interesting although loose analogy with the stability of a laminar boundary layer flow. In the laminar flow of a fluid over a flat plate, for example, two-dimensional Tollmien-Schlichting instability waves (the analog of the "orange-peel" disturbance) develop spontaneously and grow. These linear waves may reach a critical amplitude, become nonlinear and ultimately break down into turbulent flow. The transition process involves the formation of turbulent spots (the analog of the unstably boiling region), that grow to form a fully turbulent flow. In more stable flows, however, it is necessary to introduce an external boundary layer "trip" to artificially trigger a turbulent spot. This

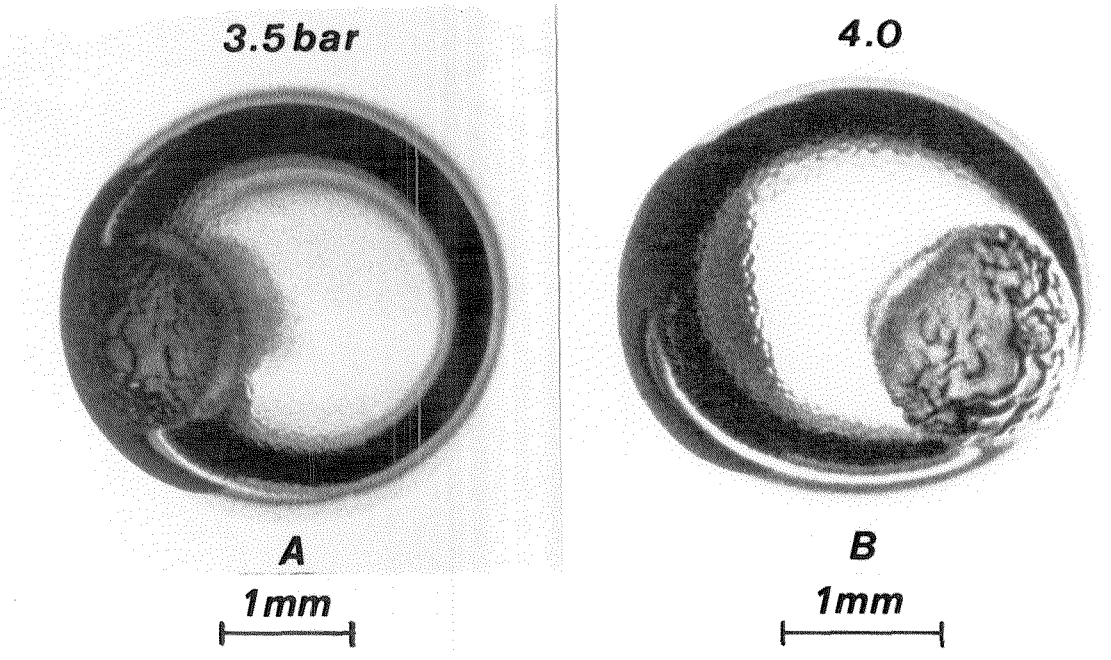

Figure 4.16 Pentane drops vapourizing in the transitional regime of stability

suggests it may be possible to externally trigger the breakdown to violent boiling by introducing a disturbance of sufficient amplitude.

4.5.4. *Two-Phase Evaporative Jet*. The transitional boiling regime is particularly useful for illustrating the physical processes that occur during unstable boiling. In this regime, the transition to violent boiling occurs after the majority of the liquid in the drop has vapourized. As a result, by viewing the bubble in profile, it is now possible to observe the interior of the bubble and the behaviour at the evaporating surface. Figure 4.17 shows two different drops shortly after the onset of unstable boiling. In picture *A*, the instability was initiated on the edge of the liquid region away from the viewer, almost out of view. A finely-dispersed cloud of liquid particles is visible near the evaporating surface. Extremely fine particles are torn from the evaporating liquid surface and the resulting aerosol or mist is propelled away from the liquid-vapour interface

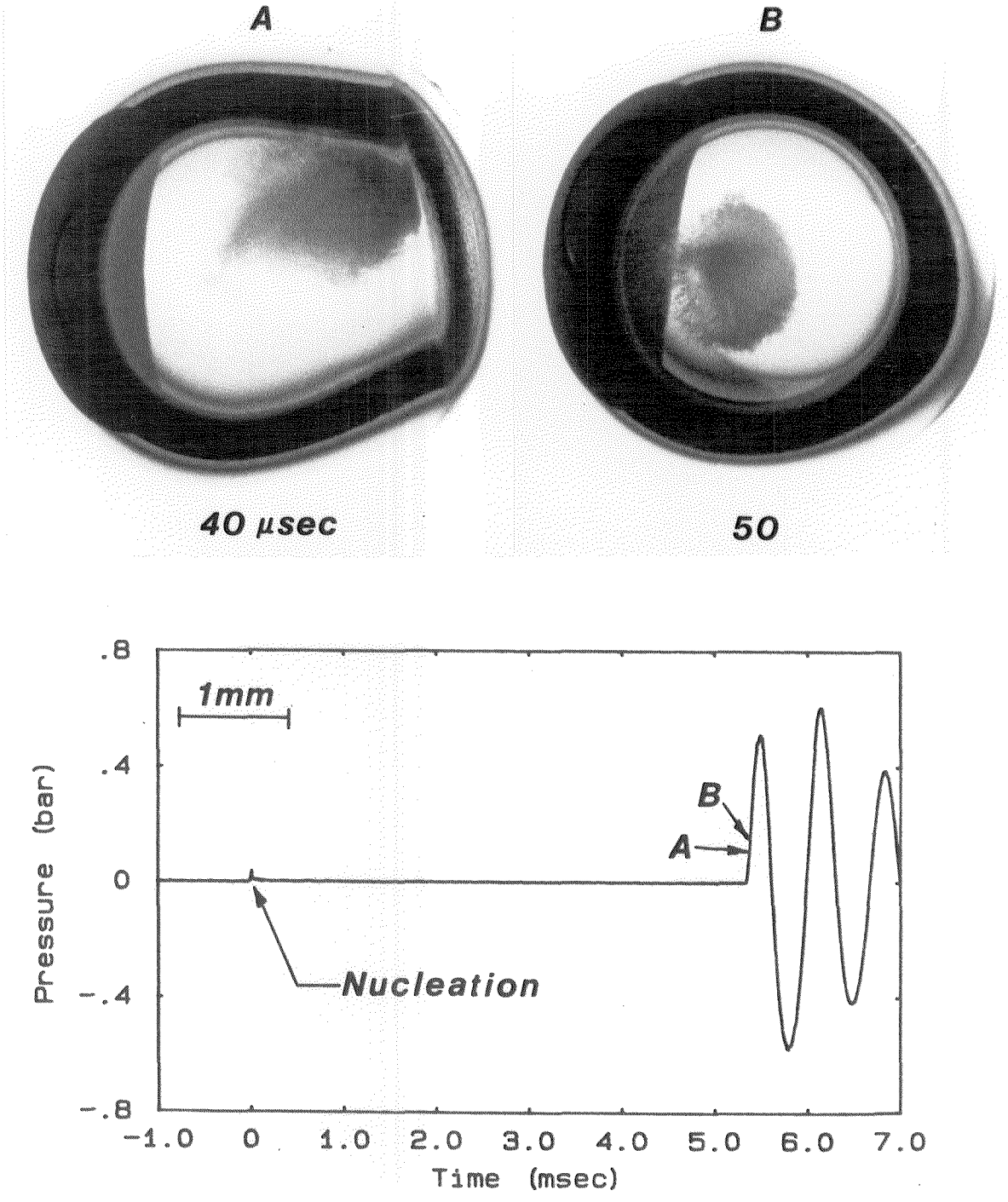

Figure 4.17 Aerosol of fine liquid particles generated by unstable boiling in ether at 3 bar

towards the interior of the bubble. Picture *B* shows a drop in which the remaining liquid is on the side of the bubble away from the viewer and the unstable evaporation forms a jet moving towards the viewer that can be viewed through the transparent bubble. The pressure trace that accompanies the photographs in figure 4.17 demonstrates that the sudden large pressure rise recorded by the transducer corresponds to the onset of the instability. The production of a two-phase flow was also observed during the vapourization of pentane in the transitional boiling regime. For example, in picture *A* of figure 4.16, the fine liquid particles are just visible near the unstable boiling region. Figure 4.18 shows the development of the two-phase evaporatively-driven jet 120 μsec after its initiation in ether.

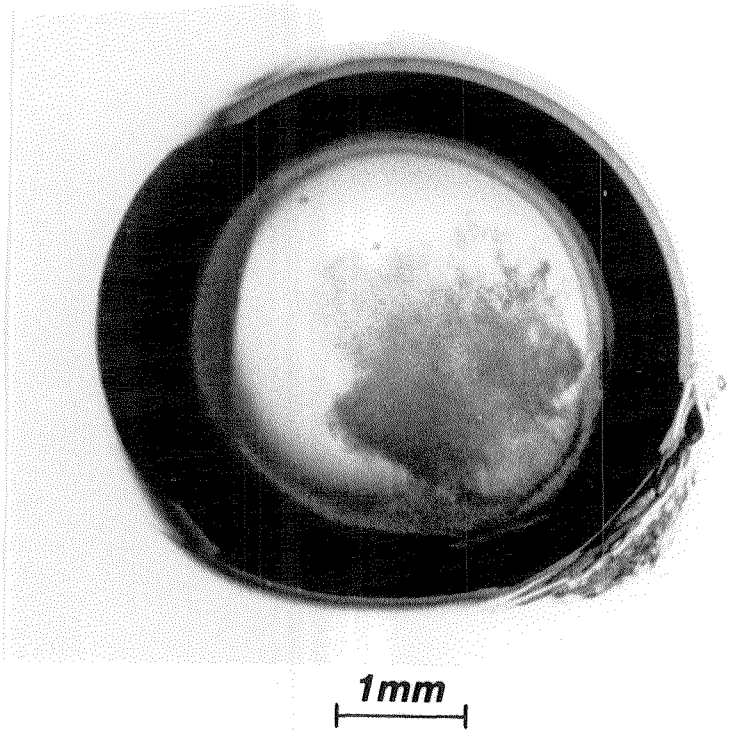

Figure 4.18 View of evaporative jet in ether at 3 bar 120 μsec after the onset of unstable boiling

The unstable boiling produces an eruption of small liquid particles that are

ejected away from the evaporating surface. Note the protrusion of the bubble surface into the host fluid that is caused by the reaction to the thrust of the jet. Occasionally liquid droplets are visible within the bubble that are apparently not related to the fine liquid particles torn from the evaporating interface. The origin of these larger droplets is related to the occurrence of multiple nucleations within the original ether drop. Some ether drops at 3 bar suffer two separate nucleations. When the bubbles grow and coalesce, in some cases a thin filament of liquid remains that breaks up into small droplets. This feature is discussed and illustrated in Appendix C.

The earlier hypothesis by Shepherd & Sturtevant (1982) that during unstable boiling a substantial amount of liquid is torn from the evaporating surface is now confirmed. They measured unstable bubble growth rates from photographs and together with far-field pressure data estimated the evaporative mass flux and the effective density within the bubble. They found that the evaporative mass flux during the unstable boiling of butane at atmospheric pressure was roughly constant at a value of 400 g/cm^2s. The density within the bubble was found to settle down to a nearly constant value of 0.13 g/cm^3 after 50 μsec. If the densities of butane liquid and vapour at the ambient temperature (105°C) are used (ρ_l = 0.46 g/cm^3, ρ_v = 0.045 g/cm^3) this implies that the two-phase flow within the bubble is 20% liquid by volume.

In the present experiments a rough estimate of the jet velocity can be made by measuring the extent of the jet from a photograph and using the time elapsed since the initiation of the jet. The jet length was measured from nine different explosions in which the jet was clearly visible, and the corresponding average jet velocities ranged from 30 to 70 m/s. Evaporation at the head of the jet is not taken into account, so the above velocities probably underestimate the actual velocity of the particles moving away from the evaporating surface. To

estimate the mass flux in the jet the jet density is needed. The densities of ether liquid and vapour at the ambient temperature (150°C) differ only by a factor of ten (ρ_l = 0.52 g/cm^3, ρ_v = 0.056 g/cm^3). Multiplying the vapour density by the average jet velocity of 50 m/s gives a lower bound of 280 g/cm^2s for the evaporative mass flux in the jet. A crude estimate of the mass loading in the jet can be made by considering the opaqueness of the jet. Figure 4.19 shows the development of an evaporative jet in an ether droplet 55 μsec after the onset of unstable boiling.

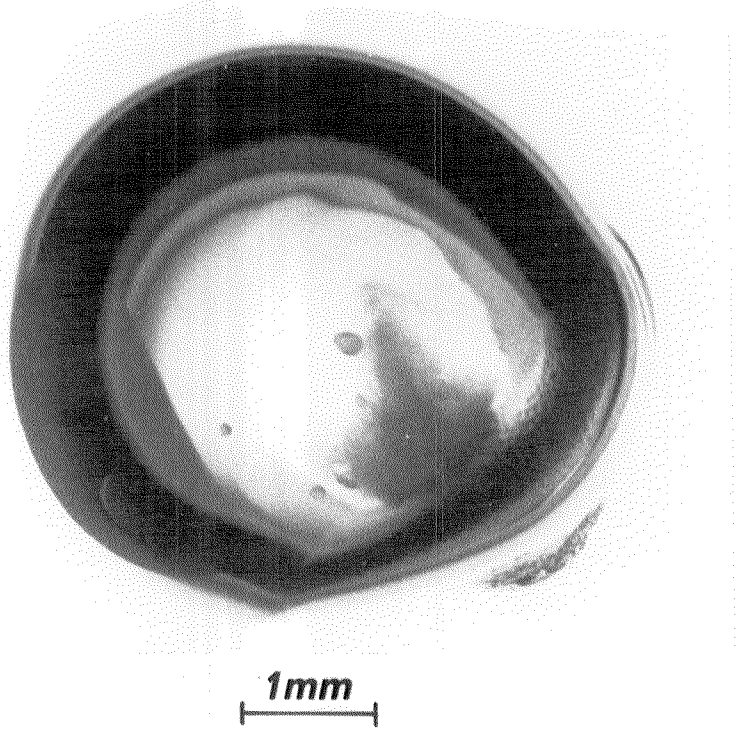

Figure 4.19 Evaporative jet in ether at 3 bar 55 μsec after onset of unstable boiling

By examining the region near the tip of the jet under large magnification, it was estimated that the jet is opaque when its thickness is greater than about 130 μm. Also an upper bound for the size of jet particles was estimated to be 10 μm. For a small particle (that is still large relative to the wavelength of light), the

effective optical cross-section far from the particle is twice the actual projected area of the particle (van de Hulst, 1981). The above information can be used in a simple geometrical calculation to estimate the liquid volume fraction in the jet and the corresponding jet mass flux is found to be about 350 g/cm^2sec. This value for the mass flux is of the same order of magnitude as estimated for butane by Shepherd & Sturtevant (1982).

In some cases, the fluid particles torn from the evaporating surface may reach the other side of the bubble before they evaporate. When the small particles contact the hot host fluid they immediately vapourize in micro-explosions that produce a splattered effect on the bubble surface. Figure 4.20 shows two photographs illustrating the roughening of the bubble surface (visible on the right side of each of the bubbles) that is caused by the internal impact of small volatile liquid droplets.

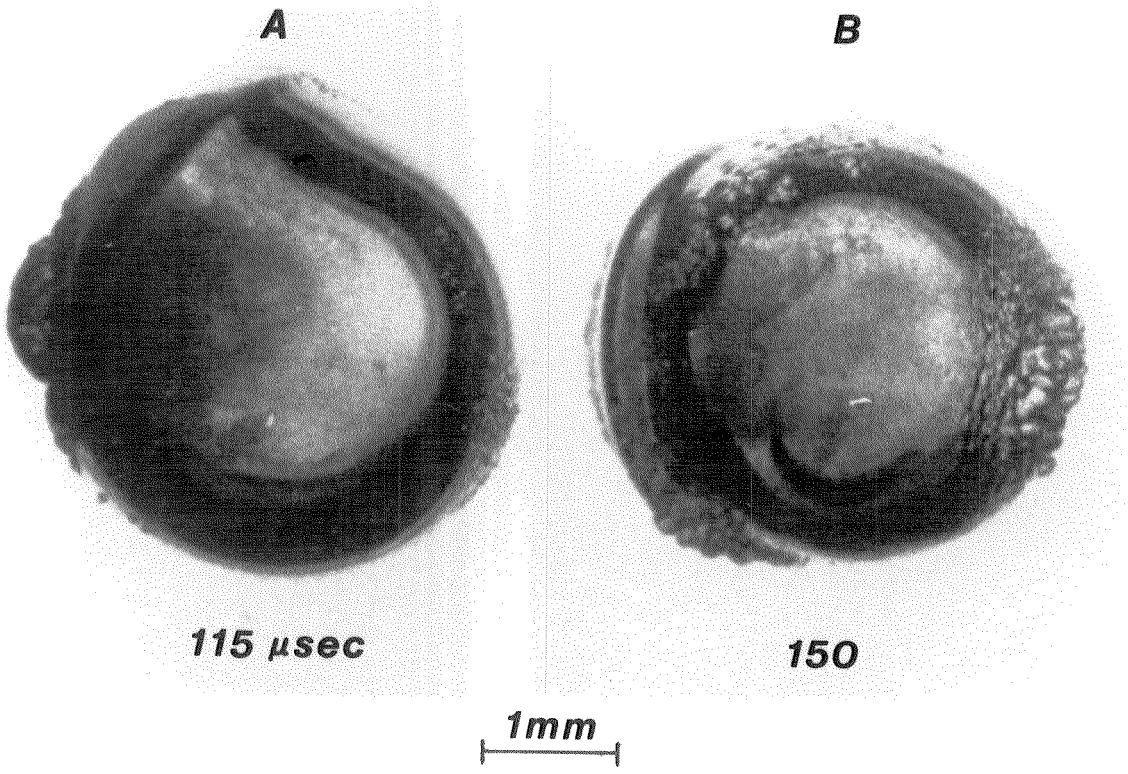

Figure 4.20 Impact of jet particles with the bubble surface

Figure 4.21 shows a photograph of an ether bubble expanding shortly after the explosive boiling phase terminates. The imprint of the liquid cap that existed just prior to the initiation of the explosion is still evident. The pressure trace below the photograph illustrates the pressure fluctuations that are recorded by the transducer as the bubble collapses and oscillates. The radiated pressure field is almost as strong as with fully unstable evaporation at atmospheric pressure. The letters *B* through *E* on the pressure trace correspond to the times for the oscillating bubbles shown in figures 4.22 and 4.23. The bubble in picture *B* was photographed while still in the initial expansion phase. The disturbances on the upper left portion of the bubble surface again indicate the position of the liquid cap just prior to the onset of unstable boiling. The hemispherical bulge on the front of the bubble corresponds to the location where the violent boiling was initiated. The disturbances on the lower right portion of the bubble surface were caused when the spray of liquid particles torn from the evaporating interface contacted the bubble surface. Picture *C* (in figure 4.22) shows the extent of the surface distortions that are caused by the Rayleigh-Taylor instability after only one rebound. The flattening of the left side of the bubbles shown in pictures *C* and *D* is a result of the proximity of the pressure transducer, just out of view to the left of the bubbles. The bubble in picture *E* (figure 4.23) was photographed after 6 volume oscillations and individual small bubbles have begun to break off from the original bubble. The bubble eventually breaks up into a cloud of small bubbles, as at atmospheric pressure.

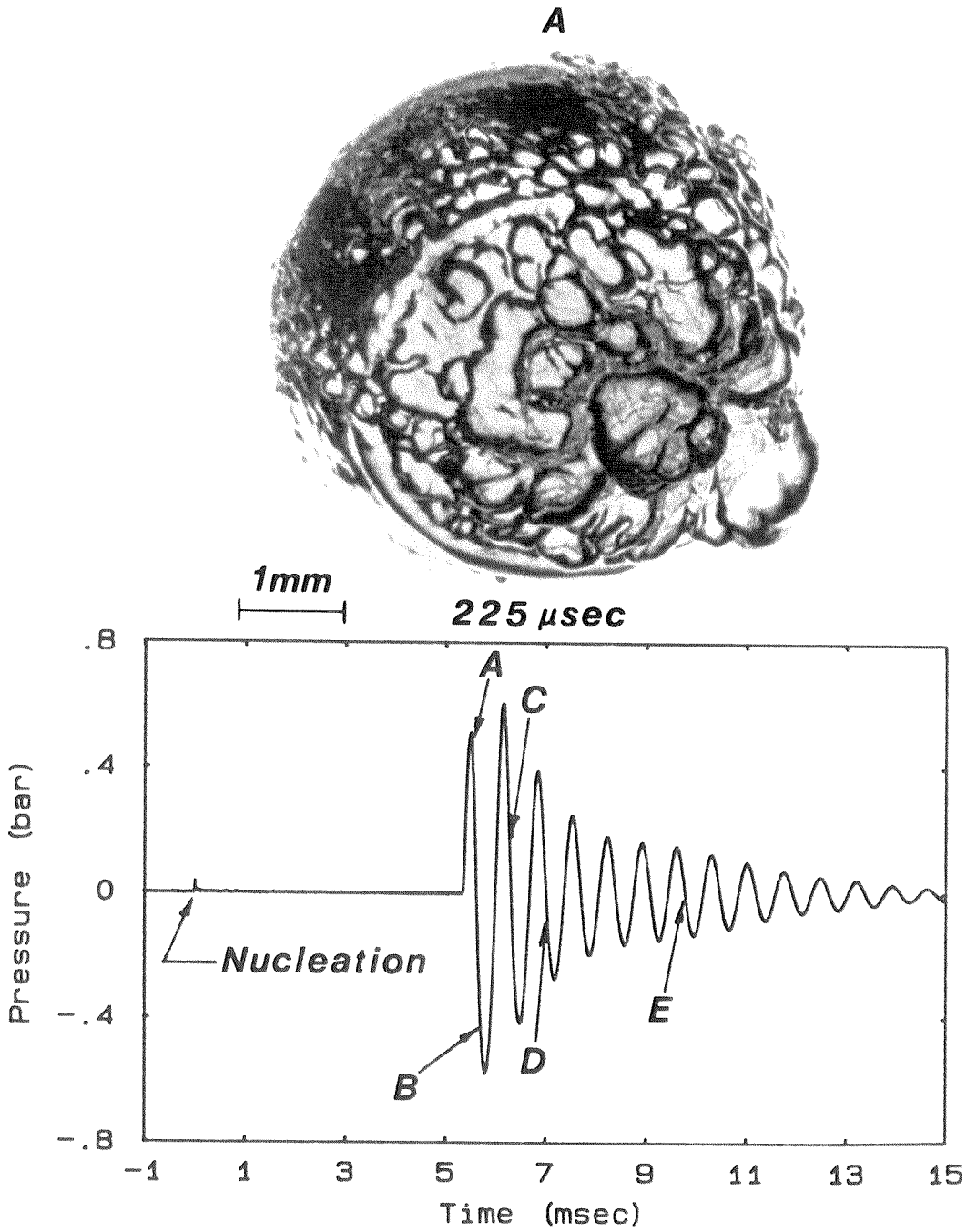

Figure 4.21 Bubble growth after the completion of explosive vapourization

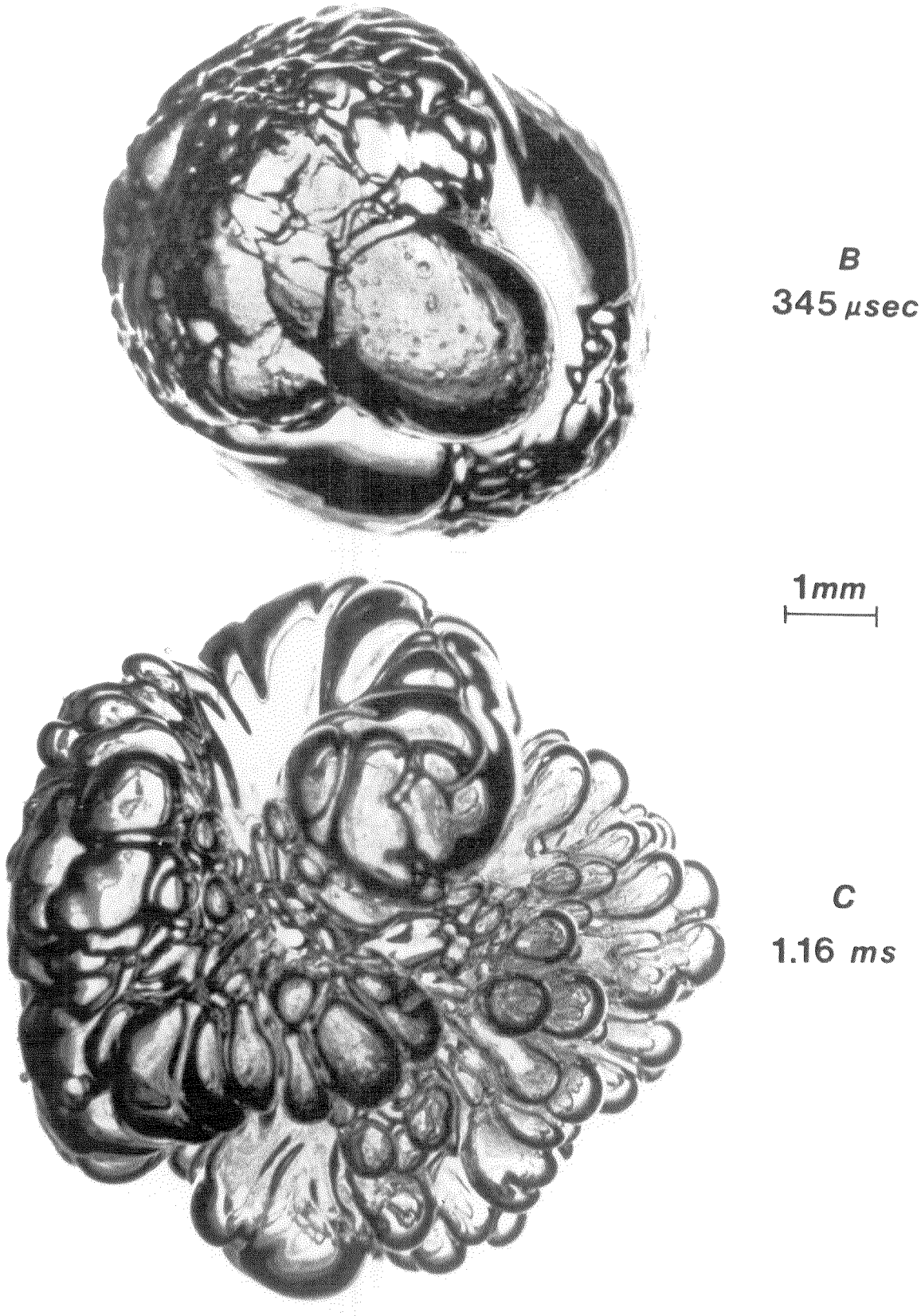

Figure 4.22 First volume oscillation of ether bubbles

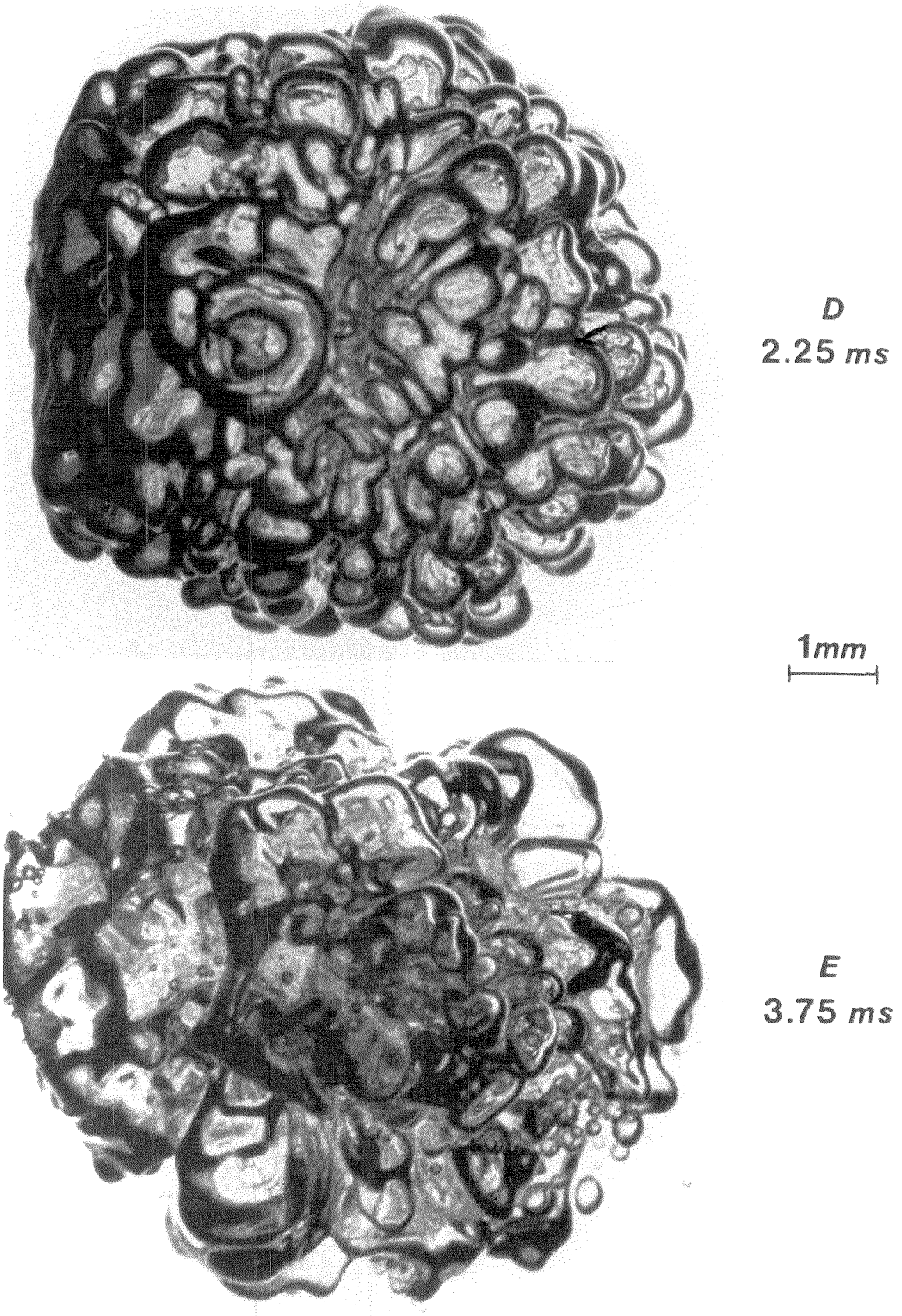

Figure 4.23 Ether bubble oscillations at 3 bar

Chapter 5

DISCUSSION

5.1. Instability Theory

The stability of a plane evaporating liquid surface has been investigated using linear stability theory by several authors, including Miller (1973), Palmer (1976), and more recently by Prosperetti & Plesset (1984). Palmer reviewed the various destabilizing mechanisms that have been proposed and the circumstances under which individual mechanisms dominate. Shepherd (1981) discussed the relative merits of various instability mechanisms for the particular case of evaporation of a liquid at the superheat limit in which the evaporative mass flux plays a dominant role. The paucity of detailed experiment studies of evaporation at extremely high superheats has hampered the testing of the existing theoretical models. At the suggestion of Prof. F. Marble, Shepherd & Sturtevant (1982) proposed that the Landau mechanism of instability, originally described in connection with the instability of laminar flames, applies to rapid evaporation at the superheat limit. In Appendix D several results, derived from the original analysis by Landau (1944), are given that illustrate the physical mechanism that leads to the instability. The Landau instability mechanism is known as the Darrieus instability in France (Marble, 1985), where it was developed independently by Darrieus (1938, 1945), also in the context of the stability of a propagating flame front. In this chapter, the quantitative application of the instability theory to rapid evaporation of a liquid, including the role of ambient pressure, will be discussed for both planar and spherical geometry.

5.1.1. *Planar Landau Instability.* The instability theory contains three physical processes that influence the stability of an evaporating interface: (i) mass flux across the liquid-vapour interface, (ii) acceleration of the fluid normal to the interface and (iii) surface tension. During the growth of a vapour bubble in a liquid boiling at the superheat limit surface tension stabilizes the bubble surface at early times, when the bubble radius is still very small. During a later, thermally-controlled stage of the vapour bubble growth (see Appendix B for a discussion of classical bubble growth theory) the deceleration of the interface stabilizes the surface. Between these two regimes the presence of substantial mass flux across the interface may lead to instability. To quantitatively investigate the stability of the interface, it is necessary to compute the growth rate of a small perturbation applied to the interface. The Landau theory (see Appendix D) yields a dispersion relation between the dimensional growth rate ω and wave number k of a small disturbance. The relation may be rewritten in nondimensional form as follows:

$$\Omega^2 + \frac{2\alpha}{\alpha+1}\Omega K + \frac{1}{\alpha+1}\left[\alpha(\alpha-1)K^2 + \frac{2N_V K + K^3}{2N_I}\right] = 0 \ , \qquad (5.1)$$

where the dimensionless growth rate Ω and wavenumber K are related to the corresponding dimensional quantities (ω, k) by

$$\Omega = \omega \frac{R}{\dot{R}} \qquad K = kR \ , \qquad (5.2)$$

and α is the density ratio ρ_v/ρ_l. In equation (5.1) the effects of surface tension and acceleration are contained in the "inertia number" and the Weber number,

$$N_I = \frac{\rho_l R \dot{R}^2}{2\sigma} \quad , \tag{5.3}$$

$$N_{\ddot{R}} = \frac{(\rho_l - \rho_v)\, R^2 \ddot{R}}{2\sigma} \quad . \tag{5.4}$$

ρ_l, ρ_v, σ, R, $\dot{R}$ and $\ddot{R}$ are the liquid density, vapour density, surface tension, bubble radius, radial velocity, and radial acceleration, respectively. N_I is defined as the ratio of the destabilizing force of the mass flux to the stabilizing force of surface tension, and $N_{\ddot{R}}$ as the ratio of the stabilizing acceleration forces to the surface tension forces. The ratio $N_{\ddot{R}}/N_I$, which is the important parameter in the low wavenumber limit, is the inverse of the Froude number. Sturtevant & Shepherd (1982) used the bubble growth theory of Prosperetti & Plesset (1978) to predict the radial growth R(t) of a smooth butane bubble at the superheat limit. For each time increment they calculated the dimensionless quantities given in equations (5.2) - (5.4), then solved equation (5.1) for the growth rate over a range of wavenumbers. Using this information they constructed a stability diagram for butane at the superheat limit. The result of a similar calculation for ether at atmospheric pressure is shown in figure 5.1. The figure illustrates the range of wavenumbers that is predicted to be unstable ($\omega > 0$) and it indicates that the bubble is subject to linear instability for times substantially smaller than the time of the earliest photographs in the present experiments. The largest length scale that is predicted to be linearly unstable at these early times is of the order of 10 μm. The observed length scale of the instability at much later times (see, for example, figure 3.8) is an order of magnitude larger than this value. Therefore, the observations documented in figures 3.2, 3.6, and 3.7 apparently depict a late, nonlinear and saturated stage of the instability.

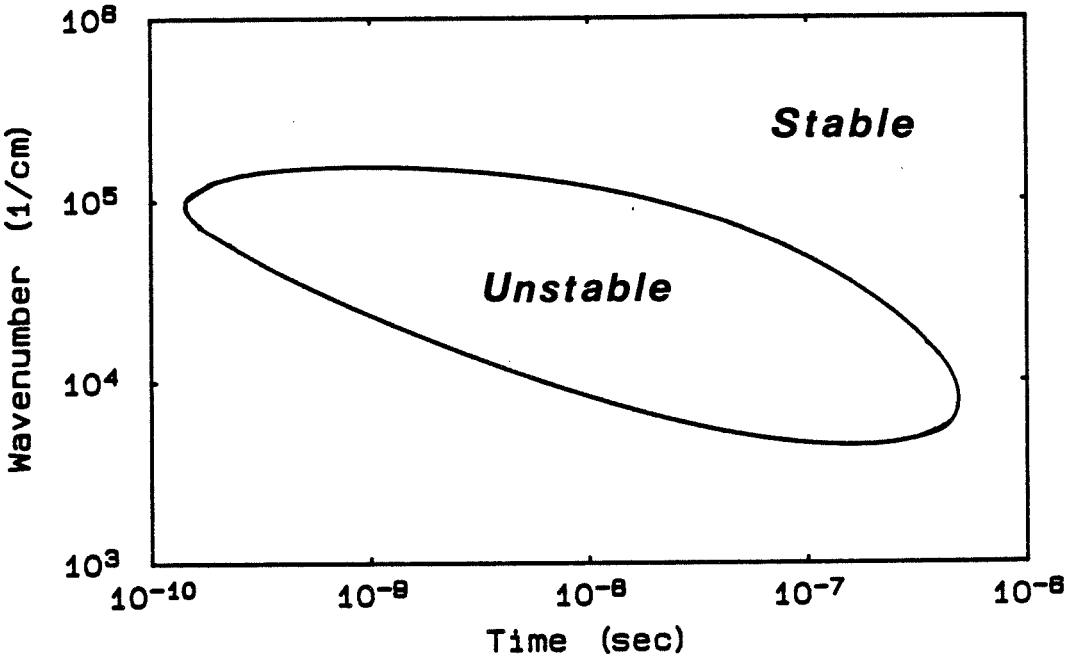

Figure 5.1 Neutral stability curve from planar theory for ether at atmospheric pressure

The nondimensional number

$$F \equiv \omega_{max}\tau \ , \tag{5.5}$$

where ω_{max} is the maximum growth rate at a given pressure and τ is the time interval during which a growing bubble is predicted to be linearly unstable, is a useful parameter to measure the effect of ambient pressure on the predictions of planar instability theory. It is a measure of the number of times the amplitude of a perturbation is exponentiated during the time interval that the interface is linearly unstable. Figure 5.2 shows the effect of ambient pressure on this "figure of merit" for ether. This plot confirms the stabilizing effect of increasing the ambient pressure.

If the behaviour of the figure of merit shown in figure 5.2 is interpreted quantitatively, the plot indicates that the instability that occurs on the surface of a

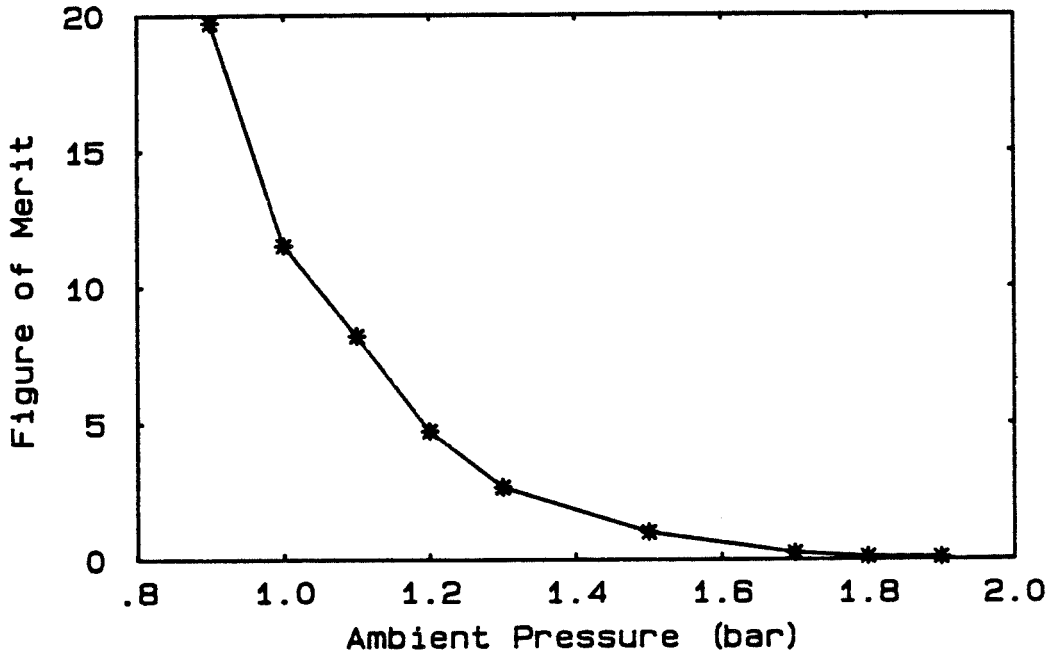

Figure 5.2 Figure of merit from planar theory showing increase of stability with increasing pressure for ether

growing ether bubble at atmospheric pressure may be completely suppressed by raising the ambient pressure to a value of 2 bar. From figure 4.4 it was shown that at 2 bar in ether the instability is suppressed at early times. However, after about 20 μsec, ***after*** the bubble comes into contact with the surface of the drop, the instability is initiated near the host fluid. The effect of the finite size of the drop and the contact of the bubble with the host fluid on the triggering of the instability are not taken into account in the instability theory. The presence of the hot host fluid particularly influences the onset of unstable boiling at early times, when the bubble just comes into contact with the host fluid, and at much later times when only a small amount of liquid remains in the drop during the transitional boiling regime. As a result, the figure of merit provides a measure of the relative susceptibility of a liquid to the instability but does not predict exactly at what ambient pressure the instability will be suppressed completely within a drop boiling at the superheat limit.

The figure of merit is a useful parameter for assessing the relative stability of different liquids. Figure 5.3 shows the variation of the figure of merit as a function of ambient pressure for three different liquids tested in the present experiments.

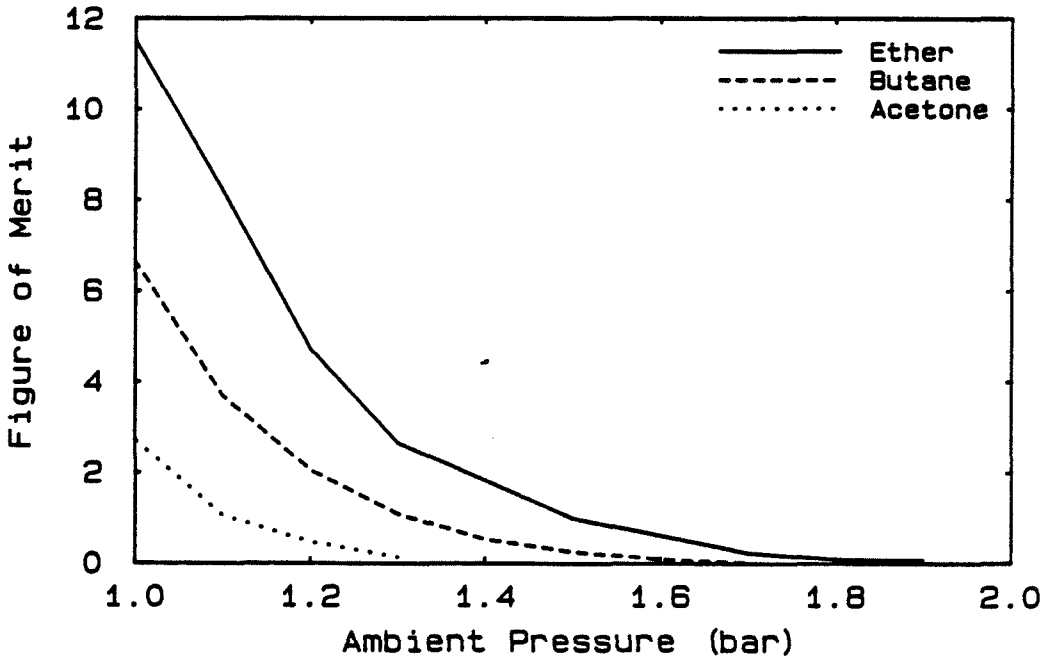

Figure 5.3 Variation of figure of merit with ambient pressure for three different fluids

The figure suggests that acetone is less prone to instability than both butane and ether. For example, at atmospheric pressure the figure of merit for acetone is 2.7, smaller than the corresponding values for butane and ether by factors of more than 2 and 4, respectively. When droplets of acetone were heated to the superheat limit it was observed that they vapourized *stably* at *atmospheric* pressure, in sharp contrast to the violent unstable boiling that occurs in butane and ether at this pressure. On the basis of the fluids tested in the present experiments, it is therefore recommended that for practical estimates of the susceptibility to instability, a figure of merit of 3 be taken as a lower limit for instability.

During stable bubble growth the volatile liquid near the evaporating surface is substantially cooled by the vapourization and the temperature of the liquid at the interface is the saturated liquid temperature corresponding to the ambient pressure. Additional heating by the adjacent host fluid may increase the temperature of the evaporating surface and cause the bubble growth to diverge from the predictions of the classical bubble growth theory (see Appendix B). Because bubble growth rate depends strongly on the bubble surface temperature (and therefore on the ambient temperature), due to the temperature dependence of vapour pressure, the calculated instability growth rates are also strongly temperature dependent. The effect of an increase in the surface temperature was quantitatively investigated for the specific case of ether boiling at an ambient pressure of 3 bar. At this ambient pressure, the instability theory predicts that the bubble surface will be absolutely stable to small disturbances. Experimentally it was found (see §4.5) that ether boils stably at 3 bar for several milliseconds before unstable boiling is triggered. To model this situation in the calculations, the stable bubble growth was allowed to proceed for 5 ms, at which point a small temperature increase was imposed at the evaporating surface to determine the effect on the stability of the surface. It was found that a temperature increase of even only 1°C caused the surface to become unstable to small perturbations. The instability growth rate was a strong function of the temperature increase. For example the calculated exponentiation time (the time for the amplitude of a disturbance to grow by a factor of e) decreases from 80 μsec to 1.2 μsec for temperature increases from 5°C to 30°C, respectively. For ether at an ambient pressure of 3 bar, the *maximum* temperature increase that may occur at the bubble surface, namely the superheat, is 80°C.

Therefore, in any real situation where temperature nonuniformities are present, departures from the quantitative predictions of the theory should be expected. In particular, it is likely that in the regime of transitional stability,

which might occur very frequently in practice, one of a number of different possible kinds of disturbances could serve to trigger a breakdown to violent instability.

5.1.2. *Spherical Geometry.* The application of the planar Landau instability theory to the growth of a spherical bubble is strictly only justified if the scale of the disturbances that develop is much smaller than the bubble diameter and the growth rate of the disturbances is much larger than the characteristic bubble growth rate. To study the effect of surface curvature on the development of the instability, the spherical analog of the Landau instability was applied to rapid evaporation. The Landau instability has been treated for spherical flames by Istratov & Librovich (1969). More recently, Matalon & Matkowsky (1984) have generated a model for the stability of a curved flame in which the effects of thermal expansion and flame structure are included.

The hydrodynamic stability analysis of Istratov & Librovich (1969) develops the perturbations in the form of spherical harmonics. The contributions of harmonics of different index are assumed to be noninteracting. A simple dimensional argument by Zeldovich (1966) shows that disturbances grow more slowly in a spherical system than for the planar case. If ε is the perturbation amplitude, λ the perturbation wavelength and U the radial velocity of the bubble, then

$$\frac{d\varepsilon}{dt} \sim \frac{\varepsilon U}{\lambda} \quad . \tag{5.6}$$

For a plane interface λ is constant and (5.6) leads to exponential growth (with growth parameter $\omega \sim U/\lambda$) for ε. However for a spherical bubble, if there is no energy transfer between modes the wavelength of a given spherical harmonic grows like the radius and (5.6) leads to algebraic growth in time for ε, i.e.,

$$\varepsilon \sim t^{\omega'} \ , \tag{5.7}$$

where ω' is now the (nondimensional) algebraic growth rate.

To apply the spherical analysis to the problem of rapid vapourization, the effects of acceleration and surface tension have been included in the boundary condition at the bubble surface. In this way a quasi-steady model may be formulated for bubbles that are growing with arbitrary velocity, assuming that the instability responds to the instantaneous acceleration and surface tension forces and that the previous history is not important. However, the surface tension terms introduce a coupling between different spherical harmonics and, hence, the assumption that the harmonics are noninteracting is not valid. The surface tension force becomes important at large values of the spherical harmonic index n, corresponding to small wavelengths. For large values of n, if one nevertheless neglects the coupling, the curvature of the interface κ (and, hence, the surface tension force), can be modelled as a function of n, the perturbation amplitude ε, and the radius R, in the following simplified form (Istratov & Librovich, 1969):

$$\kappa = -\varepsilon \frac{n(n+1)}{R^2} \ . \tag{5.8}$$

The resulting dispersion relation between ω' and n is,

$$\omega'^2 + b\ \omega' + c = 0 \ , \tag{5.9}$$

where,

$$b = 3 + \frac{n\,(1+2\alpha n)}{(n+1)\alpha + n}\ , \tag{5.10}$$

$$c = 3 + \frac{\alpha(\alpha n+1)(n^2-1) - \alpha n^2(n-1)}{(n+1)\alpha + n}$$

$$- \frac{n(n+1)\left[N_\psi - \dfrac{n(n+1)}{2}\right]}{\left[(n+1)\alpha + n\right] N_I}\ . \tag{5.11}$$

Figure 5.4 shows neutral stability contours in ether at various pressures.

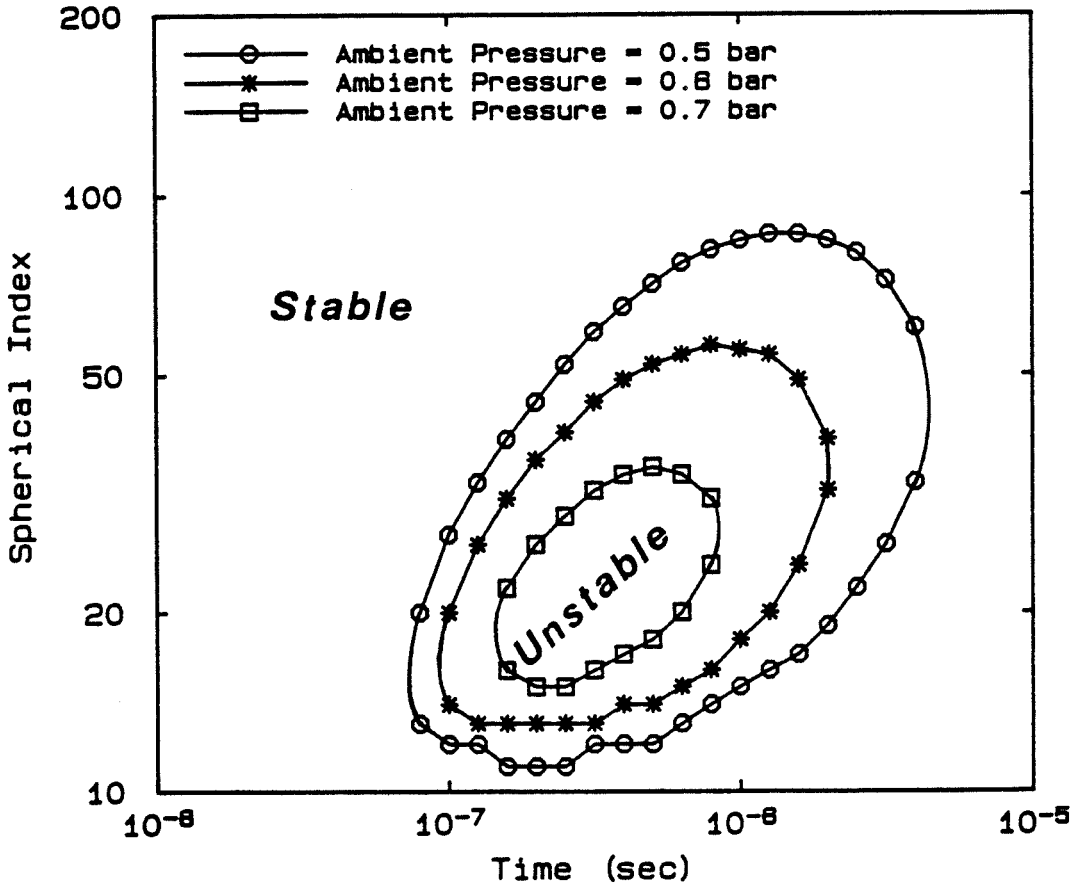

Figure 5.4 Neutral stability curves from spherical theory for ether at several ambient pressures

Kinks appear in the lower sections of the curves because only integral values of the spherical harmonic index, n, are considered due to the spherical constraint. Positive values of ω' indicate that the perturbation amplitude grows more rapidly than the radius, leading to instability. Note that the unstable region shrinks with increasing pressure and in fact at atmospheric pressure the interface is predicted to be stable at all times. This is in disagreement with the experimental results, from which it is clear that the instability is present at atmospheric pressure. Apparently the instability occurs at such small wavelengths that mode-hopping induced by surface tension causes the behaviour to be similar to a planar interface and so the spherical constraint does not hold.

An alternative explanation of the experimental observations is that the spherical theory strictly only applies at very early times in the growth of the vapour bubble, before the bubble contacts the surface of the drop. In fact, the earliest photographs taken at atmospheric pressure are consistent with the predictions of the spherical theory in that the surface of the vapour bubble appears smooth (see photographs *A* and *B* in figure 3.1). When the bubble comes into contact with the host fluid a portion of the bubble surface becomes nonevaporating and the spherical symmetry of the evaporating surface is destroyed. The onset of the instability is observed to occur shortly after the collision between the growing vapour bubble and the host fluid. When evaporation takes place across only a fraction of the bubble surface, the stability of the evaporating interface is apparently described most closely by the planar instability theory.

5.2. Behaviour of Unstable Boiling

5.2.1. *Role of Liquid Properties.* Similar dynamical features were observed during the boiling of each of the four liquids photographed in the present experiments (pentane, isopentane, ether, and butane). Some liquids were not studied over as wide a range of ambient pressures as others, so that *all* of the features have not been observed in *all* of the liquids. The instability was observed to occur in each of the fluids, although the ambient pressure at which a smooth interface is first observed varies with the liquid. The effect of surface tension and Jakob number on the behaviour of unstable boiling will now be discussed.

5.2.1.1 *Surface Tension.* Table 5.1 lists, for four different fluids, the surface tension at the saturation temperature corresponding to atmospheric pressure and the lowest ambient pressure, p_{min}, at which completely stable boiling of a least one droplet was observed.

Table 5.1. Effect of Surface Tension on Onset of Instability

Liquid	σ(@ T_{sat}) (dyn/cm)	p_{min} (bar)
Acetone	20.0	1.0
Ether	15.3	3.0
Butane	14.9	4.0
Isopentane	14.1	4.3

With increasing ambient pressure, the saturation temperature increases and the surface tension for each liquid falls although the relative ranking of surface tension between the liquids shown in table 5.1 remains the same. The general trend is that for liquids with high surface tensions a smaller increase in ambient pressure above atmospheric pressure is necessary to suppress the instability than

with liquids with lower surface tensions. This stabilizing effect of surface tension was also noted earlier in the context of the very early stages of vapourization. It was suggested that the dual appearance of the vapour region at early times (see figure 3.2) is a result of the large gradients in surface tension at the edge of the drop.

5.2.1.2 *Jakob Number*. The Jakob number, defined at saturated conditions as

$$Ja = \frac{c_p(T_{sat})(T_{sl} - T_{sat})}{L(T_{sat})} , \qquad (5.12)$$

is the ratio of the enthalpy loss in the liquid in the thermal boundary layer surrounding the bubble to the latent heat required for evaporation. Many authors also include the factor ρ_l/ρ_v in the definition for the Jakob number (also called the *Jakob modulus*). The effect of ambient pressure on the Jakob number is shown in figure 5.5. Raising the ambient pressure increases the saturation temperature. With increasing temperature the variations in both the heat capacity and latent heat (c_p increases and L decreases) tend to increase the Jakob number. However the reduction in superheat dominates the other factors in equation (5.12) and the Jakob number declines with increasing ambient pressure.

The maximum far-field overpressure from each exploding drop recorded in these experiments is a measure of the explosive force generated after the onset of instability, but is not a direct function of the Jakob number, which is a measure of the thermal energy available for evaporation. Nevertheless, to gain insight into the role of the Jakob number, it is interesting to consider whether the overpressure correlates with the Jakob number. Table 5.2 shows typical maximum overpressures recorded 5 mm away from exploding droplets of

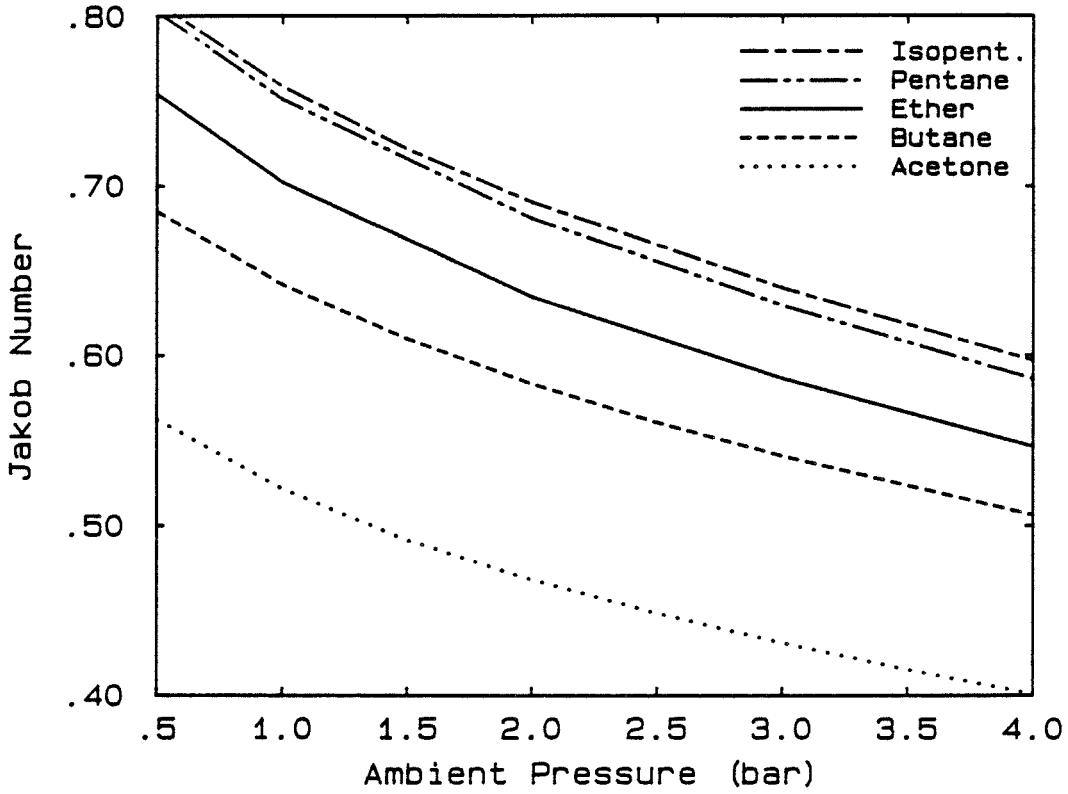

Figure 5.5 Effect of ambient pressure on the Jakob number

different fluids, each with a diameter of 1.5 mm.

Table 5.2. Selected Values of Radiated Overpressure

Liquid	Ambient Pressure (bar)	Overpressure (± 0.05 bar)	Jakob No.
Ether	3.0	0.5	0.59
Butane	3.0	0.2	0.54
Pentane	4.0	0.3	0.59
Butane	4.0	0.1	0.51

The values shown are representative overpressures generated during explosive boiling at ambient pressures of 3 and 4 bar. Other fluids tested at other

pressures show similar trends. At a given ambient pressure, the liquids with the higher Jakob numbers boiled more violently. For a given fluid, the radiated overpressure also decreases with increasing ambient pressure. Acetone has the lowest Jakob number of the liquids tested (see figure 5.5) and was the most stable. In fact, the presssure field radiated by a stably growing acetone vapour bubble had such a small magnitude that it was insufficient to trigger the electronics that produce a signal to fire the spark gap. As a result no photographs were obtained for acetone boiling at the superheat limit.

5.2.2. *Quasi-Steady Boiling.* Shepherd & Sturtevant (1982) found that after the evaporative instability becomes nonlinear the evaporation process appears to be quasi-steady, with the bubble radius increasing at a constant rate and the evaporative mass flux remaining at a roughly constant value. They presented an empirical model of evaporation after the onset of the instability that was consistent with their observations. It is now clear that during unstable boiling a two-phase jet laden with small liquid particles is generated at the evaporating surface. In light of the observations, it is instructive to consider the implications of a quasi-steady unstable boiling process for the energy balance at the interface. Suppose that β is the fraction of the liquid at the unstably evaporating interface that is converted into vapour, or in other words the mass fraction of vapour in the two-phase region. Then energy conservation at the interface may be written as

$$\frac{1}{2}J\left[W_{2\varphi}{}^2 - W_l{}^2\right] + \left[k_l \frac{dT_l}{dz} - k_{2\varphi} \frac{dT_{2\varphi}}{dz}\right] + \beta JL = 0 \ , \qquad (5.13)$$

where J is the mass flux, W is the velocity relative to the interface, k is the thermal conductivity, L is the latent heat of evaporation and the subscripts l and 2φ refer to the liquid and two-phase regions respectively. In the two-phase flow

region downstream of the interface it is assumed that there is no relative motion between the vapour and the fine liquid particles so that a single velocity, $W_{2\phi}$, may be defined in this region. The coordinate z is perpendicular to the interface and directed from the liquid into the two-phase region. The frame of reference is chosen so that the unperturbed interface is the plane $z = 0$. A small surface-entropy term has been neglected in equation (5.13) (Prosperetti, 1979). The kinetic energy terms in equation (5.13) are several orders of magnitude smaller than the latent heat term and can be neglected. If the temperature gradient in the two-phase region is also assumed to be much smaller than in the liquid, the boundary condition (5.13) may be approximated by

$$k_l \frac{dT_l}{dz} + \beta JL \simeq 0 \quad . \tag{5.14}$$

With the assumption of quasi-steady flow during unstable boiling, an estimate for the value of β may be obtained by considering the energy equation. The one-dimensional energy equation for the steady flow of an incompressible, inviscid fluid is

$$W \frac{dT}{dz} = D \frac{d^2T}{dz^2} \quad , \tag{5.15}$$

where D is the thermal diffusivity $k/\rho C_p$. A solution of this equation for the temperature in the liquid T_l, using the boundary conditions T = T_b and (5.14) at z = 0, is

$$T_l = T_b + \frac{\beta L}{C_p}(1 - e^{W_l z/D_l}) \quad . \tag{5.16}$$

Taking the limit $z \to -\infty$ in the above and solving for β gives

$$\beta = \frac{C_p(T_\infty - T_b)}{L} \quad . \tag{5.17}$$

Just after the onset of unstable boiling, $T_b \simeq T_{sat}$, so the mass fraction of vapour in the two-phase jet is initially just given by the Jakob number (for example, β = 0.59 for ether at an ambient pressure of 3 bar).

During unstable boiling, the proximity of the hot host fluid to the evaporating interface may lead to an increase in the evaporating surface temperature, particularly at late times when only a small amount of liquid remains in the drop. This behaviour was illustrated in figure 4.6 in which the last portion of liquid in drops of butane vapourized especially violently. During this late boiling stage, the evaporative mass flux is enhanced and a larger fraction of the flow generated at the evaporating surface appears to be liquid. The liquid drops that are torn from the interface are much larger than at earlier times and many do not evaporate until contacting the host fluid. This behaviour is consistent with the prediction of equation (5.17). If the interface temperature T_b increases, from (5.17) β decreases and therefore a larger proportion of the mass in the evaporative jet is liquid. In physical terms, when T_b increases, the enthalpy loss that is experienced by liquid approaching the interface (which supplies the latent heat needed for evaporation) decreases, and as a result a smaller fraction of the liquid at the interface is converted into vapour.

Chapter 6

CONCLUSIONS

The effect of ambient pressure on the dynamical behaviour of a single droplet (1-2 mm diameter) of volatile liquid boiling explosively at the limit of superheat has been studied experimentally and theoretically. The investigation was motivated by a desire to obtain a more detailed physical understanding of the evaporative instability observed earlier by Shepherd & Sturtevant (1982) during the rapid vapourization of butane droplets at atmospheric pressure. High-speed microphotography and fast-response pressure instrumentation have been used to demonstrate the occurrence of the instability in three other fluids (pentane, isopentane, and ether) at atmospheric pressure. The generality of the wide variety of phenomena observed previously in butane has been confirmed for the three other fluids tested. In addition, several remarkable new features have been documented that occur during rapid boiling at elevated pressures. The most important results of the present work are (i) that the strong moderating influence of high ambient pressure on the unstable boiling of a droplet is directly attributable to suppression of the instability, and (ii) that during violently unstable boiling small liquid particles are torn from the evaporating liquid surface. This ejection of fine droplets produces a mass flux orders of magnitude greater than that characteristic of ordinary boiling. A summary of the main experimental results is given in the following.

Raising the external pressure lowers the superheat attained at the superheat limit which decreases the vapourization rate. At high pressure (for example, above 4 bar for ether and above 4.5 bar for butane), boiling consists of normal slow vapourization from a smooth interface. The behaviour in this regime is

remniscent of that of liquids boiling at lower superheats, where the bubble surface usually has a smooth, glassy appearance. Estimated bubble growth rates show reasonable agreement with existing theories for the growth of a vapour bubble in a uniformly superheated liquid. In this stable boiling regime the vapourization process is relatively benign, in that the radiated overpressure produced by bubble growth remains at a very low level (typically less than 0.005 bar 5 mm away from the drop) during vapourization.

At intermediate pressures (for example, about 3 bar for ether and between 3.5 and 4 bar for pentane), a transitional regime of stability occurs in which a drop initially vapourizes *stably* for several milliseconds. When only a small amount of liquid remains in the drop in the shape of a thin cap, the liquid-vapour interface of the stably vapourizing liquid develops incipient instability waves (with a wavelength on the order of 100 μm) that give the interface an *orange-peel* appearance. Heat transfer from the surrounding hot host fluid to the liquid at the evaporating surface initiates violent boiling at the edge of the liquid cap. The onset of unstable boiling severely distorts the evaporating interface, greatly increasing the surface area available for evaporation. The subsequent rapid vapour production and bubble expansion generate a radiated pressure field two orders of magnitude larger than during stable boiling. Fine liquid particles ejected from the interface during unstable boiling form a high-speed two-phase jet that is propelled away from the evaporating surface. The transient jet has a high momentum flux, and a portion of the bubble surface protrudes into the host fluid in reaction to the thrust of the jet. The estimated evaporative jet mass flux in ether droplets is of the same order of magnitude as the mass flux calculated earlier by Shepherd & Sturtevant (1982) for the unstable boiling of butane. After the remaining liquid in the drop has completely vapourized, the net overpressure within the bubble is relieved by violent volume oscillations of the gas bubble. The large accelerations experienced by the bubble at

this time lead to a catastrophic deformation of the bubble surface through the action of the Rayleigh-Taylor instability.

Lowering the external pressure increases the susceptibility of a liquid to the instability by increasing the *pre-instability* mass transfer rate. As a result the time delay between nucleation and onset of unstable boiling is decreased. This effect was observed in all the liquids tested, although at a given ambient pressure some liquids are more susceptible to the instability than others. At atmospheric pressure, the instability is triggered during the initial stages of bubble growth. For example, in ether the onset of the instability occurs less than 8 μsec after nucleation, shortly *after* the initially smooth vapour bubble contacts the surface of the droplet. Heterogeneous nucleation then spreads out along the surface of the drop while disturbances (with a length scale on the order of 100 μm) distort the *unstably* evaporating interface within the drop, substantially enhancing the vapourization rate, and hence the rate of mass and energy transfer. The explosion of even a small droplet produces an audible pop in contrast with the acoustically quiet boiling at high pressure. In the present experiments, contact between the growing vapour bubble and the host fluid plays a role in the initiation of the instability although in some cases (e.g., at high pressure) it is not sufficient to trigger the instability. As a result, the occurrence of the instability for a spherical vapour bubble growing in a superheated liquid of *infinite* extent has not been conclusively demonstrated. However, under conditions in which the liquid is highly susceptible to the instability (e.g., at low ambient pressures), it is likely that the instability will occur even in the absence of contact between the vapour bubble and a nonvolatile host fluid.

The interesting dynamical effects observed after the onset of unstable boiling in earlier experiments with butane at atmospheric pressure were also observed in other liquids in the present experiments. For example, after the vapour

bubble contacts the host fluid a portion of the bubble surface becomes nonevaporating and protrudes into the host fluid. The growth of this characteristic smooth bulge is driven by the two-phase jet that leaves the evaporating surface and impinges on the surrounding fluid. At early times, droplets torn from the evaporating surface and entrained into the jet remarkably always evaporate before the jet contacts the host fluid. At late times heat transfer from the surrounding nonvolatile fluid enhances the vapourization rate and the last portion of liquid in a drop boils particularly violently. Droplets ejected from the evaporating interface at this time are large enough that they remain intact to splatter the bubble surface.

During unstable boiling, the nonevaporating portion of the bubble surface displays a considerable amount of small-scale structure that is a remnant of the contact between the highly distorted evaporating interface and host fluid. After evaporation is completed and the bubble expands, the surface becomes smoother through the action of surface tension. Droplets exploding at subatmospheric pressures experience the most rapid vapourization rates and the convoluted bubble surface exhibits a structure with a very fine scale. The shorter characteristic time for a droplet to evaporate at low pressure tends to diminish the smoothing effect of wave-spreading on the bubble surface. Ether has been tested down to an absolute ambient pressure of 0.25 bar (where the superheat attained, 145°C, is more than twice that attained at 4 bar!), and at this value temperature gradients within a drop produce spatial variations in vapourization rate. The cooler central portion of the evaporating interface is relatively smooth whereas the outer band of the surface near the hot host fluid is highly distorted, indicating intense unstable boiling.

The various liquids that have been tested display small variations in behaviour and *all* the features described above have not been observed in *all* of

the liquids. However, the stabilizing effect of increasing ambient pressure on bubble growth has been observed for each liquid although the ambient pressure at which a smooth interface is first observed varies with the liquid. Surface tension tends to stabilize an interface against onset of instability. Liquids with higher surface tensions tend to boil stably at lower pressures than liquids with lower surface tensions. The nondimensional Jakob number, the ratio of the enthalpy loss in the thermal boundary layer surrounding the bubble to the latent heat required for evaporation, is a useful parameter to correlate the relative violence of unstable boiling between different liquids. The Jakob number, like the superheat, is a measure of the departures from ordinary boiling that occur during explosive boiling at the superheat limit. Increasing the ambient pressure decreases the superheat and Jakob number, which causes the vapourization rate to decrease. For a given ambient pressure, the liquids with the higher Jakob numbers boiled more rapidly and generated higher radiated pressures (a measure of boiling violence) during bubble growth. Of the liquids tested, acetone had the lowest Jakob number and highest surface tension (@ T_{sat}), and was the only liquid to boil stably at atmospheric pressure.

The Landau mechanism for the instability of laminar flames has been adapted to the case of evaporation to investigate the effects of variable ambient pressure for a variety of liquids. The linear theory treats the stability of an interface between fluids of different density with substantial mass flux across the interface. A spherical version of the theory, applicable before the vapour bubble contacts the droplet surface, predicts absolute stability at atmospheric pressure. This is in agreement with photographs showing stable bubble growth shortly after the initial nucleation. At later times evaporation takes place across only a fraction of the bubble surface and the spherical constraint is clearly inappropriate. The instability occurs at wavelengths that are much smaller than the curvature of the evaporating interface, and planar theory

yields results in general agreement with observation. From the planar theory, a parameter has been defined as the product of the maximum growth rate and the time interval that the bubble surface is predicted to be linearly unstable. This "figure of merit" measures the sensitivity of a liquid to instability. For practical estimates of the susceptibility of a liquid to instability it is suggested that a value of 3 of this parameter be taken as a lower limit for instability. The sensitivity of the instability to temperature suggests that small temperature nonuniformities may be responsible for quantitative departures of the behaviour from predictions. Shepherd & Sturtevant (1982) noted that after the onset of instability the evaporation process seems to be quasi-steady. The implications of this relatively simple behaviour have been discussed in light of the current experimental results.

The present observations present a clear view of the substantial departures from ordinary boiling that occur when a liquid boils at the superheat limit. Extrapolating near-equilibrium models of bubble growth to the superheat limit is doomed to failure if the stability of the evaporating interface is not considered. The significant effect of the evaporative instability on the vapourization process is relevant to large-scale vapour explosions that occur in practice, and represents an additional factor that is not accounted for in existing models of fuel-coolant interactions. The applicability of the current experimental results to a larger class of fluids, particularly ones with industrial importance, still has to be verified in detail. The present results serve to emphasize that a great deal of experimental research at small scale must still be done before sufficient information is available to properly model vapour explosions and to predict their severity.

Appendix A

ASYMMETRIC BUBBLE COLLAPSE

The shape of a collapsing vapour bubble can be strongly influenced by the proximity of the pressure transducer baffle within the test section. The cylindrical transducer baffle is mounted close to the exploding droplets (see configuration A in figure 2.3) to obtain a signal that is used to trigger the light source during early times in the vapourization process. However, after the vapourization is complete, the resulting vapour bubble may come into contact with the transducer baffle. When the bubble begins to collapse, the presence of the baffle impedes the collapse of the portion of the bubble that is closest to the baffle. The resulting asymmetric collapse of the bubble is illustrated in figure A.1 which shows four different bubbles of ether vapour collapsing at atmospheric pressure. The blunt end of the cylindrical transducer baffle is visible to the left of each of the bubbles and the small dark circle on the end of baffle indicates the active surface of the pressure transducer.

Figure A.2 shows a typical pressure trace recorded by the transducer with an indication of the times that correspond to the pictures shown in figure A.1. The pressure rises sharply during the vapourization of the drop and reaches a maximum when the drop is completely vapourized. The pressure falls to a minimum as the bubble expands to its maximum size. Picture A in figure A.1 was taken shortly after the bubble has started its initial collapse. The section of the bubble farthest from the baffle develops surface distortions during collapse (picture B) and at the minimum radius a portion of the bubble nearly separates from the bulk of the bubble (picture C). Picture D was taken shortly after the bubble has begun to rebound from the initial collapse. The rapid outward radial

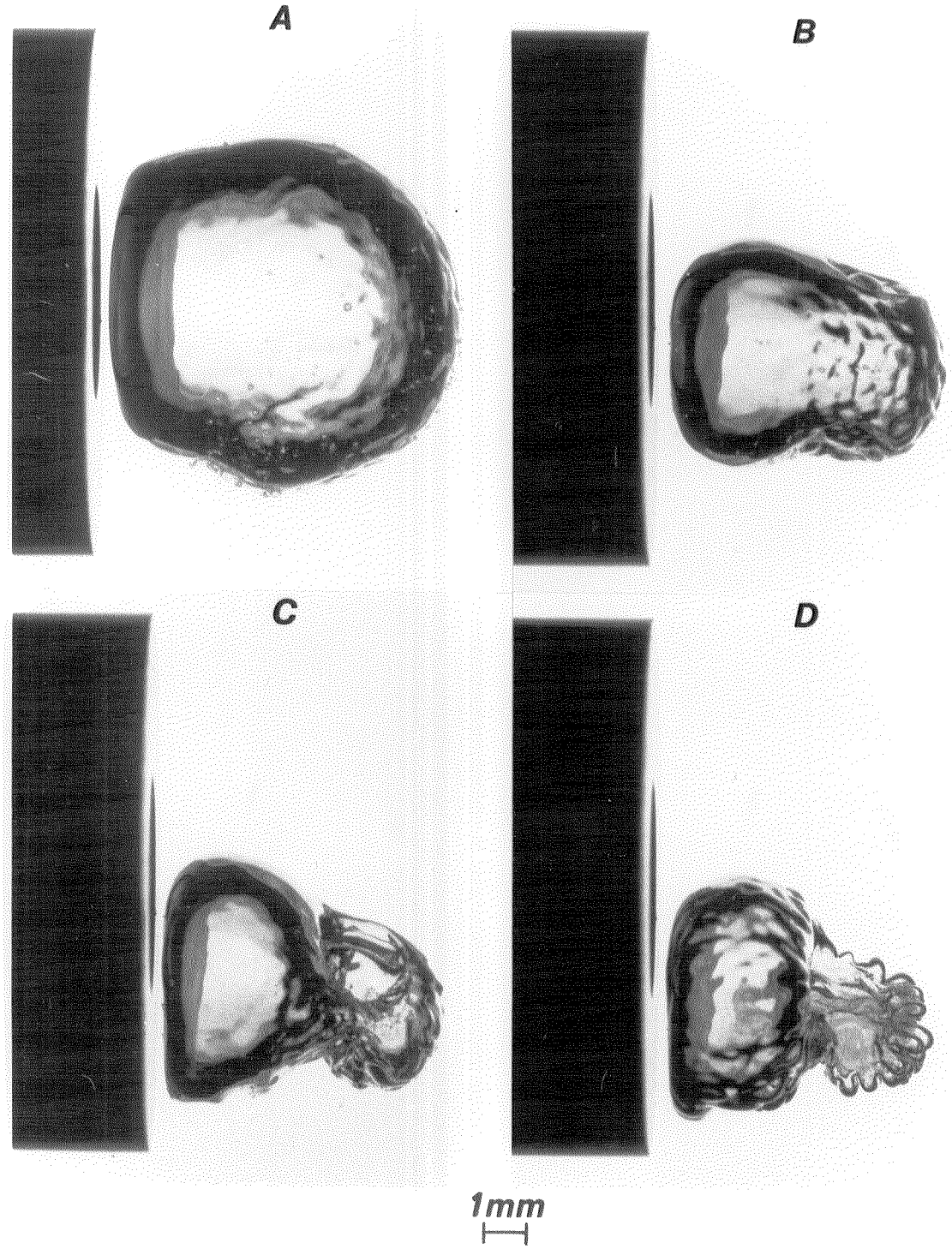

Figure A.1 Ether bubbles near the transducer baffle collapsing at atmospheric pressure

acceleration of the right part of the bubble causes the bubble surface to develop a *fingering* structure (due to the Rayleigh-Taylor instability) that is characteristic of interfaces between fluids of different density that are subject to large normal accelerations.

The asymmetrical bubble collapse shown in figure A.1 is remniscent of the behaviour of collapsing cavitation bubbles near or attached to a wall. An extensive body of experimental and numerical work (reviewed in detail by Plesset & Prosperetti, 1977) has been carried out to investigate the collapse of a cavitation bubble in the vicinity of a rigid boundary. Examples of the experimental results can be found in Benjamin & Ellis (1966) and Lauterborn & Bolle (1975), and compared with the numerical investigation of Plesset & Chapman (1971). In the dynamics of an oscillating cavitation bubble the heat transfer associated with evaporation is usually negligible and the motion is controlled by the inertia of the surrounding liquid (Plesset & Prosperetti, 1977). The dynamics of a bubble produced by the vapourization of a superheated drop differs somewhat from the behaviour of *cold* cavitation bubbles. The bubbles observed in the present experiments are filled with vapour that impedes the collapse of the bubbles. As a result, the minimum bubble radius is not nearly as small as for a typical cavitation bubble and the surface distortions at the minimum radius are readily visible.

The asymmetric collapse of a cavitation bubble near a wall leads to the formation of a high-velocity jet that is directed towards the wall. A similar strong jet has not been observed for the vapour bubbles collapsing near the transducer baffle in the present experiments. However, figure A.3 shows one photograph that provides evidence that a weak jet of vapour may penetrate the body of the bubble and impinge on the transducer baffle. The figure shows a bubble of isopentane vapour expanding after the initial collapse of the bubble. The time the

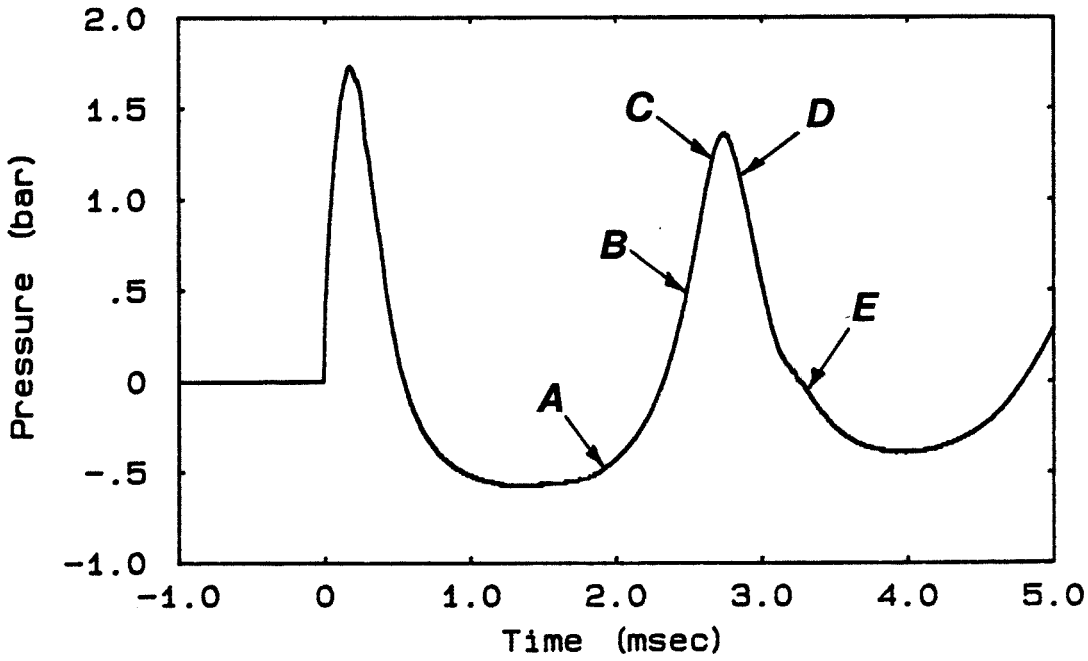

Figure A.2 Pressure recorded during bubble collapse and oscillation. The letters A to E refer to the times for the pictures shown in figures A.1 and A.3.

photograph was taken is indicated on the pressure trace in figure A.2. The small-scale roughness that is visible on the surface of the bubble closest to the transducer may have been caused by the formation of a reentrant jet of vapour during the collapse of the righthand portion of the bubble.

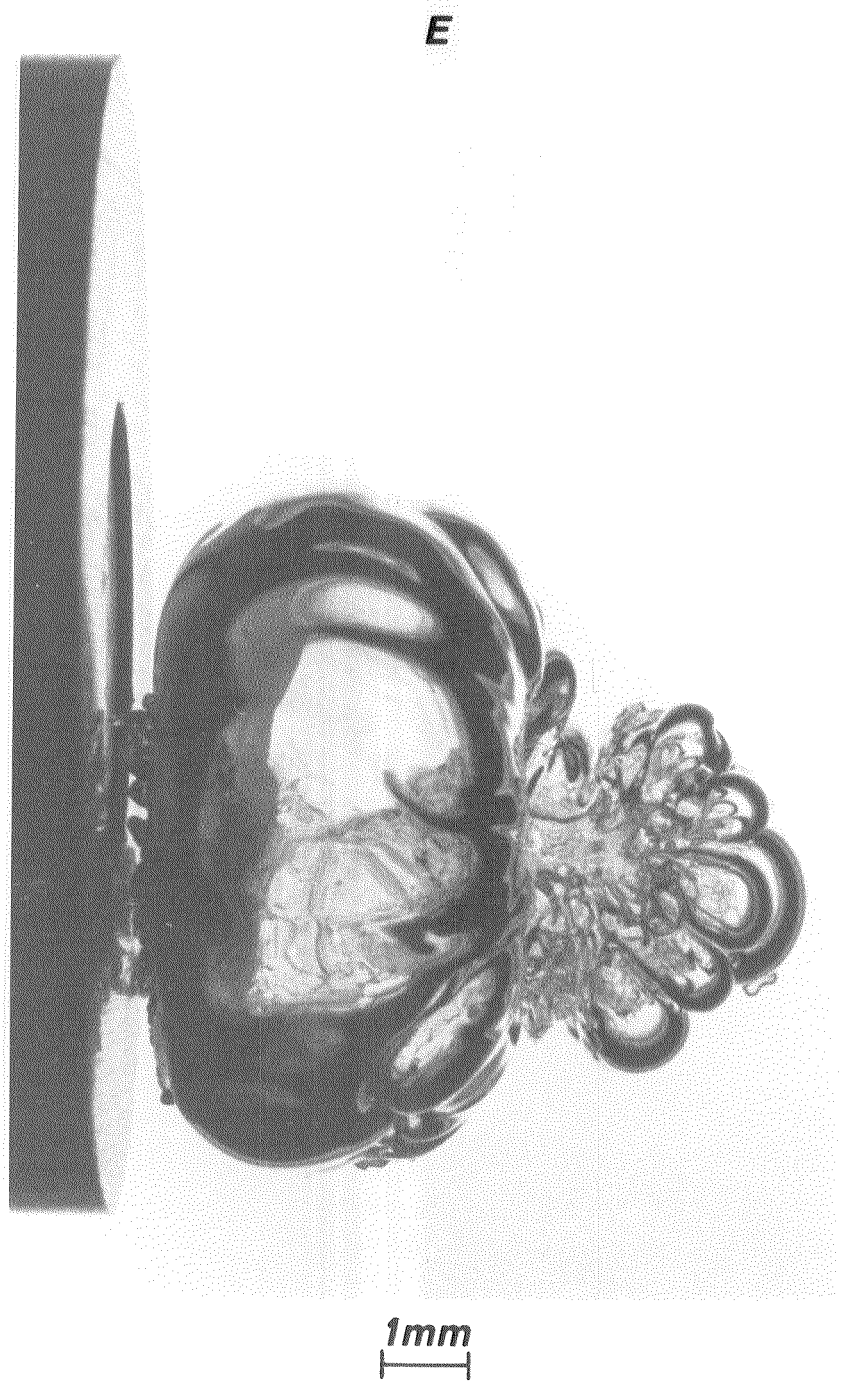

Figure A.3 Isopentane bubble rebounding after the initial collapse

Appendix B

CLASSICAL BUBBLE GROWTH THEORY

The theory referred to as the "classical theory of bubble growth" in earlier chapters describes the growth of a smooth vapour bubble from a critical nucleus in a uniformly superheated liquid. The most complete version of this theory is due to Prosperetti & Plesset (1978). The bubble growth theory shows that in a uniformly superheated liquid growth proceeds in three stages: first, a stage dominated by surface tension, in which the bubble grows from a critical radius; second, an inertially-controlled stage during which the bubble grows at a constant rate; and finally, an asymptotic stage governed by heat transfer in which the radius grows as $t^{1/2}$. Once the bubble has grown out of the surface tension dominated stage (which lasts less than 10^{-10} sec for ether at atmospheric pressure!) the growth can be described approximately by a universal equation in scaled variables. In deriving this equation Prosperetti & Plesset (1978) assumed that (i) the pressure and temperature of the vapour are uniform, (ii) the vapour is in thermodynamic equilibrium with the liquid surface, (iii) the vapour pressure is a linear function of the temperature of the liquid surface, (iv) the latent heat is constant, and (v) the surface tension is negligible. Only two variables, the bubble radius R and the bubble surface temperature T_b are independent in this theory with the above assumptions. Other variables are determined as a function of R, T_b and their derivatives.

To compare the theory with the bubble growth rates found for stable boiling in the present experiments at high pressures, rather than solving the universal equation, simple interpolation formulas suggested by Mikic et al. (1970) were used for R and T_b. However, the modified method for evaluating the vapour

pressure suggested by Theofanus & Patel (1976) was used. Prosperetti & Plesset (1978) show that these interpolation expressions are in reasonable agreement with the solutions to the universal bubble growth equation. For early times the growth of the bubble radius is dominated by liquid inertia and the radius grows linearly in time as follows:

$$R_{inertial} = \left[\frac{2}{3} \frac{P_v(T_\infty) - P_\infty}{\rho_l(T_\infty)} \right]^{1/2} t \qquad \text{(B.1)}$$

The above expression predicts a constant radial velocity of about 43 m/s for ether at 3 bar. As the bubble expands the liquid at the bubble surface cools due to the loss of heat from evaporation. The vapour pressure inside the bubble consequently falls and eventually reaches the ambient pressure when the surface temperature of the bubble falls to the saturation value corresponding to the ambient pressure. The effect of ambient pressure on the behaviour of the bubble surface temperature for ether is shown in figure B.1. The total temperature drop that occurs (which is just the superheat, $T_{sl} - T_{sat}$), decreases with increasing ambient pressure. Also the surface temperature falls more rapidly to its asymptotic value at higher ambient pressures. In this asymptotic regime the bubble growth is controlled by heat transfer and is given by the following:

$$R_{thermal} = \frac{\rho_l(T_{sat})}{\rho_v(T_{sat})} Ja \left[\frac{12D}{\pi} \right]^{1/2} t^{1/2} \quad , \qquad \text{(B.2)}$$

where D is the thermal diffusivity of the liquid evaluated at T_{sat} and the Jakob number is given by:

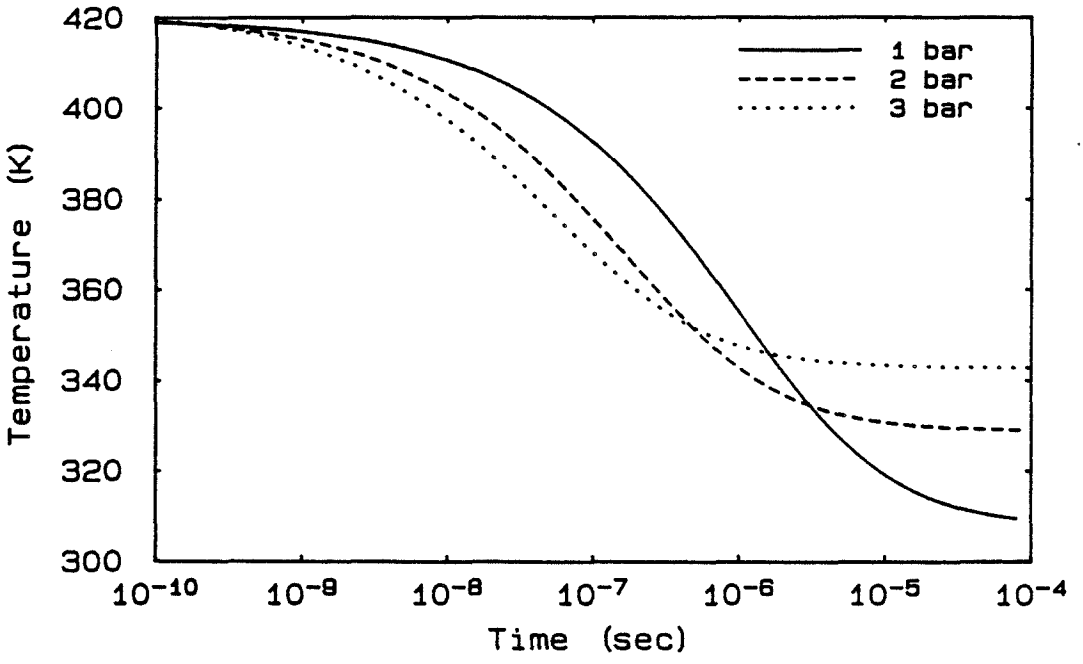

Figure B.1 Effect of ambient pressure on the variation of bubble surface temperature in ether

$$Ja = \frac{c_p(T_{sat})\,(T_\infty - T_{sat})}{L(T_{sat})} \qquad (B.3)$$

The properties of the liquid and vapour were estimated using the methods listed at the bottom of table 2.3.

Increasing the ambient pressure decreases the time duration of the inertial growth phase and slows the bubble growth velocity. For example, in ether the cross-over time between the inertial and heat transfer dominated stages (defined as the time when $R_{inertial} = R_{thermal}$) varies from 5.0 μsec at atmospheric pressure to 0.27 μsec at 3 bar. Figure B.2 shows the growth of the bubble radius as a function of time generated using the interpolation approximation to the classical theory. The theoretical curves are plotted for ether at atmospheric pressure and for 3 bar on a log-log scale and the change in slope of the curves reflects the transition from inertially-dominated bubble growth to growth

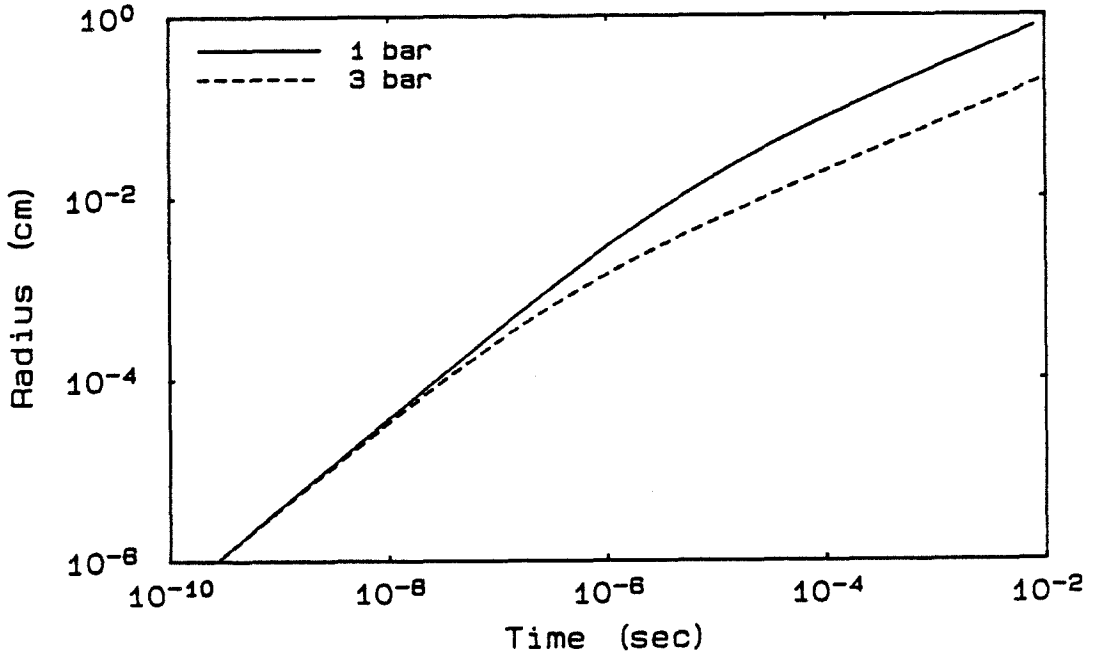

Figure B.2 Effect of ambient pressure on theoretical bubble growth rates for ether

limited by heat transfer. In figure B.3 the theoretical curves are replotted on a semi-log scale together with the experimental data estimated from the photographs shown in figure 4.8 for ether at 3 bar. The data follow the shape of the theoretical curve quite well indicating that the asymptotic growth law (equation (B.2)) is a good approximation to the bubble growth at this stage. However, the experimental points consistently lie above the theoretical predictions, suggesting that the theoretical interpolation equation slightly underestimates either the inertial growth rate at early times or the duration of the inertially-dominated growth regime. In any case, the discrepancy between the theoretical curve and experimental results is not surprising considering the fact that the finite size of the drop and heat transfer from the host fluid to the evaporating surface and to the vapour in the bubble are not accounted for in the theory.

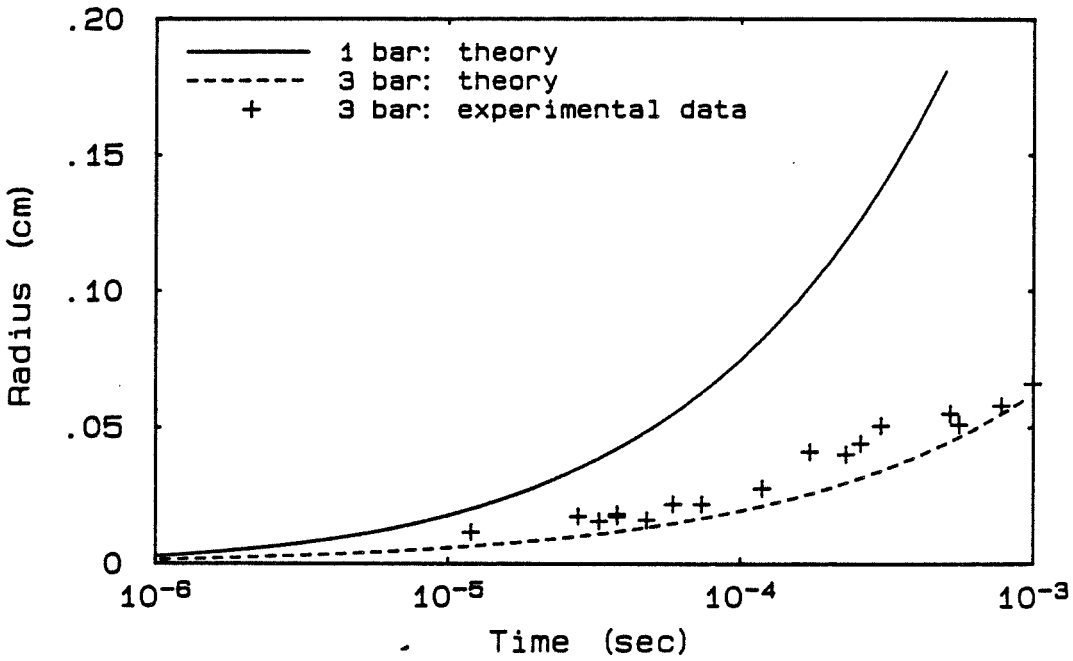

Figure B.3 Experimental and theoretical stable bubble growth in ether

Appendix C

MULTIPLE NUCLEATIONS

At atmospheric pressure the unstable vapourization of a superheated drop is always observed to proceed by the formation and growth of a single bubble within the drop. At high ambient pressures, when the instability is suppressed, the smooth vapour bubble grows much more slowly and quite often two or more nucleations are observed to occur within a single drop. The formation of each bubble nucleus generates a small-amplitude pressure pulse that is recorded by the pressure transducer. The recorded pressure trace can then be examined together with a photograph to determine if more than one bubble nucleated within the drop. In this appendix the occurrence of multiple nucleations in ether drops vapourizing in the transitional regime of instability will be illustrated.

Figure C.1 shows two vapour bubbles growing within a drop of ether boiling at 3 bar. From the pressure trace it can be determined that the second bubble formed about 55 μsec after the initial bubble. The photograph was taken 500 μsec after the second nucleation occurred. An example of a more rare triple nucleation event is documented in figure C.2. With reference to the pressure trace, the nucleation history of the rather bizarre looking drop shown may be reconstructed. Following the first nucleation the second bubble formed after a delay of 785 μsec. The drop was photographed after an additional delay of about 2 ms and the bubbles form the two lobes that are visible on each end of the drop. The two faint curved lines that are just visible through the central part of each bubble are the intersections of the bubbles with the remaining liquid in the drop on the side of the bubbles away from the viewer. The pressure

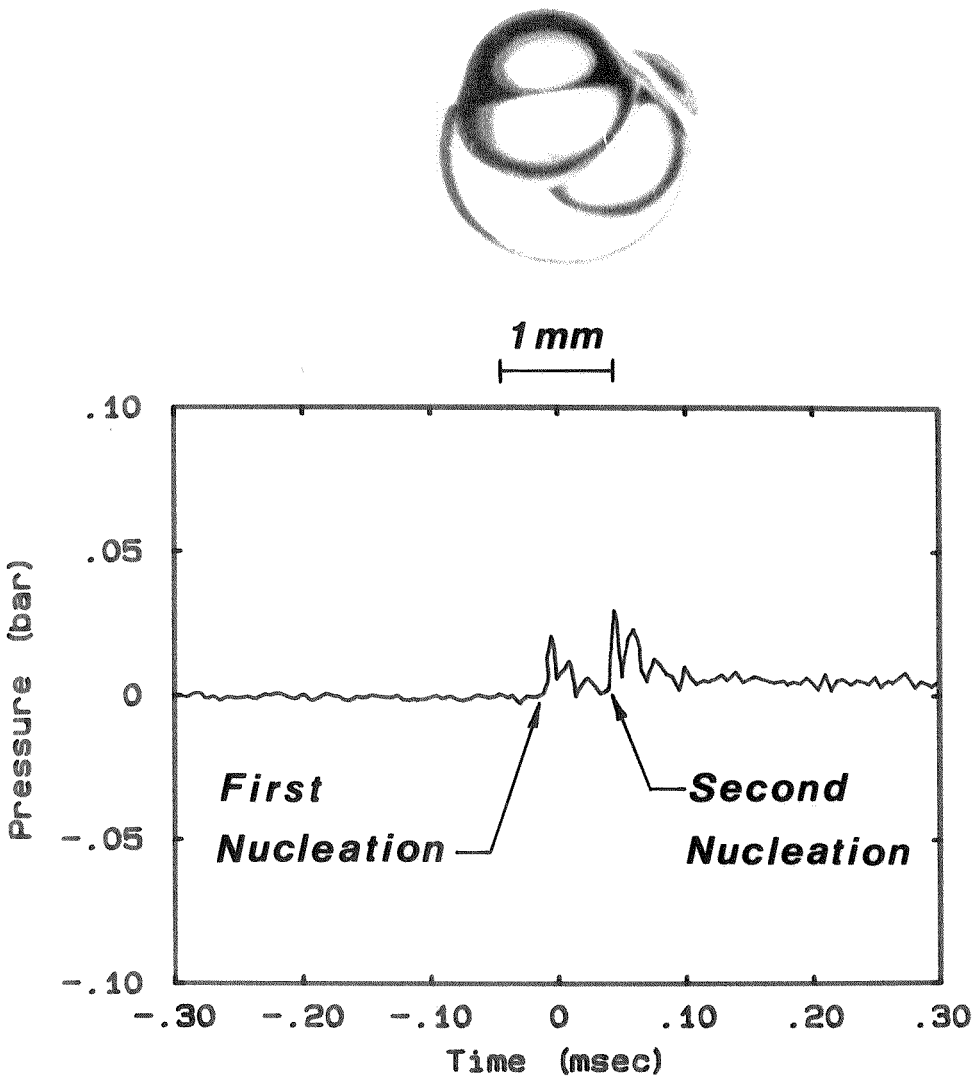

Figure C.1 Double nucleation within an ether droplet boiling stably at 3 bar

trace indicates that the third bubble nucleated a mere 35 μsec before the spark gap fired to photograph the drop. The third nucleation occurred in the remaining liquid located behind the large bubble on the right side of the drop. The small bubble (less than 0.2 mm in diameter) can be viewed through the centre of the larger bubble in front of it.

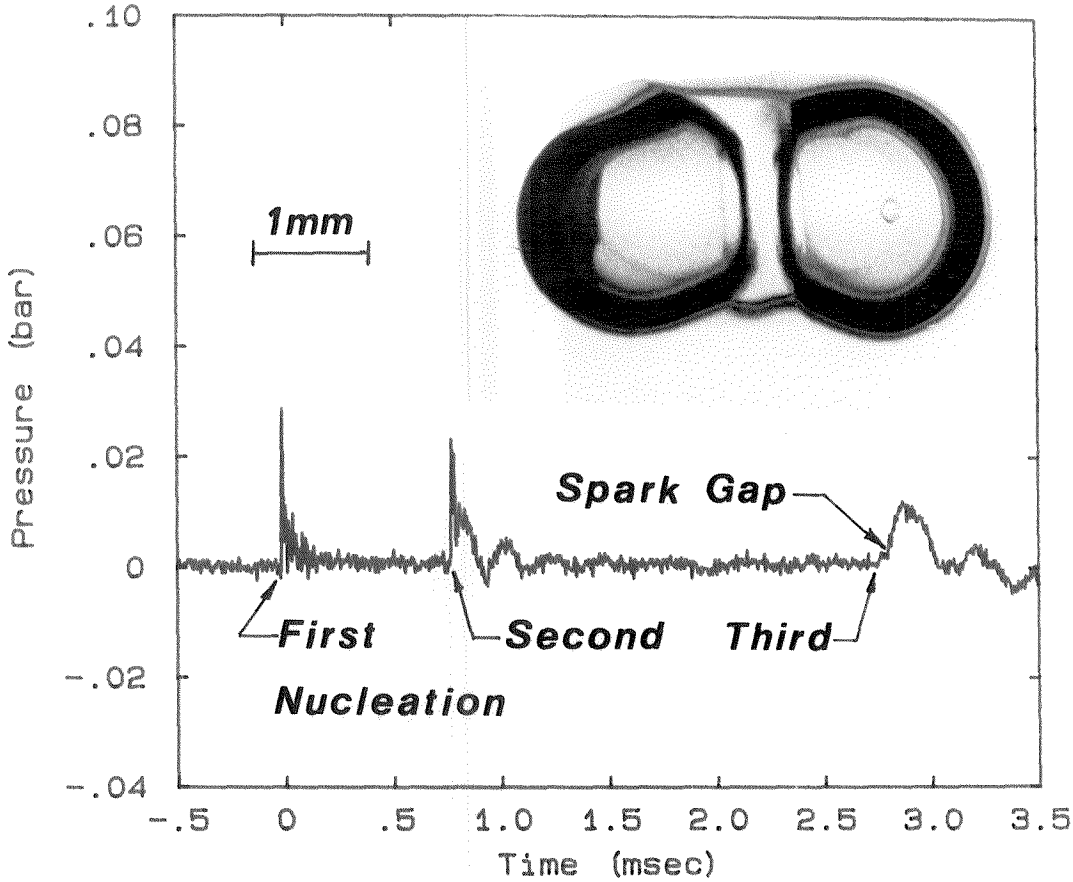

Figure C.2 Triple nucleation within an ether droplet boiling stably at 3 bar

When two bubbles grow within a drop and merge, a thin filament of liquid is often left behind after the coalescence of the bubbles. Figure C.3 shows two examples of this in drops that suffered two nucleations. Picture A was photographed 35 μsec *before* and picture B 65 μsec *after* the initiation of the explosion. In the right photograph it can be seen that the explosive jet combines with the large droplets of the fluid filament.

The merging of two bubbles within a drop usually causes a disturbance that is sufficient to initiate the violent instability. Droplets that remain from the fluid filament are often observed within bubbles photographed shortly after the onset of unstable boiling. Figure C.4 shows a drop photographed 35 μsec after the

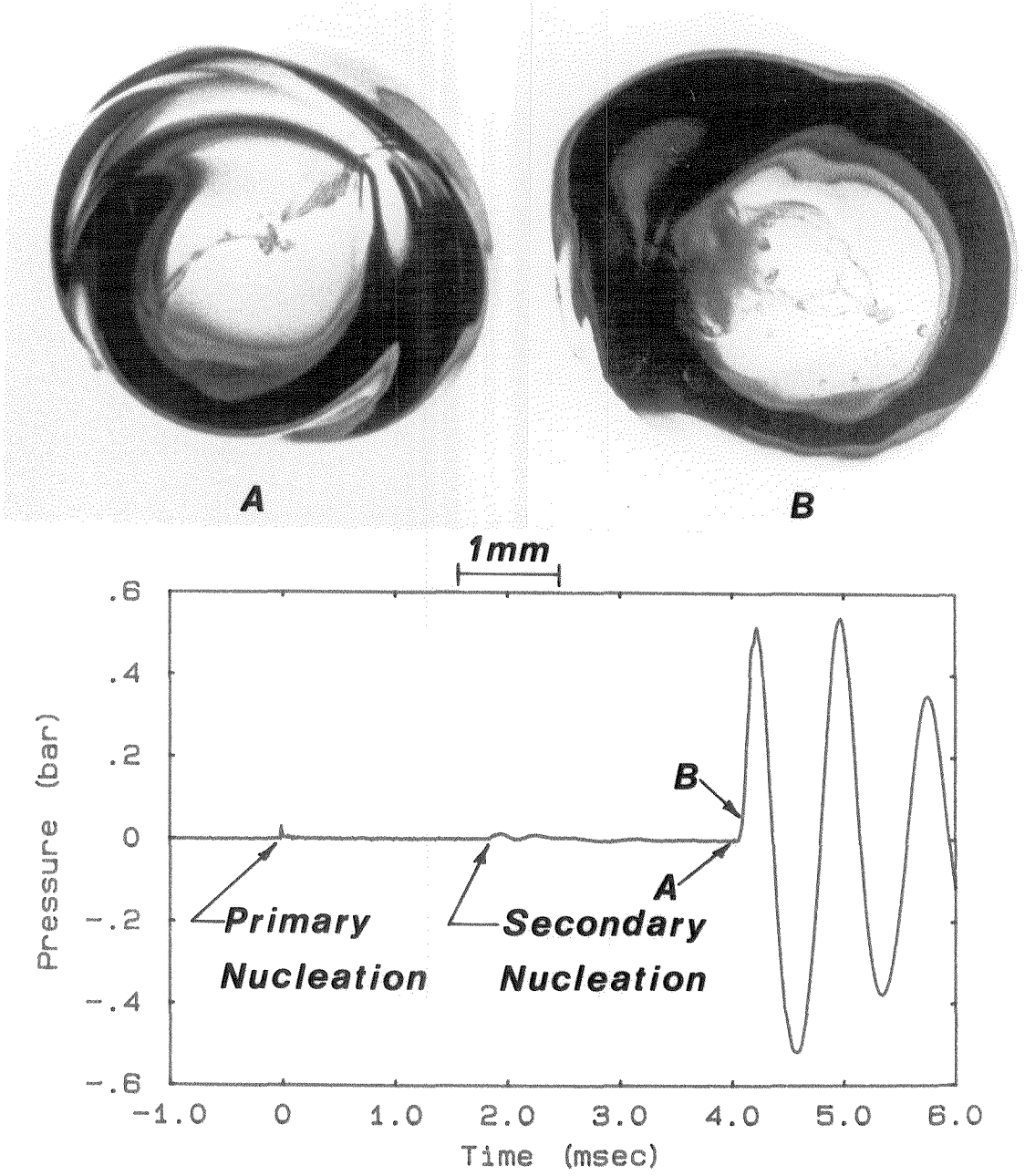

Figure C.3 Liquid filament resulting from the merging of two bubbles growing within a drop

unstable vapourization was triggered in the lower portion of the drop. Small droplets are visible within the bubble that are unrelated to the fine mist of particles that is generated at the evaporating interface. When bubbles nucleate on

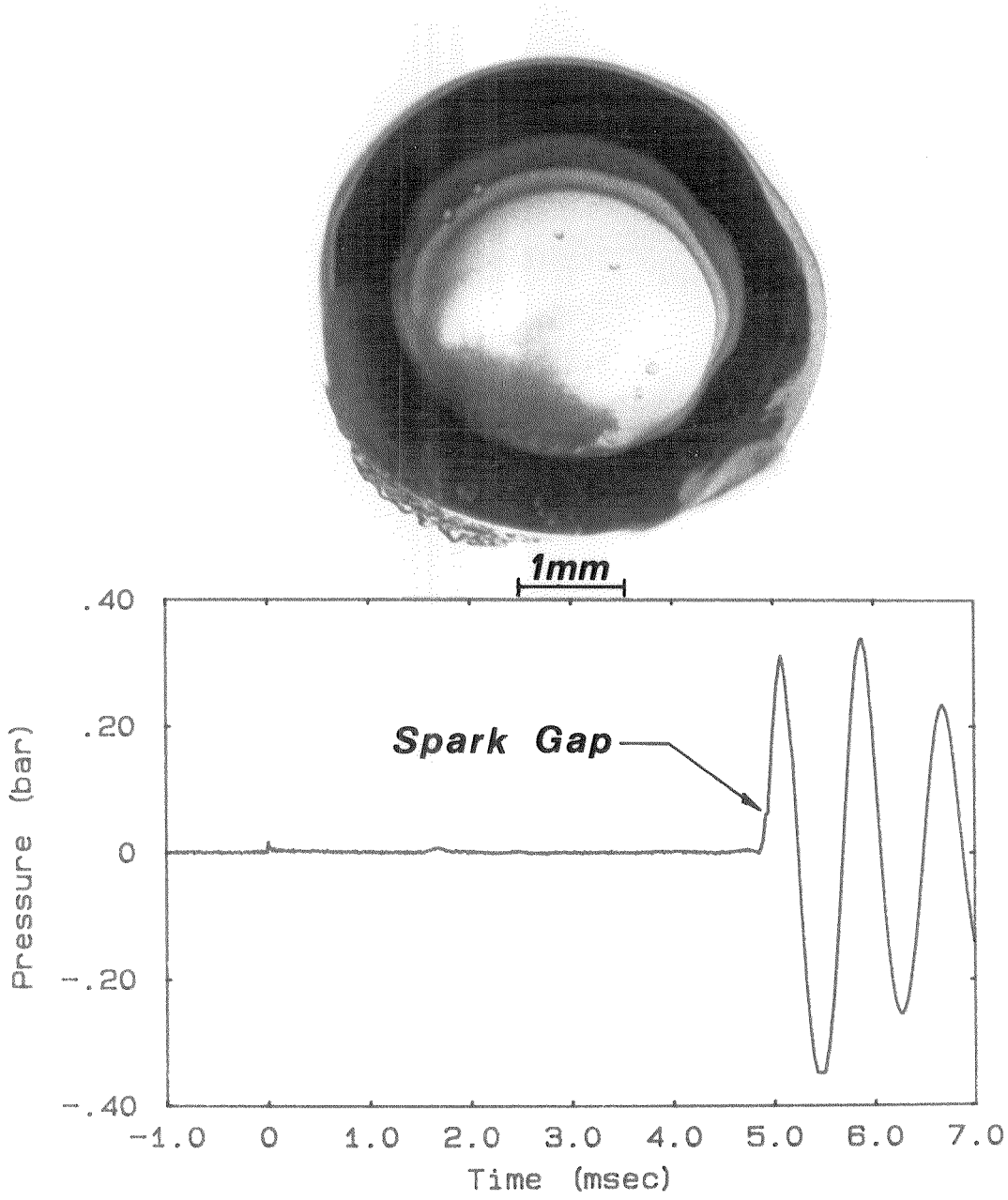

Figure C.4 Ether bubble shortly after onset of instability

opposite sides of a drop, grow and meet, large distortions of the bubble surface can occur as shown in figure C.5. The stably vapourizing liquid trapped between the two growing bubbles began to boil unstably 60 μsec before the photograph was taken.

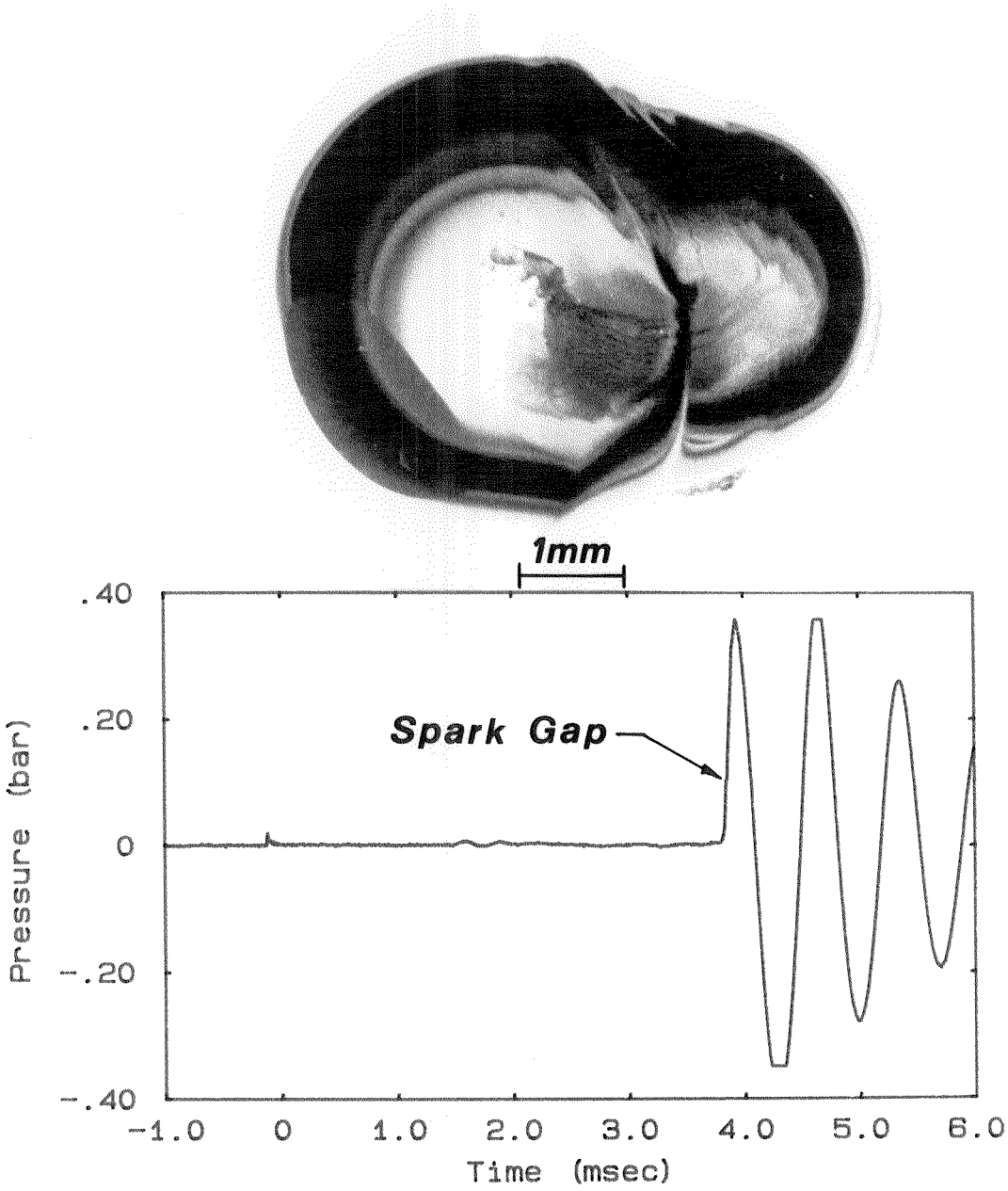

Figure C.5 Unstable boiling following double nucleation

Appendix D

LANDAU INSTABILITY RESULTS

Landau (1944; cf. also Landau & Lifshitz 1959) investigated the stability of a plane flame front with respect to small disturbances. The analysis considers the dynamical behaviour of an interface between two fluids of different density with mass flux across the interface. No thermal effects are included and the effect of surface tension and fluid accelerations at the interface enter into the theory through the boundary condition on the pressure. Figure D.1 shows a schematic of the interface $\eta(y,t)$ with nomenclature appropriate for evaporation at the interface.

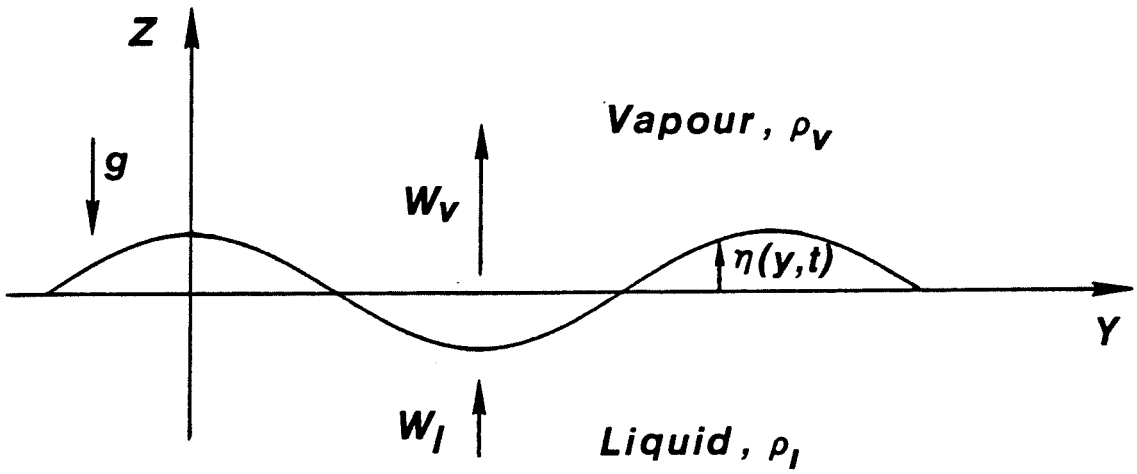

Figure D.1 Schematic of interface coordinates

In this frame of reference the unperturbed interface is the plane z = 0 and W_l, W_v are the velocities respectively of the liquid and vapour relative to the interface. By specifying perturbations to the velocities and pressure, and assuming exponential growth of the perturbed interface, i.e.,

$$\eta(y,t) = \eta_0 \, e^{\omega t} \cos(ky) \quad , \tag{D.1}$$

Landau derived a quadratic relation for the dimensional growth rate ω. Solving this dispersion relation for the larger root gives the following expression for the growth rate as a function of the wavenumber, k:

$$\omega = -k \, \frac{W_l W_v}{W_l + W_v} + \left[\frac{k^2 W_l W_v (W_v^2 + W_l W_v - W_l^2)}{(W_l + W_v)^2} - \nu_0^2 \right]^{1/2} \quad . \tag{D.2}$$

In solving for the above expression, the continuity of mass flux J at the interface, i.e.,

$$J = \rho_v W_v = \rho_l W_l \quad , \tag{D.3}$$

was used and the natural frequency of ordinary surface waves, ν_0, given by

$$\nu_0^2 = \frac{gk(\rho_l - \rho_v) + \sigma k^3}{\rho_l + \rho_v} \quad , \tag{D.4}$$

was introduced, where σ is the surface tension. If the terms involving mass flux in equation (D.2) are set to zero, the growth rate becomes imaginary ($\omega = i\nu_0$) indicating oscillatory behaviour.

The growth of the perturbation of the interface is driven by the mass flux across the interface. For example, for small values of the wavenumber the contribution from ν_0^2 in equation D.2 may be neglected, and if it is assumed that $\rho_l >> \rho_v$, the growth rate is linearly proportional to the mass flux as follows:

$$\omega = \frac{k}{(\rho_l \rho_v)^{1/2}} J \quad . \tag{D.5}$$

Equation (D.5) does not hold at high wavenumbers when the assumption that ν_0 is negligible is no longer valid. For large values of k, the surface tension term in ν_0 becomes important and ν_0^2 dominates the other term within the square brackets in equation (D.2). As a result ω becomes complex with a negative real part indicating a stable configuration.

The Landau instability is characterized by the presence of vorticity in the vapour region. The presence of the vorticity is fundamental to the instability mechanism and comes about as a result of the requirement of continuity of tangential velocity at the interface (Marble, 1985). The incoming liquid flow is irrotational but vorticity is produced by the flow transition at the interface. The vorticity is generated through the action of the baroclinic term ($\nabla \rho$ x ∇p) in the vorticity equation. Figure D.2 shows a schematic of the interface showing the direction of the density and pressure gradients and indicating the direction of the vorticity that is produced in the vapour.

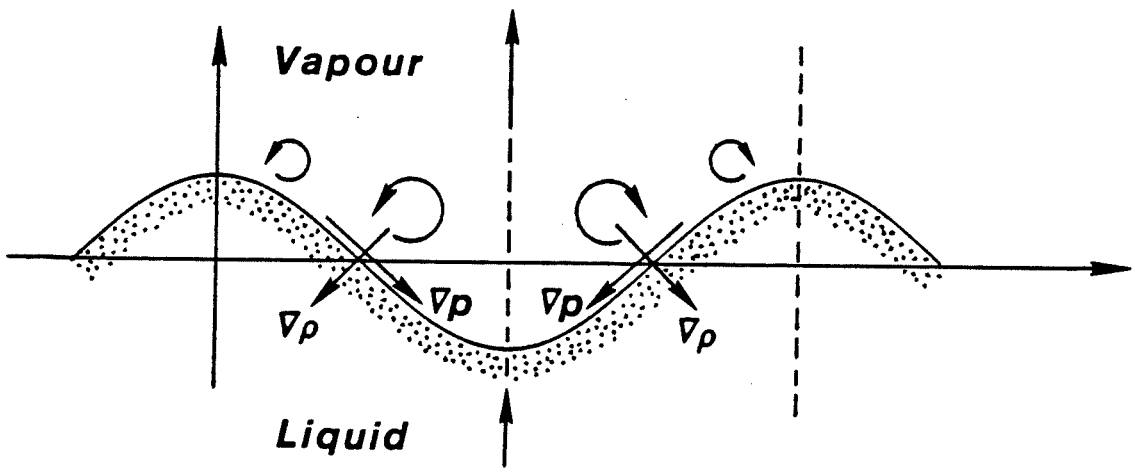

Figure D.2 Baroclinic generation of vorticity at the evaporating interface

An expression for the vapour vorticity may be derived from the Landau theory by taking the curl of the fluctuation velocity in the vapour. The resulting expression for the vorticity, ζ, is as follows:

$$\zeta = \eta_0 k \sin(ky)\left[1 + \frac{\omega}{k W_v}\right]\left[k(W_v - W_l) - 2\omega\right] e^{\omega(t - x/W_v)} \quad . \tag{D.6}$$

The vorticity is 90° out of phase with the perturbed interface and the maximum vorticity is produced at the inflection point in the interface as shown in figure D.2. The vorticity produced decreases as the growth rate ω decreases, but remains the same sign when the real part of ω becomes negative.

To obtain a better physical feel for the instability mechanism, it is instructive to examine the pressure fluctuations that are generated in the vapour and liquid. From the Landau theory the pressure perturbations in the liquid and vapour can be expressed as follows:

$$p_l' = -\eta_0 \rho_l \omega(W_l + \omega/k)\cos(ky)\, e^{(\omega t + kx)} \tag{D.7}$$

$$p_v' = -\eta_0 \rho_v (W_v - \omega/k)\left[\frac{k(W_v - W_l) - \omega(1 + \frac{\omega}{k W_v})}{1 - \frac{\omega}{k W_v}}\right]\cos(ky)\, e^{(\omega t - kx)} \quad . \tag{D.8}$$

For the unstable case ($\omega > 0$), with the same assumptions used in writing equation (D.5), the pressure perturbations can be written as follows:

$$p_l' = p_v' = -\frac{\eta_0 k}{\rho_v} J^2 \cos(ky) e^{(\omega t - k|x|)} \quad . \tag{D.9}$$

So the motion of the interface produces a lateral pressure variation that is at a maximum at the interface and decays on either side of the interface. The pressure perturbation grows exponentially in time with growth rate ω as a result of the fundamental unsteady behaviour at the interface. The pressure perturbation is 180° out of phase with the interface as shown in the drawing on the left in figure D.3.

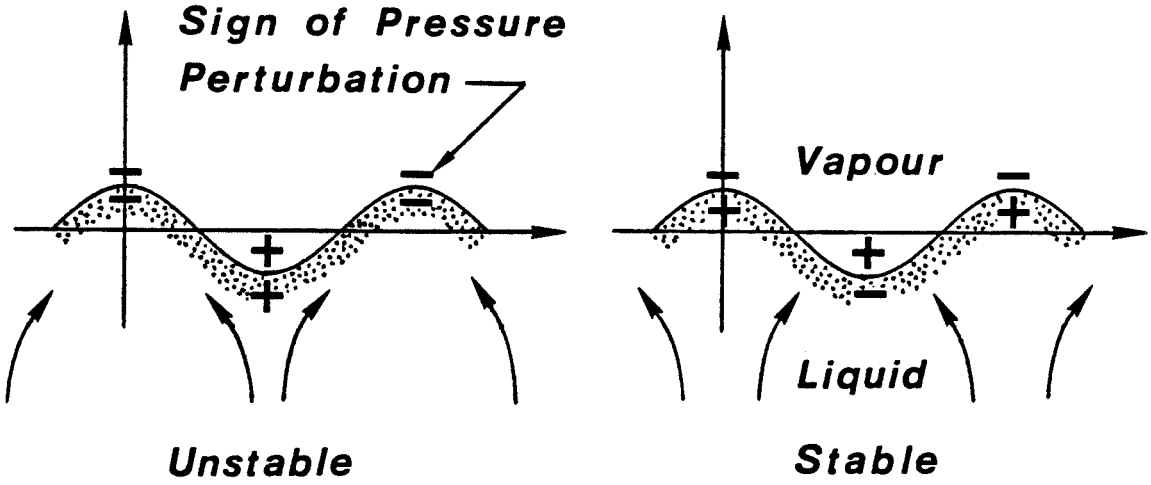

Figure D.3 Deflection of fluid streamlines due to pressure fluctuations in the liquid

The incoming fluid streamlines are deflected away from the liquid troughs and into the fluid crests causing the amplitude of the interface perturbations to grow. The evaporating surface may become so convoluted that liquid particles are ejected downstream into the vapour region, greatly enhancing the mass flux.

For low values of the mass flux the real part of ω is negative and the surface is stable. In this case, from equation (D.7), p_l' has the opposite sign as for unstable growth (p_v' remains the same sign but decreases in magnitude) and the

situation is depicted in the drawing on the right in figure D.3. Now the liquid moving towards the interface is deflected towards the liquid troughs tending to decrease the initial disturbance and leading to a stable configuration.

1. References

ANDERSON, R.P. & ARMSTRONG, D.R. 1974 Comparison between vapor explosion models and recent experimental results. *A.I.Ch.E. Sym. Series* **70**(138), p. 31.

APFEL, R.E. & HARBISON, J.P. 1975 Acoustically induced explosions of superheated droplets. *J. Acoust. Soc. Am.* **57**, p. 1371.

AVEDISIAN, C.T. 1982 Effect of pressure on bubble growth within liquid droplets at the superheat limit. *J. Heat Transfer* **104**, p. 750.

AVEDISIAN, C.T. & GLASSMAN, I. 1981a Superheating and boiling of water in hydrocarbons at high pressures. *Int. J. Heat Mass Transfer* **24**(4), p. 695.

AVEDISIAN, C.T. & GLASSMAN, I. 1981b High pressure homogeneous nucleation of bubbles within superheated binary liquid mixtures. *J. Heat Transfer* **103**, p. 272.

BAINES, M., BOARD, S.J., BUTTER, N.E. & HALL, R.W. 1980 The hydrodynamics of large-scale fuel-coolant interactions. *Nucl. Tech.* **49**, p. 27.

BENJAMIN, T.B. & ELLIS, A.T. 1966 The collapse of cavitation bubbles and the pressures thereby produced against solid boundaries. *Phil. Trans. Roy. Soc. A* **260**, p. 221.

BLANDER, M. & KATZ, J.L. 1975 Bubble nucleation in liquids. *A.I.Ch.E. J.* **21**(5), p. 833.

BOARD, S.J., FARMER, C.L. & POOLE, D.H. 1974 Fragmentation in thermal explosions. *Int. J. Heat Mass Transfer* **17**, p. 331.

BUCHANAN, D.M. 1974 A model for fuel-coolant interactions. *J. Phys. D:Appl. Phys.* **7**, p. 1441.

BUCHANAN, D.J. & DULLFORCE, T.A. 1973 Mechanism for vapor explosions. *Nature* **245**, p. 32.

DALLE DONNE, M. & FERRANTI, M.P. 1975 The growth of vapor bubbles in superheated sodium. *Int. J. Heat Mass Transfer* **18**, p. 477.

DARRIEUS, G. 1938 La mecanique des fluides. *La Technique Moderne*, p. 15.

DARRIEUS, G. 1945 Propagation d'un front de flamme. Presented at *Le Congres de Mecanique Appliquee*, unpublished.

DERGARABEDIAN, P. 1953 The rate of growth of vapor bubbles in superheated water. *J. Appl. Mech.* **20**(4), p. 537.

DERGARABEDIAN, P. 1960 Observations on bubble growth in various superheated liquids. *J. Fluid Mech.* **9**, p. 40.

DRUMHELLER, D.S. 1979 The initiation of melt fragmentation in fuel-coolant interactions. *Nucl. Sci. & Eng.* **72**, p. 347.

FLORSHUETZ, L.W., HENRY, C.L., & KHAN, A.R. 1969 Growth rates of free vapor bubbles in liquid at uniform superheats under normal and zero gravity conditions. *Int. J. Heat Mass Transfer* **12**, p. 1465.

GROLMES, M.A. & FAUSKE, H.K. 1974 Axial propagation of free surface boiling into superheated liquids in vertical tubes. *Proc. 5th Int. Heat Transfer Conf.*, Paper B1.7, Japan Soc. Mech. Engrs and Soc. Chem. Engng, Japan, p. 30.

HALL, R.W. & BOARD, S.J. 1979 The propagation of large scale thermal explosions. *Int. J. Heat Mass Transfer* **22**, p. 1083.

HENRY, R.E. & FAUSKE, H.K. 1979 Nucleation processes in large scale vapor explosions. *J. Heat Transfer* **101**, p. 280.

HENRY, R.E., FAUSKE, H.K. & McUMBER, L.M. 1975 Vapor explosions with subcooled freon. *Trans. Am. Nucl. Soc.* **22**, p. 413.

HEWITT, H.C. & PARKER, J.D. 1968 Bubble growth and collapse in liquid nitrogen. *J. Heat Transfer* **90**, p. 22.

HOOPER, F.C. & ABDELMESSIH, A.H. 1966 The flashing of liquids at higher superheats. *Proc. Third International Heat Transfer Conference*, Chicago, **5**, p. 44.

ISTRATOV, A.G. & LIBROVICH, V.B. 1969 On the stability of gasdynamic discontinuities associated with chemical reactions. The case of a spherical flame. *Astron. Acta.* **14**, p. 453.

JARVIS, T.J., DONOHUE, M.D. & KATZ, J.L. 1975 Bubble nucleation mechanisms of liquid droplets superheated in other liquids. *J. Colloid and Interface Science* **50**, p. 359.

JONES, JR., O.C. & ZUBER, N. 1978 Bubble growth in variable pressure fields. *J. Heat Transfer* **100**, p. 453.

KOSKY, P.G. 1968 Bubble growth measurements in uniformly superheated liquids. *Chem. Engng. Sci.* **23**, p. 695.

LANDAU, L.D. 1944 On the theory of slow combustion. *Acta Physiochimica U.R.S.S.* **19**, p. 77.

LANDAU, L.D. & LIFSHITZ, E.M. 1959 *Fluid Mechanics*. Pergamon, New York, problem 2, p. 479.

LAUTERBORN, W. & BOLLE, H. 1975 Experimental investigations of cavitation-bubble collapse in the neighbourhood of a solid boundary. *J. Fluid Mech.* **72**(2), p. 391.

MARBLE, F. 1985 Private communications, California Institute of Technology, Pasadena, California.

MIKIC, B.B., ROHSENOW, W.M. & GRIFFITH, P. 1970 On bubble growth rates. *Int. J. Heat Mass Transfer* **13**, p. 657.

MILLER, C.A. 1973 Stability of moving surfaces in fluid systems with heat and mass transport - II. Combined effects of transport and density difference between phases. *A.I.Ch.E. J.* **19**, p. 909.

NELSON, L.S. & BUXTON, L.D. 1978 Effects of pressure on steam explosion triggering in Corium-E Simulants. *Am. Nucl. Soc. Trans.* **28**, p. 448.

PALMER, H.J. 1976 The hydrodynamic stability of rapidly evaporating liquids at reduced pressure. *J. Fluid Mech.* **75**, p. 487.

PENG, D.Y. & ROBINSON, D.B. 1976 A new two-constant equation of state. *Ind. Eng. Chem. Fund.* **15**(1), p. 59.

PLESSET, M.S. & CHAPMAN, R.B. 1971 Collapse of an initially spherical vapour cavity in the neighbourhood of a solid boundary. *J. Fluid Mech.* **47**, p. 283.

PLESSET, M.S. & PROSPERETTI, A. 1977 Bubble dynamics and cavitation. *Ann. Rev. Fluid Mech.* **9**, p. 145.

PLESSET, M.S. & ZWICK, S.A. 1954 The growth of vapor bubbles in superheated liquids. *J. Appl. Phys.* **25**(4), p. 493.

PROSPERETTI, A. 1979 Boundary conditions at a liquid-vapor interface. *Meccanica* **14**, p. 34.

PROSPERETTI, A. & PLESSET, M. 1978 Vapour-bubble growth in a superheated liquid. *J. Fluid Mech.* **85**(2), p. 349.

PROSPERETTI, A. & PLESSET, M.S. 1984 The stability of an evaporating liquid surface. *Phys. Fluids* **27**(7), p. 1590.

RACKETT, H.G. 1970 Equation of state for saturated liquids. *J. Chem. Eng. Data* **15**, p. 514.

REID, R.C. 1976 Superheated liquids. *Amer. Scientist* **64**, p. 146.

REID, R.C. 1978 Superheated liquids: a laboratory curiosity and, possibly, an industrial curse. *Chem. Engng. Ed.* **12**, p. 60.

REID, R.C. 1983 Rapid phase transitions from liquid to vapor. *Adv. Chem. Eng.* **12**, p. 105.

REID, R.C., PRAUSNITZ, J.M. & SHERWOOD, T.K. 1977 *The Properties of Gases and Liquids*. McGraw-Hill, New York.

SHEPHERD, J.E. 1981 Dynamics of vapor explosions: rapid evaporation and instability of butane droplets exploding at the superheat limit. Ph.D. Thesis, Caltech.

SHEPHERD, J.E. & STURTEVANT, B. 1982 Rapid evaporation at the superheat limit. *J. Fluid Mech.* **121**, p. 379.

SKRIPOV, V.P. 1974 *Metastable Liquids*. John Wiley & Sons, New York.

STREHLOW, R.A. 1980 Accidental explosions. *Amer. Scientist* **68**, p. 420.

STURTEVANT B. & SHEPHERD, J.E. 1982 Evaporative instability at the superheat limit. *Appl. Sci. Res.* **38**, p. 85.

TAYLOR, G.I. 1950 The instability of liquid surfaces when accelerated in a direction perpendicular to their planes. I. *Proc. R. Soc. Lond. A* **201**, p. 192.

THEOFANOUS, T., BIASI, L., ISBIN, H.S. & FAUSKE, H. 1969 A theoretical study of bubble growth in constant and time-dependent pressure fields. *Chem. Engng. Sci.* **24**, p. 885.

THEOFANOUS, T.G. & PATEL, P.D. 1976 Universal relations for bubble growth. *Int. J. Heat Mass Transfer* **19**, p. 425.

THOMPSON, P.A. & SULLIVAN, D.A. 1979 A simple formula for saturated-vapor volume. *Ind. Eng. Chem. Fund.* **18**, p.1.

VAN DE HULST, H.C. 1981 *Light Scattering by Small Particles*. Dover Pub., Inc., New York, p. 107.

WITTE, L.C., COX, J.E. & BOUVIER, J.E. 1970 The vapor explosion. *J. of Metals* **22**(2), p. 39.

WITTE, L.C., VYAS, T.J. & GELABERT, A.A. 1973 Heat transfer and fragmentation during molten-metal/water interactions. *J. Heat Transfer* **95**, p. 521.

ZELDOVICH, Y.B. 1966 Stability of chemical processes: the Semenov's theory and its progress. *Chemical Kinetics and Chain Reactions*. Moscow, p. 574.

ZUBER, N. 1961 The dynamics of vapor bubbles in nonuniform temperature fields. *Int. J. Heat Mass Transfer* **2**, p. 83.